STUDIES OF CHARGED-PARTICLE-INDUCED RESIDUAL RADIONUCLIDES PRODUCTION CROSS-SECTIONS USING AVF CYCLOTRON FOR MEDICAL APPLICATIONS

AHMED RUFA'I USMAN

FACULTY OF SCIENCE
UNIVERSITY OF MALAYA
KUALA LUMPUR

2017

STUDIES OF CHARGED-PARTICLE-INDUCED RESIDUAL RADIONUCLIDES PRODUCTION CROSS-SECTIONS USING AVF CYCLOTRON FOR MEDICAL APPLICATIONS

AHMED RUFA'I USMAN

THESIS SUBMITTED IN FULFILMENT OF THE REQUIREMENTS FOR THE DEGREE OF DOCTOR OF PHILOSOPHY

FACULTY OF SCIENCE
UNIVERSITY OF MALAYA
KUALA LUMPUR

2017

UNIVERSITY OF MALAYA

ORIGINAL LITERARY WORK DECLARATION

Name of Candidate: **AHMED RUFA'I USMAN**

Matric No: **SHC130040**

Name of Degree: **Doctor of Philosophy**

Title of Thesis:

STUDIES OF CHARGED-PARTICLE-INDUCED RESIDUAL RADIONUCLIDES PRODUCTION CROSS-SECTIONS USING AVF CYCLOTRON FOR MEDICAL APPLICATIONS

Field of Study: **EXPERIMENTAL NUCLEAR PHYSICS**

I do solemnly and sincerely declare that:

(1) I am the sole author/writer of this Work;
(2) This Work is original;
(3) Any use of any work in which copyright exists was done by way of fair dealing and for permitted purposes and any excerpt or extract from, or reference to or reproduction of any copyright work has been disclosed expressly and sufficiently and the title of the Work and its authorship have been acknowledged in this Work;
(4) I do not have any actual knowledge nor do I ought reasonably to know that the making of this work constitutes an infringement of any copyright work;
(5) I hereby assign all and every right in the copyright to this Work to the University of Malaya ("UM"), who henceforth shall be owner of the copyright in this Work and that any reproduction or use in any form or by any means whatsoever is prohibited without the written consent of UM having been first had and obtained;
(6) I am fully aware that if in the course of making this Work I have infringed any copyright whether intentionally or otherwise, I may be subject to legal action or any other action as may be determined by UM.

Candidate's Signature Date:

Subscribed and solemnly declared before,

Witness's Signature Date:

Name:

Designation:

ABSTRACT

The charged-particle-induced nuclear reactions by using cyclotrons or accelerators with a moderate energy have become a very vital feature of the modern nuclear medicine. Based on the well-measured excitation functions, the optimum production parameters of the important radionuclides can be easily determined. Realising the importance of excitation functions for the efficient production of radionuclides, a comprehensive study of residual radionuclides production cross-sections was performed using a stacked-foil activation technique combined with offline HPGe γ-ray spectrometry. In the first phase of the study, a 24 MeV deuteron energy was used as the bombarding particles on two separate stacks, both containing nickel (Ni) and titanium (Ti) foils as the main targets metals. In the 2nd phase, a 50.4 MeV alpha-particle beam energy was used as the projectile on a stack containing holmium (Ho), Ti and copper (Cu) foils. The experiments were performed using the AVF cyclotron of RI Beam Factory, Nishina Centre for Accelerator-Based Science, RIKEN, Wako, Saitama, Japan. Deuteron-induced cross-sections of the ^{nat}Ni(d,x)$^{55\text{-}58,60}$Co, ^{57}Ni, ^{52g,54}Mn and ^{61}Cu reactions were measured from the respective threshold energies up to 24 MeV. From the second phase, the excitation functions of the ^{nat}Cu(α,x)^{66,67}Ga,^{65}Zn,^{57,58,60}Co nuclear reactions have been measured in the energy range of 50 MeV down to 3.2 MeV. Similarly, the excitation functions of ^{nat}T(α,x)^{43}K,$^{43,44m,44g,46\text{-}48}$Sc, ^{48}V and ^{48,49,51}Cr from natural titanium as well as the excitation functions of ^{165}Ho(α,nx)$^{165\text{-}168}$Tm radionuclides from holmium target have also been measured. The accuracy of the measured cross-sections was confirmed by, in addition to the beam current, the simultaneously measured monitor reaction excitation functions of ^{nat}T(d,x)^{48}V and ^{nat}T(α,x)^{51}Cr for the first and second phase of the studies, respectively. The results were compared with previous experimental data (if available) and with the theoretical TALYS 1.4 and 1.6

nuclear reaction codes evaluated in the TENDL-2014, 2015, libraries. Present results show reasonable agreement with some of the reported experimental data while a partial agreement is found with the evaluated (theoretical) data. The integral thick target yields (TTY) of ^{55}Co and ^{56}Co radionuclides via deuteron irradiation on nickel have been calculated. From the stack bombarded by the 50.4 MeV alpha beam energy, the present study also calculated the integral thick target yields for ^{43}K, $^{43,44m,44g,46-48}$Sc, ^{48}V and ^{48,49,51}Cr from the titanium targets. The measured data are useful to reduce the existing discrepancies among the literature, to improve the nuclear reaction model codes and to enrich the experimental database towards various applications. The ^{nat}Ni(d,x)^{61}Cu cross-sections recommended by the IAEA overestimate recent experimental ones, and their upgrade has been proposed. Some of the radionuclides reported in this study have been investigated via their study route for the first, second or third time.

ABSTRAK

Tindak balas nuklear yang disebabkan oleh zarah bercas dengan menggunakan siklotron atau pemecut dengan tenaga yang sederhana telah menjadi ciri yang sangat penting dalam perubatan nuklear moden. Berdasarkan kepada fungsi pengujaan yang diukur dengan baik, parameter untuk pengeluaran radionuklid penting yang optimum, dapat ditentukan dengan mudah. Menyedari kepentingan fungsi pengujaan untuk pengeluaran radioniklid yang berkesan, kajian yang komprehensif telah dijalankan ke atas keratan rentas sisa pengeluaran radionuklid dengan menggunakan teknik pengaktifan timbunan kerajang logam yang digabungkan dengan spektrometri HPGe sinaran-γ luar talian. Dalam fasa pertama kajian ini, tenaga deuteron sebanyak 24 MeV telah digunakan sebagai zarah pembedil bagi dua susunan yang berasingan, di mana kedua-dua susunan ini mengandungi kerajang logam nikel (Ni) dan titanium (Ti) sebagai sasaran logam utama. Dalam fasa kedua, tenaga pancaran zarah alfa sebanyak 50.4 MeV telah digunakan sebagai peluru pada timbunan yang mengandungi kerajang logam holmium (Ho), Ti dan tembaga (Cu). Kajian ini telah dilakukan dengan menggunakan siklotron AVF dari RI Beam Factory, Nishina Centre for Accelerator-Based Science, RIKEN, Wako, Saitama, Jepun. Keratan rentas yang disebabkan oleh deuteron, bagi tindak balas ^{nat}Ni (*d*, *x*) $^{55\text{-}58,60}$Co, ^{57}Ni, $^{52g,\ 54}$Mn dan ^{61}Cu, diukur dari tenaga ambang masing-masing sehingga 24 MeV. Daripada fasa kedua, fungsi pengujaan daripada tindak balas nuklear ^{nat}Cu(α, x)^{66,67}Ga, ^{65}Zn, ^{57,58,60}Co telah diukur dalam julat tenaga 50 MeV turun kepada 3.2 MeV. Fungsi pengujaan bagi ^{nat}T(α, x) ^{43}K, $^{43,44m,\ 44g,\ 46\text{-}48}$Sc, ^{48}V dan ^{48,49,51}Cr dari titanium semulajadi dan juga fungsi pengujaan bagi radionuklid ^{165}Ho(α, nx) $^{165\text{-}168}$Tm dari sasaran holmium, juga telah diukur. Ketepatan yang diukur keratan rentas telah disahkan oleh arus pancaran serta fungsi pengujaan tindak balas panduan oleh ^{nat}T(d, x)^{48}V dan ^{nat}T(α, x)^{51}Cr bagi fasa

pertama dan kedua kajian , masing-masing. Semua keputusan telah dibandingkan dengan data eksperimen terdahulu (jika ada) dan juga dengan teori TALYS 1.4 dan kod tindak balas nuklear 1.6 yang dinilai dalam perpustakaan TENDL 2014, 2015. Keputusan terkini menunjukkan persetujuan yang munasabah dengan beberapa data eksperimen yang telah dilaporkan sebelum ini, manakala persetujuan separa telah didapati dengan data (teori) yang dinilai. Kamiran hasil sasaran tebal (TTY) bagi radionuklid ^{55}Co, ^{57}Co dan ^{58}Co melalui penyinaran deuteron ke atas nikel telah dikira. Dari timbunan yang dibedil oleh 50.4 MeV tenaga pancaran alfa, Kamiran hasil sasaran tebal bagi ^{43}K, $^{43,44m,\ 44g,\ 46-48}$Sc, ^{48}V dan ^{48,49,51}Cr dari sasaran titanium. Data yang diukur adalah berguna untuk mengurangkan percanggahan yang sedia ada di antara kesusasteraan, untuk meningkatkan kod model tindak balas nuklear dan untuk meningkatkan pangkalan data eksperimen terhadap pelbagai aplikasi. Keratan rentas bagi ^{nat}Ni(d, x) ^{61}Cu yang disyorkan oleh IAEA telah memberikan jangkaan yang lebih tinggi dalam eksperimen-eksperimen terbaru, dan penaikkan taraf telahpun dicadangkan. Sebahagian daripada radionuklid yang dilaporkan dalam kajian ini telah disiasat melalui laluan kajian mereka buat kali pertama, kedua atau ketiga.

ACKNOWLEDGEMENTS

All praises and profound gratitude are due to the Allah, the creator of heaven and earth, the initiator of knowledge for the life, health, wisdom and passion He bestowed on me to reach this level of education and write this final research qualification. I would forever be thankful and grateful for this special honour He bestowed on me.

My special gratitude and regards go to my “super” supervisor, Associate Prof. Dr Mayeen Uddin Khandaker, whose endless guide on and off the research field made me what I am today. His regular laboratory visits of his students, going around to every student desk, asking for students’ progress and problems would forever remain in my memory. Similarly, I must specifically mention his connections with other research groups which made it possible for my enrolment as a PhD research student at Nishina Centre of accelerator-based Science, RIKEN, Japan, without which this work would have never been possible.

I am highly indebted to my entire family members and friends in the following fashion: To my great and lovely parents Alh Usman Abubakar Alkali, Saratu Adamu and Asma’u Usman for their parental care, education and prayers; to all my brothers and sisters for their constant prayers and good wishes. Moreover, I would like to say a special thank you to my caring wife, Khadija, for the special dishes she made during the program, which always reminds me of my beautiful culture despite being about 14 flight hours away from my country. Her perseverance and endurance of my late homecoming as well as occasional unintentional transfer of PhD shocks on her are much now belatedly recognised and regretted.

This brings me to another point of my sincere appreciations to the entire members of the Nishina Centre of accelerator science research group, especially the team leader, Dr Hiromisu Haba as well as to other members of the group such as Dr Musashi Murakami and Dr K. Komori for their unquantifiable assistance during and after my visits to their

laboratories. The management of RIKEN is also at this moment acknowledged for making such policies that absorbed students.

I most also recognise here the very helpful and valuable knowledge I got from Dr N. Otsuka, the head of Nuclear data centre of the International Atomic Energy Agency (IAEA). His assistance in the literature data evaluations, fruitful discussions on uncertainties on cross sections as well as many other aspects during writing manuscripts for publication are much appreciated.

The entire radiation laboratory colleagues here at UM such as Asadussaman Khandoker, Hauwa Kulu, Farhad, Kolo Mathew, Michael O., Nor Baini, and Zaffan need to be mentioned and acknowledged. Their contributions in one way or the other were significant. Equally I want mention other names such as Lurwan Garba Gaya, Mustapha Bala Ruma and Muhammad Lawal Danrimi.

I would like to end my acknowledgement message with a sincere appreciation to the Umaru Musa Yar'adua University, Katsina, Nigeria as well as the Nigerian Government for award of the PhD study fellowship under the Tertiary Education Trust Fund (TETFund) scheme. This privilege would never be forgotten.

TABLE OF CONTENTS

LIST OF FIGURES

LIST OF TABLES

LIST OF SYMBOLS AND ABBREVIATIONS

(d, x)	:	Nuclear reaction with incident deuteron particle and emitted x particle
(α, x)	:	Nuclear reaction with incident alpha particle and emitted x particle
$\Delta\sigma$	:	Uncertainty in cross section
^{44m}Sc	:	Metastable state of scandium-44 radionuclide
^{52g}Mn	:	Ground state of magnesium-52 radionuclide
Al	:	Aluminium
ALICE	:	It is nuclear reaction code
AME	:	Atomic Mass Evaluation
AVF	:	Azimuthally Variable Cyclotron
B	:	Barrier
C	:	Counts
Co	:	Cobalt
Cu	:	Copper
D (or d)	:	Deuteron
E	:	Energy
EC	:	Electron Capture
EMPIRE	:	It is nuclear reaction code
ENSDF	:	Evaluated Nuclear Structure Data File
EOB	:	End of bombardment
EOI	:	End of Irradiation
E_{th}	:	Threshold energy
Ex	:	Experiment
E_{γ}	:	Gamma energy
FWHM	:	Full Wave at Half Maximum

Ga	:	Gallium
GM	:	Geiger Muller
GNASH	:	It is nuclear reaction code
Ho	:	Holmium
HPGe	:	Hyper Pure Germanium Detector
IT	:	Isomeric transition
I_γ	:	Gamma intensity (emission probability)
mb	:	Milli barn
MBq/C	:	Mega Becquerel per coulomb
MeV	:	Mega electron volt
Mn	:	Magnesium
n	:	Neutron
nA	:	Nano ampere
NaI	:	Sodium Iodide detector
^{nat}Cu	:	Natural copper
^{nat}Ho	:	Natural holmium
^{nat}Ni	:	Natural nickel
^{nat}Ti	:	Natural titanium
Ni	:	Nickel
NNDC	:	National Nuclear Data Centre, Brookhaven national laboratory
Norm	:	Normalized
Norm*	:	Normalized and multiplied with atomic weight of the element
Norm+	:	Normalized and summed
NuDat	:	Nuclear Data
p	:	Proton

PET	:	Positron Emission Tomography
R	:	Reaction rate
RF	:	Radio frequency
RI	:	Radioactive isotope
SA	:	Specific Activity
SCC	:	Super Conducting Cyclotron
SPECT	:	Single Photon Emission Computed Tomography
SRC	:	Superconducting Ring Cyclotron
SRIM	:	Stopping and Range of Ions in Matter
TALYS	:	It is nuclear reaction code
t_{coo}	:	Cooling time
TENDL	:	Talys Evaluated Nuclear Data Library
t_h	:	Thickness
t_{irr}	:	Irradiation time
Tm	:	Thulium
t_{mea}	:	Measurement time
TRIM	:	Transport of Ions in Matter
TTY	:	Thick target yield
uAh	:	Micro Ampere hour
x	:	Emitted particle
Y	:	Yield
Z	:	Atomic number
Zn	:	Zinc
α	:	Alpha particle
β	:	Beta particle

γ	:	Gamma ray
ε_γ	:	Gamma efficiency
Φ	:	Flux
λ	:	Decay constant
ρ	:	Atomic density
σ	:	Cross section

LIST OF APPENDICES

CHAPTER 1: INTRODUCTION

1.1 Introduction

Nuclear Technology proved to be one of the most important developments of the 20th century. The multitude applications of nuclear science in many fields of human endeavour we are now witnessing were initially founded by the works of the pioneers in this field. In particular, the work of Marie Curie and Pierre Curie formed a spectacular foundation to the knowledge of radioactive materials. With the belief of Marie Curie that a pitchblende, a material she was working on, contained a more active element than uranium, she succeeded in 1898 to isolate two previously unknown elements; polonium (after her country of origin, Poland) and radium (named after its high activity). In 1911, the first notable practical use of radioactive isotopes was tested by, at that time, a young Hungarian student G. de Hevesy, who was working with naturally occurring radionuclides in Manchester University. He used the radioisotopes to confirm the suspicion he had that the meals they were served at the boarding school were from a leftover of the preceded day.

Another milestone in the history of nuclear physics was recorded in 1919 by Ernest Rutherford when he directed the alpha particle emission of a polonium sample on to a nitrogen gas. The result he obtained shows that proton was emitted from the disintegrated nitrogen. Rutherford, however, realised later that some more energetic particles with energy more than the energy of the natural radiation are necessary to effectively disintegrate matter and thus the new demand for higher fluxes of energy so that man-controlled nuclear reactions can be achieved. For some years there was no progress, until in 1928 when independent works by Gurney and Gamov predicted tunnelling, and from the development, it was understood that a 500 keV energy could just be sufficient to split an atom (Bryant, 1994). In fact, it was documented that a year

before this prediction, Rutherford delivered a speech (at the annual address to royal society, 1927) where he publicly expressed the need for the scientific community to accelerate charged particle with energy greater than the natural alpha-decay so that nuclides of higher energy than nitrogen could be disintegrated. He then challenged the participants to fulfil this, his long-time desire, of the rich supply of higher energy projectile particles other than the natural low energy emission (Steere, 2005). With this prediction, Rutherford thus immediately encouraged Cockcroft and Walton to start designing a particle accelerator capable of delivering 500 keV energy. In 1932, only four years after Rutherford's suggestions, these scientists were able to produce the particle accelerator which they used to split the Li atom by 400 keV energy of proton (Cockcroft & Walton, 1932a; Cockcroft & Walton, 1932b) and consequently earned them the noble price of 1951 (Bryant, 1994). However, their accelerator has energy limitation as it was in few keV energy and the further quest for higher energy continue. In almost the same period (1929), E. O Lawrence, a young associate professor and non-German speaking at the University of California, was searching through some German publications, when he suddenly came across the work of Wideroe (Steere, 2005), a reported work in German on the same acceleration of particle issues. Although Lawrence could not understand the German language, the figure he saw was enough to motivate him. Inspired by such a figure, he successfully constructed the first cyclotron and further works with his graduate students for its enhancement (Lawrence & Cooksey, 1936; Lawrence & Livingston, 1932; Sloan & Lawrence, 1931), and the period thus becomes the turning point of radioisotope production (Ruth, 2003). Lawrence's contributions were recognised as he later received the Nobel Prize in 1939.

Due to the uncovering of the electromagnetic field, as the core principles for sustaining accelerations of particles around 1930, this period was quite a remarkable one in the history of accelerators.

Although applications of radioisotope started in the 1920s, the practically limited available naturally occurring radioactive isotopes at that time suddenly hindered the early development of this field to a wider scope in the period. The practical, full-scale potentials of radioisotope applications only began to be realised when artificial radioisotopes could be produced.

1.2 Common Routes for Radionuclides Productions

While in general term, nuclear reactions can occur naturally through radioactivity, a control nuclear reaction requires certain procedures for its occurrence and maintenance. To produce specific radioactive products of interest, several considerations are necessary ranging from appropriate target selection to the use of specific energy of the bombarding particle. In principle, to effectively produce artificial radionuclides, the colliding of a projectile (the bombarding particle) onto a target is necessary. There are three major techniques for the production of (controlled) radionuclides for hospital usage:

1.2.1 Nuclear Reactor

In nuclear reactors, the initial reaction of a neutron with ^{235}U pave the way to produce more particles such as neutrons, protons, deuterons, alpha particles, and so on. These produced particles can be used for further nuclear reactions to produce the desired radionuclides. Description of reactor-produced radionuclides is out of the scope of this thesis.

1.2.2 Generators

These are useful alternatives to the use of the cyclotron or reactor sources. A (radioactive) generator is a long half-life radionuclide called 'mother" which decays to a short-half-life radionuclide called 'daughter' that can be used for imaging procedures in hospitals. A nuclear reactor is typically utilised to produce this long-lived radionuclide and then shipped in a 'generator'. When needed, the 'daughter' radionuclide is combined with radiopharmaceuticals for designed application. Replacement of generators in hospitals is usually monthly, depending on the half-life of the 'mother' radionuclide. The very popular radionuclide ^{99m}Tc ($T_{1/2}$= 6.02 h) (daughter) is the most prominent radionuclide in use in the hospitals and is derived from the long-lived ^{99}Mo ($T_{1/2}$= 66 h) serving as the 'mother'. Statistics show that more than 80% of all hospital diagnostic procedures (about 36,000 daily medical procedures in the United States) are performed using ^{99m}Tc (Srivastava, 1996). The 'mother' ^{99}Mo is produced in a reactor. This system is called '^{99}Tc generator'. Studies on 'daughter' – 'mother' generator system are well established, with some studies nowadays focusing on other procedures such as electrochemical separation technique, which are useful especially when low specific activity parents are used (Chakravarty et al., 2012). In recent years, several studies have investigated the direct cyclotron production of ^{99m}Tc (Lagunas-Solar et al., 1991; Takacs et al., 2015) via proton bombardments and much more radionuclides (McCarthy et al., 1997; Moustapha et al., 2006).

1.2.3 Cyclotron

The use of the cyclotron is by far the most efficient production method for radioisotopes. A brief history of cyclotron was already presented in the previous section of this chapter. There are many studies on production of radioisotopes using cyclotrons, and a lot more are ongoing. The present thesis is a product of experimental

measurements from a cyclotron as well. Thus, most part of chapter two is devoted to the general description of the main procedures and targets involved in radioisotope productions and cross sections measurements. Some clear advantages of accelerator-produced radionuclides are (Ruth, 2009; Schmor, 2011);

- Targets and products radionuclides are different chemical elements. This benefit is connected to the following other advantages;
- A suitable physical or chemical separation technique is possible due to the variation of target and product.
- Radioactive impurities can be minimised by proper selection of specific irradiation energy window.
- As the target and products are different elements, a high specific activity (SA) preparation is possible.

More so, regarding widely usage and acceptability, the following three major reasons have made the accelerator-produced radionuclides to excel over those from its counterpart, the nuclear reactor;

- Radionuclides produced from accelerator have more favourable decay characteristics (half-life, emitted particles, gamma rays, and so on).
- Reactor only produces radionuclides with, in general term, low specific activities (SA).
- Access to a reactor is usually very limited, owing to political reasons. This has earlier been predicted (IAEA, 2008) and has even led to several studies on direct cyclotron production of ^{99m}Tc.

As this thesis is on radioisotopes production in a cyclotron, it will, therefore, dwell heavenly on this aspect and related procedures throughout the thesis.

1.3 Author's Experience at RIKEN Research Centre

During the author's candidature, he was privileged to have been enrolled as a research student at Nishina Centre for Accelerator based-science, one of the very active research laboratories of RIKEN research centre, Wako, Saitama, Japan. RIKEN is one of the world leading scientific research centres, with most of their facilities up to date and capable of competing with sister research peers. Recently, one of their contributions in scientific world has been recognised by IUPAC through recognition of their discovery of element 113 (named recently as nihonium, Nh) (Riken, 2017).

As a registered research student, the author had the opportunity to visit the centre on three different occasions, each time with different set of experiments. In addition to the experiments presented in this thesis, the author also participated in some other experiments, beyond the scope of this thesis, such as deuteron bombardment of a stack of Ti, Ce and Tb in one occasion and Ti, Sc and Al foils in another.

The experimental exposure provided the author with some volume of practical experience regarding target preparations, irradiation and measurements of activities as well as very invaluable teamwork experience. Though the author's work was done using the AVF cyclotron of the centre, the author was also opportune to have visited most of the accelerators of the centre, including their latest and recently completed Superconducting Ring Cyclotron(SRC). Using the SRC, now RIKEN can accelerate the heavy ions, up to uranium.

1.4 Background of the Study

Studies on radioisotope production via nuclear reactor and proton only cyclotrons for medical applications are vast in the literature, and their practical applications in PET are well established. Although deuteron production route has recently been attracting large

literature, its practical applications are not yet common in the hospitals owing to other problems. The radioactive isotope productions via alpha bombardments are yet the less investigated production channel and are still work in progress. Exploration of this route can play a major role in nuclear data analysis.

To optimise radionuclides productions, sufficient nuclear data from all production routes are crucial. It thus may involve a proper selection of energy range for the projectile particle so as to maximise the product (radionuclides) production yield and also minimise radioactive impurities (Qaim et al., 2002). In practice, while chemical separation is an ideal way of removing non-isotopic impurities, the suppression of the isotopic impurities is mainly achieved by using targets of enriched isotopes or through careful energy selection of the incident bombarding particle. The selection of appropriate energy for particular radioisotope production is possible in cyclotrons with large energy interval. The adverse effects of radioactive impurities are; first, the additional radiation dose to patients and secondly, it affects the imaging quality through its effect on a 'line spread function' (Qaim et al., 2002). These disadvantages, therefore, jeopardise the importance of the radionuclide in question and thus necessitate the need for other production routes of the desired radionuclide instead of the conventional method.

The cyclotrons produced radionuclides are very efficient in diagnostic and therapeutic studies via some popular techniques such as positron emission tomography (PET) and Single Photon emission tomography (SPECT). Over the last few decades, there has been a sharp increase in the number of cyclotrons, which further enhanced the developments of these modalities. The PET technique as an example has now become a well-developed imaging modality. The PET is performed through labelling radiopharmaceuticals with short-lived positron emitting radionuclides such as ^{15}O (T1/2

= 2 min), ^{11}C (T1/2 = 20.4 min), ^{18}F ($T_{1/2}$ = 110 min), etc. However, the short half-life nature of these radionuclides, except ^{18}F, necessitate the need for an on-site cyclotron (Aslam & Qaim, 2014) or a (radionuclide) generator system, depending on the radionuclide of interest. Furthermore, despite the large success of these radionuclides, the use of these short half-lives radionuclides in PET is sometimes associated with other problems and thus limit the prospects in the PET technique. More precisely, when studies of slow biological processes or labelling of peptides and proteins as in the case of brain tumour studies, the short half-lived positron emitting radionuclides are quite deficient (Qaim, 2004). The continuous expansions of PET procedures demand that more versatile radionuclides be used for diverse applications. The longer-lived radionuclides, also called non-standard positron emitters, are required for some more successful investigations in slow metabolic procedures (Amjed et al., 2016). The longer lived positron emitters could be useful when labelling of compounds of organic origin such as halogens, to prepare metallic complexes or even in the pharmacokinetics (Qaim, 2004). On the other hand, these radionuclides can also serve as a positron emitting analogue label for quantification of the radiopharmaceuticals in SPECT and are also very useful as therapeutic radionuclides (Qaim, 2004).

A recent study strictly emphasises on the need for the developments of new positron emitters for the new challenges (Qaim, 2004). The present thesis, therefore, considered these non-standard radionuclides (radionuclides with half-lives ranging from few hours to several days) as future radionuclides and intend to either validate the available literature (where available) or report newly observed radionuclides in the studied production routes.

1.5 Objectives of the Study

To effectively study some the non-standard radionuclides for medical applications, the following objectives were set in this work:

- To measure the excitation functions of $^{nat}Ni(d,x)^{x}Y$ nuclear reactions in the frame of 24 MeV deuteron beam
- To study the cross sections and thick target yields of scandium radionuclides from 50.4 MeV alpha-induced reactions on $^{nat.}Ti$
- To measure the excitation functions of $^{nat}Cu(\alpha,x)^{66,67}Ga,^{65}Zn,^{57,58,60}Co$
- To investigate the excitation functions of the short-lived radionuclides via alpha production route on holmium foils.

1.6 Scope of the Study

The present thesis is designed as a purely experimental study, with the output of Talys code used for cross-checking the agreement between the experimental work and the theoretical predictions. Furthermore, the work is designed to use deuteron and alpha particles as the main ion beam projectiles of interest to produce several radioisotopes from selected targets mention in the objectives. Specifically, the use of proton was not considered because of the vast literature on the subject. Similarly, the work reports the results obtained from Ni, Cu, Ti and Ho but not all the metals used in the experiments. The use of natural targets plays important roles for different reasons. One of such advantage is that it helps to estimate the level of such impurities since when enriched isotopes are used the product radionuclides may still be contaminated due to a small proportion of the natural isotopic composition. The theoretical Talys nuclear reaction code, a powerful prediction code, was used via TENDL-library for cross checking the agreement between theoretical and the experimental results of this thesis.

1.7 Outline of the Thesis

This section gives a brief overview of the whole thesis based on the sequence of chapter presentation style of the thesis. The chapter one of this thesis is designed such that a clear picture of the entire study is made. The chapter, therefore, presents a brief introduction to the history of radioisotope production, the major methods for the practical radioisotopes production for medical applications and challenges encountered during the productions. The chapter also describes background or solid foundations leading to the study, the scope and objectives of the thesis.

In chapter two, a general literature review related to the objectives of the thesis is presented. The review focuses on the definition of some basic radionuclide production terms, the cyclotrons and their major types, and the ion sources in cyclotrons. The chapter also examined the previous literature on the use of nickel, titanium and holmium targets about the objectives of this thesis. The review of some specific applications relevant to each studied radionuclide has not been provided in chapter two but in the relevant chapters of which the radionuclide is mentioned. This is in accordance with the format of the thesis.

The method, results and a short conclusion of the first objective of the present thesis are presented in chapter three. Using 24 MeV deuteron as the projectile beam on natural nickel, the excitation functions of $^{nat}Ni(d,x)^{55\text{-}58g+m,60g+m}Co$, ^{57}Ni, $^{52g,54}Mn$ radionuclides have been studied and presented in the chapter. The thick target yields of some of the radionuclides have also been calculated. The uncertainties in cross sections were evaluated in an elaborate way, based on the experimental conditions of the present study.

Chapter four presents the methodology and results obtained from bombarded titanium target. In this chapter, elaborate discussions of the tabulated values of cross sections and plotted excitation functions of some scandium and chromium radionuclides have been reported. The excitation function of ^{48}V was also presented. Details of gamma energy separation of two or more interfering gamma lines (having same or very close gamma energies) are also provided in this chapter. The thick target yields of the studied radionuclides have been calculated, plotted along with available literature where available and presented in this chapter with discussions following the results. A short conclusion following the results of the chapter was also provided at the end of the chapter.

In chapter five, results of gamma spectra from copper, a metal that also served as energy degrader, were evaluated. The excitation functions of $^{nat}Cu(\alpha,x)^{66,67}Ga,^{65}Zn,^{57,58,60}Co$ nuclear reactions in the alpha beam have been reported.

Chapter six is the last experimental chapter of this thesis. The chapter presents relevant experimental procedures on the measured cross sections of thulium radionuclides. The excitation functions of the studied thulium radionuclides of this work, obtained from the bombardment of holmium foils, as well as the experimental literature data,are presented in this chapter. The TENDL-2015 library was used for comparing the current result to the theoretical predictions of TALYS nuclear reactions code.

The final chapter, chapter seven, presents the major summaries of the various results and conclusions of the previous chapters before it of this thesis, based on the initial set objectives. The limitations of the present study are enumerated under this chapter. The

chapter also presents, in a more direct way, the main contributions of the study to the research area. The final item under this chapter presents some recommendations for further research.

It is acknowledged that, due to the presentation and thesis style adopted in this thesis (article style), based on the University of Malaya guide (format), some information may be found unavoidably repeated in some sections of the thesis.

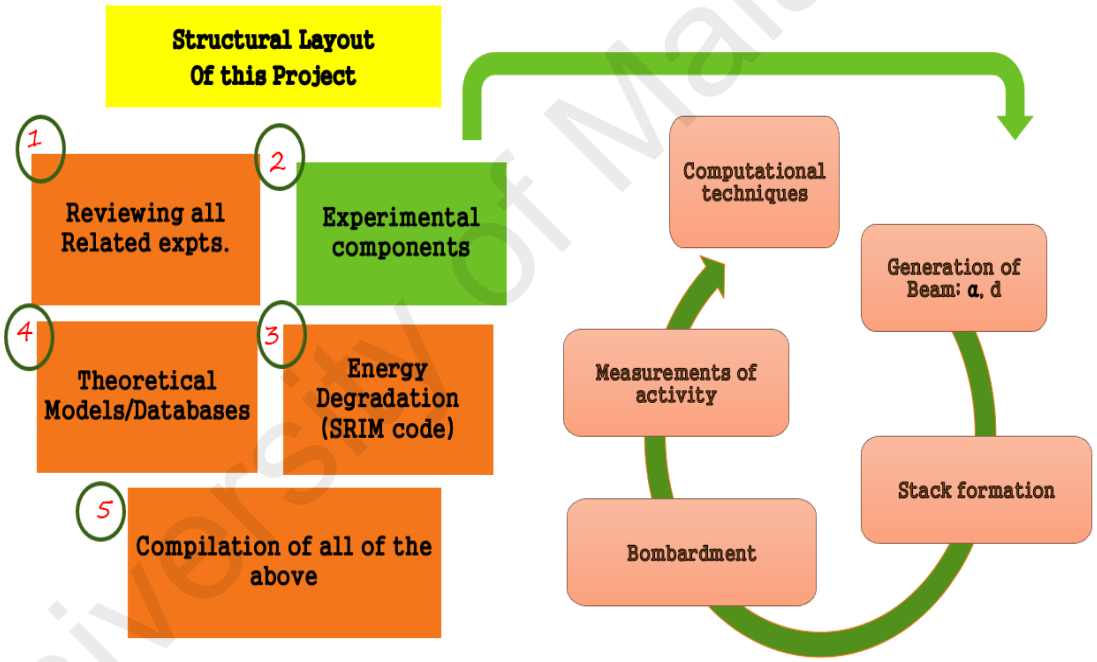

Figure 1.1: Schematic Summary of the Major Components of this Thesis.

CHAPTER 2: LITERATURE REVIEW

2.1 Introduction

This chapter introduces the concepts of medical applications of radionuclides and their production techniques. It also provides basic definitions of some terminologies relevant to radioisotope productions as well as introducing the general concept and basic developmental stages of nuclear accelerators, especially the cyclotrons, for the production of medical isotopes and other applications. Some little information on radiopharmaceuticals has also been provided. The chapter ends with some specific reviews on the main target metals used for the bombardments in this study, where in each case, a tabular summary of the comprehensive review of the previous works has been provided.

In the production of radioisotopes for medical applications by metallic bombardments, the light-charged protons are currently the most efficient and widely used tools. The production machines are readily available in many hospitals of developed and developing countries and research laboratories all over the world. Proton only cyclotrons (and sometime deuteron also) are frequently used for Positron Emission Tomography (PET) or other related techniques in the medical field (Qaim et al., 2016). However, sometimes, using other charged particles such as deuteron or alpha particles can give a tangible result or even better, depending on the requirement or problem at hand.

A recent review (Qaim et al., 2016) on alpha-induced nuclear reactions has quantified several applications of alpha-induced nuclear reaction in nuclear medicine, nuclear data, material science, and so on. The applications of alpha-induced reactions are due to the basic properties of alpha particles in their ability to scatter, ionise or activate a matter they encounter. In particular, the accelerators operating at medium

energy alpha particles (below 40 MeV) are of great importance in nuclear research, in both the investigative- and application-oriented senses (Uddin & Scholten, 2016).

Commercial cyclotrons for alpha bombardments have not yet been available for radioisotope productions due to other reasons beyond the scope of this chapter. Despite this, more research, especially in the recent years, are developing more interest in the use of the deuteron and alpha particles for radioisotope production. These researches could likely pave the way for commercial deuteron only and alpha only cyclotrons in the near future. In this chapter, the author has reviewed previous works on the irradiation of nickel, titanium and holmium metallic targets in relation to the employed production routes of the present study (deuteron and alpha-particles beams). The summaries of the reviewed information have been presented in several Tables of this chapter.

2.2 Medical Applications of Accelerator-Produced Radionuclides

The broad applications of radionuclides cannot be confined to a narrow area as their applications are found in many fields such as medical applications, scientific research, agriculture, oceanography, mineral exploration, etc. Radionuclides or radioisotopes are nowadays crucial diagnostic and therapeutic agents in many hospitals.

The use of radionuclides as tracers for the assessment of functions of certain body parts is very much in practice. These radionuclides can usually be injected, embedded, ingested or induced by activation in the body (IAEA, 2008; Ruth, 2009; Schmor, 2011). On the other hand, therapeutic applications are also standard practice in many tumour treatment centres. There are even more expectations of much more radionuclides for therapeutic applications (Schmor, 2011).

A review on tracing of tissues and therapeutic potentials of most of the studied radionuclides have been presented in various chapters of this thesis relevant to the investigated radionuclides.

2.2.1 Radiopharmaceuticals

In nuclear medicine, radionuclides are combined with other compounds to form radiopharmaceuticals which can localise in body organs (Schmor, 2011). They differ from usual pharmaceuticals in that they are administered in a, relatively, very small concentration such that they do not elicit any pharmaceutical response (Schmor, 2011).

The following are properties of an ideal radiopharmaceutical;

i. Short half-life,
ii. Rapid biological distribution
iii. Absence of particulate emissions
iv. Target specifications
v. Photon energy range of 150 to 250 keV

Each of the above properties has some specific advantages. As an example, the use of a short half-lived radiopharmaceutical to a patient is to transfer the least possible radiation dose to the patient. The longer the half-life of a radionuclide to be used with a carrier, the higher or the longer (radiation exposure time) the radiation dose to the patient.

2.3 Circular Accelerators

The circular form of the accelerator is, in contrast to the linear accelerator, the type of machine or accelerator in which charged–particles or ions are constrained to flow in closed quasi-circular path or orbit through the action of the magnetic field. All circular accelerators possess some characteristics in their design such as having a vertical

magnetic field which ensures the bending of the particle trajectories and one or more gaps coupled to inductively isolated cavities for the accelerations of particles. Resonance circular accelerators are also characterised by synchronisation between oscillating acceleration fields and particles revolution frequency.

One of the major advantages of circular resonance accelerators over resonance frequency (RF) LINACS is the particle recirculation. The particles usually pass through the same acceleration gap for a significant period (about 10^2 to 10^8 times). This gives the particle very high energy in a relatively low voltage. The ability to attain high energy with smaller length in circular accelerators also serve as another advantage over its linear counterpart.

There are many different designs of circular resonance accelerators now in the world, with some having certain advantages over others while others exist only to follow the historical development. With the exceptions of some designs, we can broadly classify circular resonance accelerators into either cyclotrons or synchrotrons. These exceptions are the Microtron, a technologically like LINAC, and synchrocyclotrons.

2.4 Cyclotrons: Design and Classifications

This class of circular accelerators is characterised with a constant magnitude of the magnetic field and constant RF frequency. The design of cyclotrons is such that they generate beam micro-pulses in a continuous manner. The amount of beam energy is mainly limited by relativistic effects, which destroys the synchronisation between particle orbits and rf fields. Thus, cyclotrons are primarily useful for ion accelerations. They have large area magnetic fields which confine ions from zero magnetic fields to certain level of output energy.

2.4.1 Uniform Field Cyclotron

In nuclear physics research, the uniform field cyclotron has a historical position. They are the first categories of cyclotrons or accelerators used in the generation of multi-MeV particle beams. The vertical field is azimuthally uniform. Similarly, the field magnitude is almost constant in radial direction, with small positive field index which allows vertical focusing. The resonance accelerations of this class of cyclotron are dependent on the constancy of the non-relativistic gyrofrequency. This category does not have synchronous phase. Uniform-field cyclotrons have an energy range of 15-20 MeV for light ions beams, determined by a relativistic mass increase as well as a decrease in magnetic field strength with radius.

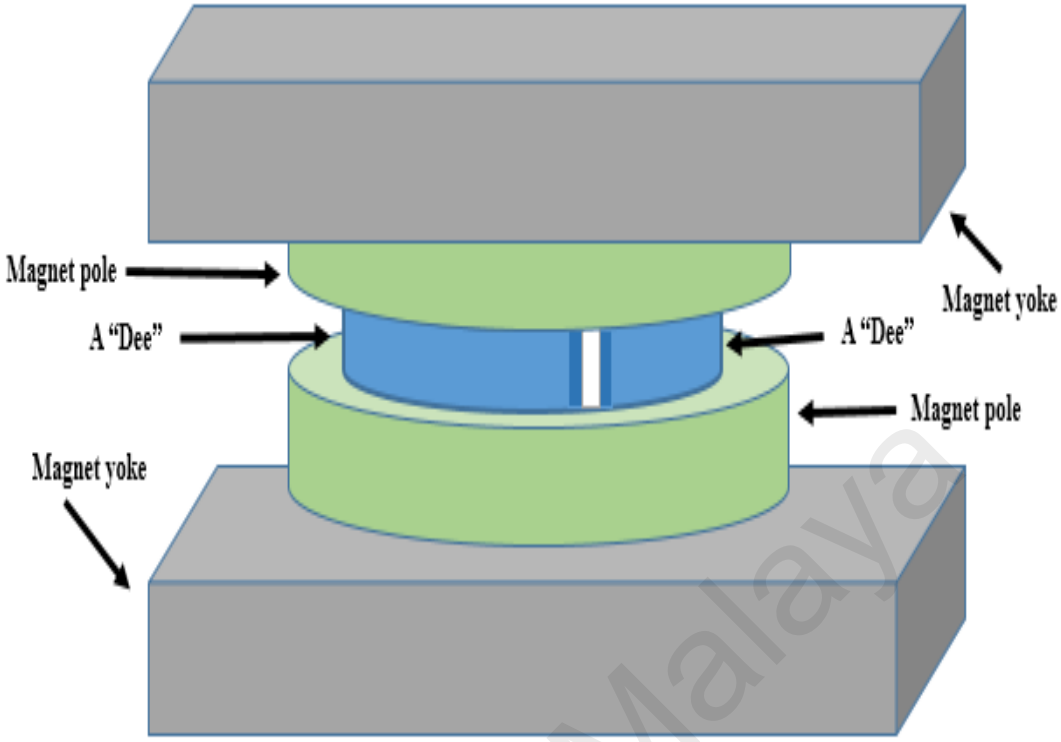

Figure 2.1: The layout of the uniform-field cyclotron's beam acceleration region

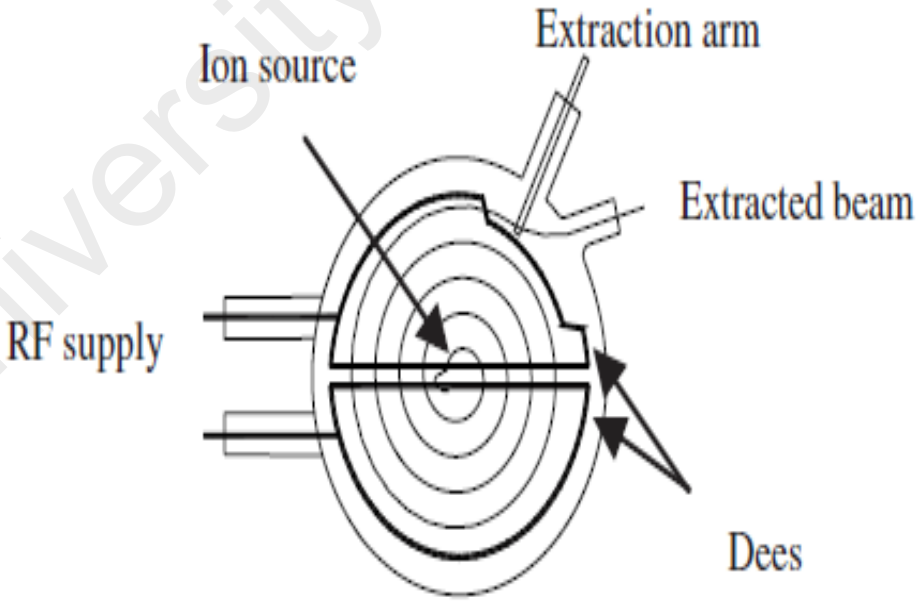

Figure 2.2: Basic principles of the uniform-field Cyclotrons (Credit: Ruth, 2003)

2.4.2 Azimuthally-Variable-Field (AVF) Cyclotrons.

Sequel to the success achieved in the uniform-field cyclotron, the AVF cyclotron serve as a major improvement to the former through improvement in interior designs. The confining magnetic field has been improved through attachments of wedge-shaped inserts at periodic azimuthal positions of the poles of the magnet. It is possible to tolerate an average negative-field index so that the bending field is proportional to the cyclotron radius. Vertical focusing is also enhanced through the horizontal field component. Similarly, in the AVF cyclotrons, the magnetic field variation balances the relativistic mass increase followed by an achieved constant revolution frequency. These important properties are only achieved by careful selection of focusing elements and field index variation and such AVF cyclotrons with properties are called isochronous AV cyclotrons. AVF cyclotrons offer higher intensity beams through the above explained stronger vertical focusing. The AVF cyclotrons have thus take the place of the former uniformed-field ones even for low energy applications.

2.4.3 Separated Sector Ring Cyclotrons.

A typical limitation of isochronous cyclotron during accelerations of protons (ions) is the focusing limit of the magnet. The spiral angle, at a certain stage, cannot be further increased, and the only way for increasing the axial focusing is by increasing the flutter, F (Heikkinen, 1994). To achieve this, the valleys must be decreased. The separated sector cyclotrons are a special class of AVF cyclotrons (or isochronous cyclotrons). The variations in the azimuthal field result from, in contrast to AVF cyclotrons, the splitting of the bending magnet into several sectors. The magnet of a separated sector cyclotron consists of only hill sectors and no iron in the valleys. This means practically no magnetic field in the valleys. There is also the separate exciting wound of coils around each of the sectors (Craddock & Symon, 2008). This arrangement or design is not compatible with low-energy injection, thus

requiring a pre-accelerator (which can be a smaller cyclotron), leading to an initial large orbit radius; thus, the term ring cyclotron. This design makes the separated sector cyclotrons to offer two basic advantages:

- Separation of the functions through the modular magnet construction – this allows much freedom in designing how the diagnostic equipment, injection and ejection components and RF accelerating cavities are to be mounted in the virtually field-free space between sectors.
- The pole gap can be smaller thereby reducing the power requirements of the used magnet and increasing the flutter, F, so that the F is no longer restricted to ≈0 (Craddock & Symon, 2008).

Though the design does not give the possibility of a particle to be accelerated from low energy, this feature may also be of benefit in some cases, especially as beam of better coherence (lower emittance) are produced when an independent accelerator is used in low energy acceleration. Some of the separated sector cyclotrons in the world include the TRIUMF K520 in Vancouver Canada (first beam:1974), the GANIL K380 cyclotron in France (first beam:1982), the RIKEN K540 in Japan (first beam:1986), and so on. The number of the sectors varies from 4 to 6.

2.4.4 Spiral Cyclotron

As the name implies, the spiral cyclotrons have pole inserts with spiral boundaries. Although spiral shaping is also used in the standard separated-sector and AVF machines, in a spiral cyclotron, the ion orbits have an inclination at the boundaries of the high-field regions. The edge focusing helped in the enhancement of the vertical confinement. Thus, the overall effects of the edge focusing and defocusing compound to further vertical confinement.

2.4.5 Superconducting Cyclotrons (SCC)

Most of the existing cyclotrons operate using conventional magnets (room temperature magnets) in which, due to iron saturation, 2 T is the maximum magnetic field. Beyond this limit, superconducting field coils must be used (Heikkinen, 1994). On the other hand, SCC can give more than 6 T magnetic field between the hills (e.g., MSU K1200 SCC has 6.2 T) (Heikkinen, 1994). With the superconductivity (high magnetic field), it is possible to construct cyclotrons with small magnets that can deliver relatively high energy. Superconducting coils supply the magnetisation force which consumes little power. These cyclotrons can deliver high energy particles using small magnets and has a low operation cost as well, an important feature of SCC. Structurally, the superconducting cyclotrons are compact machines and are operated at high fields, much above the iron poles saturation level. This condition allows all magnetic dipoles in the poles to be aligned, leading to accurate net field prediction.

To give some examples of in use SCC, the following cyclotrons can be are cited: The Harper Hospital K100: a very compact SSC, has 30 cm extraction radius, 50 MeV focusing limits, 100 MeV bending limits, used for neutron therapy, and is comparably light (weighs only 25 US tons), which makes it easy for rotating it around a patient during treatment (Heikkinen, 1994). The SCC example can also be seen in RIKEN research centre as one of their latest installations.

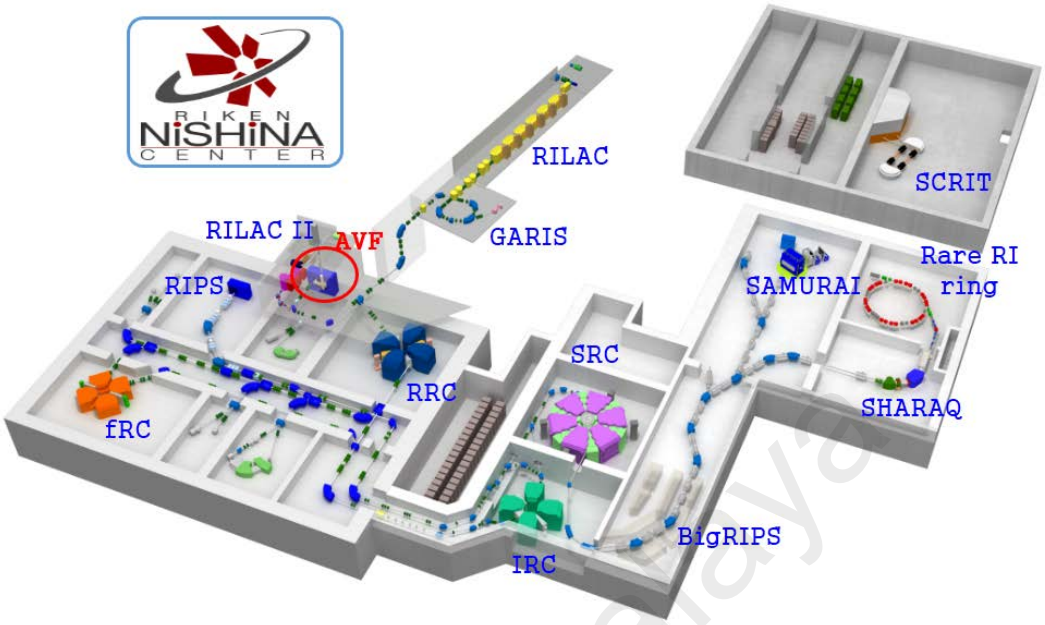

Figure 2.3: The topology of the RIKEN accelerators.

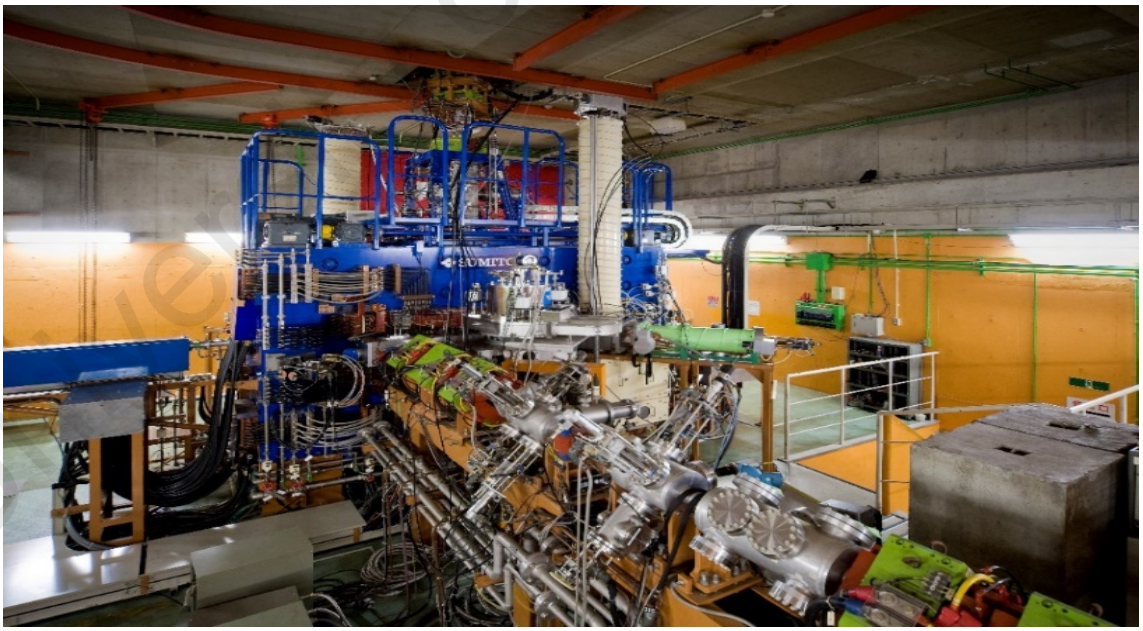

Figure 2.4: The AVF cyclotron of RIKEN

2.5 Other Types of Circular Cyclotron

2.5.1 Synchrocyclotron

Synchrocyclotron represents, on the history line of the accelerator, a stage of the conceived idea of expanding the cyclotron observed energy limit. This class of circular machines are thus considered as a preliminary stage of the more advanced stage, the synchrotron. Just as in uniform-field class, this category also has similar geometry to uniform-field class and constant magnetic field, except that it also has a variable RF frequency which during the relativistic regime, helps to maintain particle synchronisation. In other words, the focusing limits observed in isochronous cyclotrons can be overcome in synchrocyclotron by frequency modulation (FM), in which the frequency is decreased as the particle mass increases (Heikkinen, 1994). Furthermore, synchrocyclotron present, in comparison to a conventional cyclotron, a much lower time-averaged flux. Despite these advantages at higher energies, however, the ability of AVF cyclotron to give a continuous flux at sub-GeV energy range (lower energies below 1 GeV) make it supervened upon the synchrocyclotron.

2.5.2 Synchrotron

These are the modern circular accelerators and are designed such that both RF frequency and magnetic field can be varied. This property helps to sustain a synchronous particle in the machine at a constant orbit radius, an important feature of this class. The significance of this constant-radius property is that the feature helps in bending and focusing fields over a small ring-shaped volume, thus minimising the cost of the larger magnet while also allowing the possibility of generating high energy up to hundreds of GeV ion energy, through the construction of larger-diameter machines. This much higher ion energy is usually achievable except due to the cost of the building of the machines and availability of site for the construction. Synchrotrons have typical 15 – 60 Hz range of cycle frequency. Synchrotrons are playing very important roles in

particle physics researches and both ions, and charged particles can be accelerated, although there is a limitation in energy in the electron synchrotron due to synchrotron radiation.

2.6 The Ion Sources and Beam Extraction System

The ions for accelerations in cyclotrons can be sourced either within the cyclotron (internally ion source) where the ions are generated from the central region of the cyclotron or from its outside (external ion source) where the ions are injected into the core region of the cyclotron. There are advantages and disadvantages to each type of ion source. There are several available ion sources, each having their peculiar operating properties. Regardless of the source being internal or external, the ions used in the cyclotrons can be either positive or negative. The procedure for the extraction of either a positive or negative ion from a source to the central part of a cyclotron is partly dependent on the characteristics of the ion source. There are also studies on the improvement of the extraction system in many accelerators, one of such study was also performed at RIKEN research centre (Kohara et al., 2004) in which a single-turn extraction was found to be easily achieved via Flattop acceleration technique.

2.6.1 The Positive Ion source

The cyclotrons using positive ions source can have the activation of targets either by internal targets (targets inside the cyclotrons) or external targets (outside the cyclotrons) through the external beam line. Both methods have the disadvantage of activating the cyclotron components. Moreover, a considerable beam loss along the trajectory is also observed when the beam is extracted to external targets, and can consequently lead to total failure. In this case, the use of internal targets help to avoid this energy loss via beam extraction but with high unavoidable residual activation of the components of the cyclotron (Schmor, 2011). A positive ion accelerating cyclotron is compact, reliable,

versatile and energy–efficient, designed usually to accelerate some range of light ions for radionuclides production.

2.6.2 The Negative Ion Source

Most of the modern cyclotrons use negative ion source. The negative ion accelerating cyclotron can have much higher extracted beam intensities and thus high extraction efficiency.

Electrons, in this case, are generated or stripped from the ion by allowing the beam to traverse a thin stripping foil, and the now-positive ion trajectory is altered to exit the cyclotron. Beam extracted through this means are of usually high quality and have to be further enlarged to meet the target's energy density limit. The presence of efficient vacuum conditions is however necessary in his case for the cyclotron to avoid activation of components. The cyclotrons with internal targets are the most cost-effective machines, but this solution, however, introduces a gas source and also limit the maximum achievable current of the cyclotron (Schmor, 2011). This problem can be overcome and thus accelerate larger current with less components activation when the cyclotron uses external ion source coupled with greater complicity in the design.

2.7 Cyclotron Targets and Target Holders

Production of specific radioisotopes requires proper selection of targets which would be irradiated with a beam of the desired projectile. These targets are placed in the path of the accelerated beam. In the fast, several cyclotrons use inbuilt target. However, there were some obvious shortcomings associated with using inbuilt targets. Most of the current cyclotrons use external targets. Accelerator targets can be in the form of solids, liquid or gas. The targets are mostly placed in a targets holder or container which are usually separated from accelerator vacuum by a thin window (Schmor, 2011). For the improvement of yield and reduction of contaminants in commercial production of

specific radionuclides, enriched forms of elements are used. However, the costs of high purity enriched isotopes are very high and play roles in the selection of radionuclides of interest and the corresponding production pathway. The targets are made such that it is possible to quickly remove and transfer them to the hot cell for further action. On the other hand, the designed thing window is very critical for optimised radionuclide production and must thus be able to withstand pressure difference and beam energy loss parameters (like thermal conductivity, Melting temperature, activation, chemical reactivity and tensile strength) (Schmor, 2011).

2.8 Medical Versus Research Cyclotrons

Since the Lawrence and Livingston's invention of the first cyclotron 1930 (Heikkinen, 1994; Schmor, 2011), many cyclotrons have been completed and several more under construction. In 1941, the installation of the first dedicated cyclotron to medical applications was made in Washington University at St Louis. The cyclotron was used in the production of radionuclides of arsenic, iron, sulphur and phosphorus (IAEA, 2009a). Since that period, there has been a rapid development of this area, especially around the 1980s. Apart from the sourcing medical isotopes from the nuclear reactor which has been a much popular way, recently both cyclotron research centres and dedicated cyclotrons are good sources of these radionuclides and often supplied to hospitals. Commercial production of radionuclides for medical applications is even more developed in recent years, with several compact cyclotron designs available in hospitals (Schmor, 2011) which only occupy a small space. Some research centres readily provide radionuclides to hospitals. The RIKEN research centre, Japan (Goto, 1989; Kohara et al., 2004; Toprek et al., 1999; Vorozhtsov et al., 2008; Yano, 2007) is a well-known centre which also provides radionuclides to their clients, among many other centres in America, Canada, and a large part of Europe, etc. There are several reviews on cyclotrons usage in medical applications, where details of the produced

radionuclides, their specific applications and the class of the cyclotron involved for such production are given (Milton & Triumf, 1995; Papash & Alenitsky, 2008; Qaim, 2004; Qaim et al., 2002; Schmor, 2011).

2.9 Radionuclides Production: Principles and Theory

The principles in radionuclides production show it is a true alchemy, in that atom of one element is converted into another. The main feature in the conversion is through alteration of the nucleons (proton and or neutrons) of the target atom. If the reaction is such that a neutron (reactor is the main source of the neutron) is added to the target and without emission of particles, then the produced nuclide would have the same chemical properties as of the target atom or nuclide. On the other hand, when charged particles (proton, deuteron, alpha, and so on) are used for the target bombardment, the produced nuclide is usually an entirely different element. Different kinds of nuclear reactions are produced when a charged particle bombards a target nucleus and each of those reactions depends on certain parameters such as type and energy of the projectile (bombarding) particle. There are a number of online tools such as Qtool system (Qtool, 2011) which help to give complete reactions products and threshold energy of the reaction when the target and energy of the projectile are completely specified. Under this section some important properties and components of radionuclide productions are discussed;

2.9.1 Nuclear Reactions and Kinematics

There are several factors involved for certain reaction product to be produced when one projectile particle bombards a target. Two potential barriers a charged projectile particle should overcome are first, the electrostatic repulsion between its self (positively charged) and the positively charged nucleus (Coulomb barrier) and secondly, the Q-value, which entirely depends on whether the reaction is endothermic or exothermic. Nuclear reaction from a classical point of view, between a nucleus and a charged

particle, can never occur if the centre-of-mass energy of the two colliding objects is less than the Coulomb barrier. Thus, to produce radionuclides in cyclotrons, this means that the bombarding charged particle should possess an energy larger than the electrostatic repulsion of the target atom given by the following equation;

$$B = \frac{Zze^2}{R} \quad (2.1)$$

Where B represent the barrier of the reaction, Z and z are the respective atomic number of projectile and target species, e is the electric charge and R is the distance (cm) separating the two species.

The values of Coulomb barrier of the charged projectile species vary as a function of the atomic number (Z values) of the target species, and further details are available elsewhere (IAEA, 2009a).

On the other hand, the Q-value and threshold energy play roles of which reaction path-way and exit particles are possible based on the energy of the incident projectile. The Figure 2.5 below represents an example such of exit possibilities with the corresponding q-values.

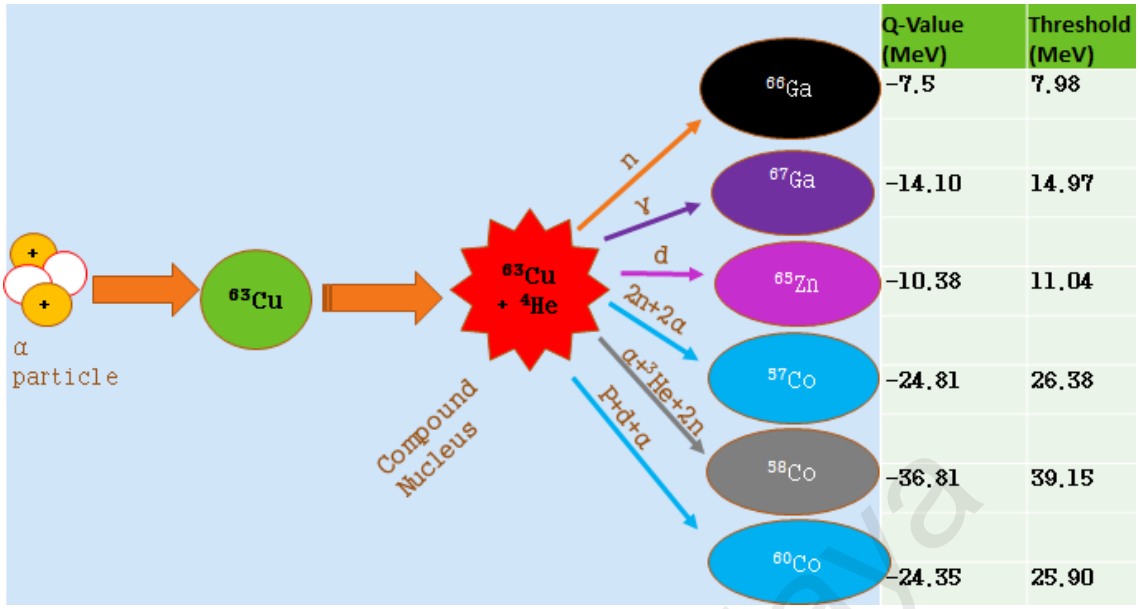

Figure 2.5: Possible exit channels of alpha bombardment on ^{63}Cu.

2.9.2 Reaction Models and Estimation of Cross-section

Nuclear reaction cross section represents the total probability of formation and decomposition of a compound nucleus via a reaction channel. Thus, the two critical stages of a nuclear reaction are the formation of a compound nucleus from the collision of target and projectile; and the decay of the compound nucleus to some reaction products. There are some theoretical models that try to estimate the reactions cross section when one particle bombard another. The nuclear reaction theoretical models are vital in virtually all stages of nuclear data evaluation in both general phenomena of data analysis and to estimate cross-section in the cases of insufficient experimental data or even where the available data is discrepant. The compound nucleus model, proposed by Bohr (Bohr & Wheeler, 1939; Brink, 1990; Mahaux & Weidenmuller, 1979) is the major basis of nuclear reaction theory. The pre-equilibrium models, which also received modification based on exciton model have been combined with the compound nucleus model to form some major computer codes for the estimation of cross sections. In fact, these models can be regarded as 'a model in model' as most of these models were based on some other models. Some of the popular model and codes available are the ALICE,

GNASH, and more recently, EMPIRE and TALYS. Each of these models have several versions which have been developed over time, making them much more reliable by enhancing their predictive powers. Moreover, some online databases are now also available for some of the evaluated cross sections based on these models. As an example, the Talys code (Koning & Rochman, 2012) has been evaluated for most reactions up to 200 MeV and made available on online library called Talys Evaluated Nuclear Data Library, TENDL (Koning et al., 2014b), with the latest Library update as TENDL-2015 which was evaluated based on Talys 1.8 code.

2.9.3 Specific Activity

This is an important property of radionuclide in biological or physiological processes. It is the number of radioactive atoms relative to the total number of atoms present in the sample. Specific activity (SA) is usually expressed in radiation units per mass units, and thus the most traditional unit is Ci/mole (also Ci/g) or even a fraction of these (recently being expressed as GBq/mole) (Ruth, 2009). In a situation where the only atoms present in the sample are of the radioisotope, in such a case the sample is called carrier-free. As an example, if a compound was labelled with ^{211}At, then the compound would be carrier-free as all isotopes of astatine are radioactive (unstable). In most cases, however, there exist some small quantity of stable atoms (nonradioactive), serving as carrier and have similar chemical properties, acting as a pseudo-carrier. The short half-lived radionuclides usually have much higher SA.

Using radioactivity decay equation below, the number of radioactive atoms in a given samples can be calculated;

$$-\lambda N = \frac{dN}{dt}, \tag{2.2}$$

where $\lambda\left(ln(2)/t_{1/2}\right)$ is the decay constant and $\frac{dN}{dt}$ is the rate of disintegration.

Specific activity of a radiopharmaceutical or an Isotope is useful in determination the biological or chemical effect the substance may have on a system under study (Ruth, 2009).

2.9.4 Experimental Cross sections and Radionuclide Production Rate

The reaction cross section of a reaction, A(x,y)B, is denoted by σ and is measured in historically in barns (1 barn =10^{-28} m^2 or 10^{-24} cm^2), with smaller units of barns, such as millibarns (mb) also in use. The reaction cross section is also referred to as integral cross section when integrated over all angles (Mohamed, 2006). The relationship observed (graphically) between the cross sections and the incident projectile energy is referred to as the excitation function of the radionuclide(Mohamed, 2006).

There are several factors which determine the rate at which radionuclides are produced from a given bombardment. These include;

1. The incident energy of the bombarding particle.
2. The intensity of the projectile beam. This parameter is associated to beam current.
3. The magnitude of the reaction cross section. This is usually expressed as a function of energy.
4. The target thickness (nuclei per cm^2).

We can thus express the rate of production, assuming a constant cross section, as;

$$R = n_T I \sigma \tag{2.3}$$

In which n_T represent target thickness in nuclei per cm^2. More elaborately, R can be express as;

$$-\frac{dn}{dt} = R = nI\left(1 - e^{-\lambda t}\right) \int_{E_s}^{E_{in}} \left\{\frac{\sigma(E)}{dE/dx}\right\} dE \quad (2.4)$$

Where; R represent number of formed nuclei per second, n is the target thickness (nuclei per cm^2), I is for the incident particle flux (this term is related to beam current), t is the irradiation period, E_{in} and E_s are the initial (incident) and final energy of the of the incident or projectile particle, x is the distance travel by the projectile particle and $\sigma(E)$ represent the cross section. Other symbols in the equation maintain their usual meaning.

There are several simplifications of these formulae. There are also modifications to the equation for cases when the target is a compound rather than a pure element.

Some very commonly used forms of the R and σ equations for cyclotron produced radionuclide, and using gamma counts are given below;

$$R = \frac{\lambda C(E)}{\varepsilon_\gamma I_\gamma NQ(1 - e^{-\lambda t_i})(e^{-\lambda t_c})(1 - e^{-\lambda t_m})}, \quad (2.5)$$

And

$$\sigma\,(E) = \frac{RNQ}{t_h \varphi N_d}, \quad (2.6)$$

Where; *C*(E) represent counts (gamma counts for gamma detectors), N is the number of target atoms, N_d is the number density of the target atom, Q is the beam current t_h is the target thickness and φ represent the flux.

2.9.5 Production Yield

The reaction cross section obtained from a thin targets i considered constant throughout the targets due to the light thickness of the target. This is, in other word, due to negligible energy loss because of the thin nature of the target when compared to

required energy range for the effect to be observed on cross sections. On the other hand, the cross section from a thick target would vary along the thickness of the target as the thickness could likely be comparable or even larger than the energy of the incident particle.

The production yield (Y) of a radionuclide from a given target thickness in nuclear reaction can be express (IAEA, 2009a; Mohamed, 2006) as in the following equation;

$$Y = \frac{N_A F}{M} I_b \left(1 - e^{-\lambda t}\right) \int_{E_s}^{E_{in}} \left\{\frac{\sigma(E)}{dE/dx}\right\} dE \qquad (2.7)$$

From which N_A is the Avogadro's constant ($6.022045(31) \times 10^{23}$ atoms per mol), F represent the fraction of the target isotope, I_b is for beam current, M is the atomic weight of the target material, dE/dx represent the stopping power of the target, and other symbols have their usual meaning.

As the beam traverse through the target, the beam energy is gradually loss due to stopping power of the target material and thus the cross section is depending on the energy degradation. Suppose those values are constant in within a successive thickness interval 1 MeV corresponding to stopping power of the material, the yield calculation is performed by integrating over the entire energy range irradiation (Mohamed, 2006).

Many researchers have calculated the yields of various radionuclides in different studies (Cata-Danil et al., 2008; Ditrói et al., 2008; Dmitriev, 1986; Dzoyem et al., 2016; Khandaker et al., 2007; Murakami et al., 2014; Nassiff, 1983; Shahid et al., 2015a; Shahid et al., 2015b). However, there are several definitions of yield by many researcher such that a recent review by EXFOR compilers of IAEA (Otuka & Takacs, 2015) recommended that researchers should properly define their yield clearly using appropriate units. The review further suggested sticking to, to avoid confusions, the

units of MBq/uA for the EOB (End of Bombardment) and saturation thick targets yields and MBq/C for physical tick target yields. It also discourages researchers from the use of MBq/uA.h for the physical tick target yields, except if they want report it separate, in addition to MBq/C, for practical reasons.

The yield values calculated represent the expected maximum values from irradiation of a given material (target). In practical sense, the yield obtained under high current runs is always lower than the corresponding theoretically calculated ones because of likely heterogeneity of incident beam, radiation damage effect, recoil loss of targets material (especially thin foil) from energetic beam, and so on.

2.9.6 Saturation Factor

As expected, the production reaction rate of a radionuclide is affected by the fact that produced radionuclide is itself radioactive (undergoes decay itself), and is even more prominent for radionuclides of very short half-lives. In the production of short-life radionuclides, since the rate of decay is proportional to the number of radionuclides present, the competing nuclear reaction rates, production and decay achieve equilibrium at a long and sufficiently irradiation times (Ruth, 2009). This point at which equilibrium is reached is called saturation. This indicate that further irradiation does not bring any benefit since the production rate already equals the rate of decay and thus no additional product would be produced. For the shorter bombardment times, the fraction of the yielded product is related to the saturation factor given by $\left(1 - e^{-\lambda t}\right)$, in which t is the irradiation time and λ is the decay constant of the decaying radionuclide (Ruth, 2009). It has been found that a bombardment equivalent to one half-life usually results to a saturation factor of 50%, and for practical reasons, irradiations hardly exceed 3 half-lives (90% saturation), except in the case of a shortest lived radionuclides (Ruth, 2009).

2.9.7 Target Stopping Power

The stopping power (dE/dx) can also be defined as the slowing or loss of kinetic energy (by any means) of a charged particle when it traverses through a matter or target. The stopping power and ranges of ion in matter is a property of different materials and can be calculated using the well-known code, Stopping and Range of Ions in Matter, SRIM/TRIM code (Ziegler, 2004). SRIM code is its self a group of some programs which calculate the stopping and range of ions up to 2 GeV/u through matter using a quantum mechanical treatment of ion and atom collisions. Its calculations are very efficient through the use of statistical algorithms in which free ion jump between calculated collisions are allowed and then computing the average of the results of the collisions over the intervening gap (Ziegler, 2003). It is a very powerful code as to can be used to perfumed varieties functions in different field of knowledge, including material science and nuclear technology. In addition to energy loss application in nuclear science, it can also be used to estimate the thickness of some materials. The SRIM code has several versions with its recent version being SRIM 2013, available at online at (Ziegler, 2003).

2.10 Effect of Recoil Energy on Cross Sections and Yield Calculations

Recalling from our basic knowledge of the principle of collisions, that collided particles may tend to move together after collision. In this case, when a very high energetic beam of particles bombards a group of target atoms, the projectile particle may be energetic enough to knock out some of the atoms from the target group of atoms to the next available layer behind the target.

To give more specific example relating to the present thesis, that is during radioisotope production, let us consider the following scenario where a projectile particle bombards a target as in the following sketch.

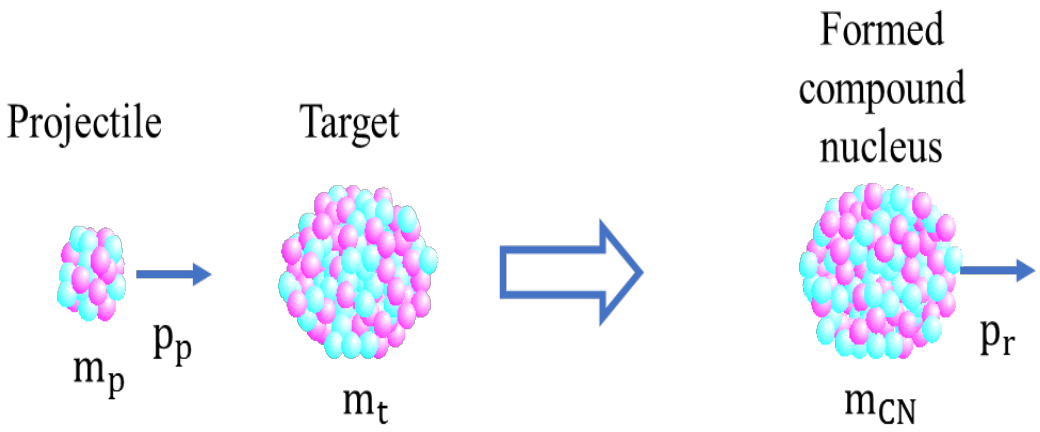

Figure 2.6: Demonstration of momenta of a projectile, target and compound nucleus during nuclear collisions.

The following steps are to simplify description of the collision process:

a. From the Figure above, a projectile with a mass m_p moves with momentum p_p, just before the nuclear reaction (collision). The projectile approaches a stationary target of mass, m_t.

b. After the nuclear reaction, a compound nucleus (CN) is formed with a momentum p_r. The CN therefore has **recoil energy, E_r** as follows:

$$E_r = \frac{p_r^2}{2m_{CN}} \tag{2.8}$$

where m_{CN} is the mass of compound nucleus.

c. But the momentum conservation law shows that, $p_p = p_r$.

d. This implies that,

$$p_p^2 = p_r^2 \tag{2.9}$$

And

$$2m_p E_p = 2m_{CN} E_r \tag{2.10}$$

$$E_r = \frac{m_p}{m_{CN}} E_p. \quad (2.11)$$

e. From equation 2.11, we can therefore say that;

- The recoil energy E_r increases as the kinetic energy of projectile E_p increase.

- If a heavier projectile is used, the recoil energy E_r becomes higher (E_r is proportional to the E_p).

f. If the produced nucleus has enough recoil energy, E_r, to leave the target and penetrate a recoil-catcher (foil) behind it (say a metal foil, in the case of a stacked foil), it will then penetrate the foil and will be stopped by it or even by another foil after the second foil, depending on its energy.

g. Because of this recoil loss, measured yield in the target (first foil) is lower than actual one.

h. To correct this effect, the yield in the next foil should be added to the measured yield of the previous foil (reference foil).

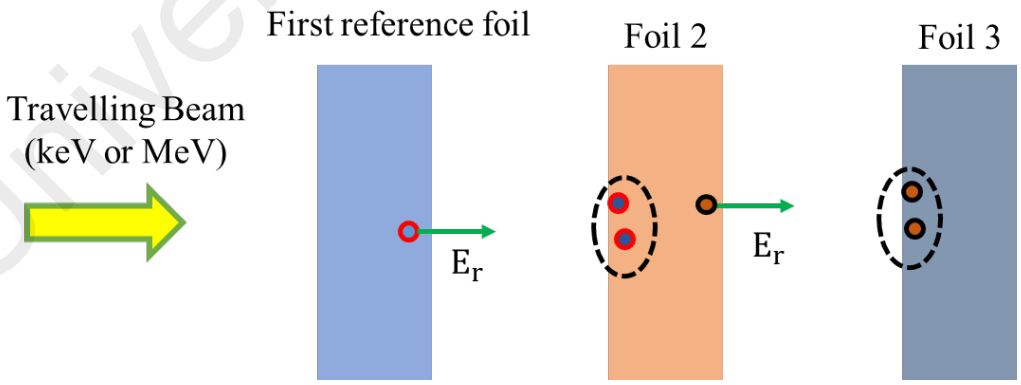

Figure 2.7: Recoil loss demonstration in irradiated stacked foils by a beam.

2.11 Review of Nickel Bombardment

Survey of literature indicates several studies have used nickel (powder, oxide or solid metal) as target for deuteron bombardment. Tracing the earliest works in EXFOR database, 3 sets of independent studies were reported in 1963 on cross section measurement from nickel bombardment by deuteron.

The Blann and Merkel (1963) first of those groups reported the experimental cross sections of ^{57}Ni, $^{55\text{-}57}$Co and ^{55}Fe radionuclides. A closer look on the experimental details of Blann's group revealed that the authors measured the activities of the reported radionuclides using, among other detectors, sodium Iodide crystal detector (NaICR). It is also clear that the decay data of the investigated radionuclides have over the years been updated in contrast to the data used by the group as at that time, even though the literature data found in Exfor database (Otuka et al., 2014) did not explicitly state the decay data used by the group. It would be seen latter in chapter 3 that a more comprehensive comparison is made by plotting the reported cross-sections of this group on the same graph with the present work and other literature data. A certain level of discrepancy has been observed from the plots.

The second observed work on this subject in the same 1963 was the reported work by Budzanowski's group (Budzanowski et al., 1963) which reported only ^{61}Cu radionuclide. The work was performed using a 120-cm cyclotron of the Institute of Nuclear Physics at Cracow, with a single metal foil and therefore a single data of cross-section at an energy of 12.8 MeV.

Similarly, Baron's group (Baron & Cohen, 1963) was reported to have used deuteron beam on nickel within the same period. The available literature data indicate several metallic targets, in addition to Ni, were used as targets material for the irradiation in either powdered or solid metal form, but does not clearly state the form of nickel target

(powder or foil) used. The literature however clearly stated that the group employed both ^{27}Al and ^{209}Bi foils to serve as monitors. The other metals used in the experiments along with the nickel were gallium, lanthanum and indium targets.

Slowly, after 1963, the use of nickel as a target for deuteron bombardment for radioisotopes production gradually attracts greater attentions from various research groups, especially due to growing interest in the radiation technology and also due to more potentials of the investigated radionuclides. Some more elaborate potential applications of the radionuclides emitted from deuteron bombardment of nickel are presented in Chapter 3 of this thesis. Recently, especially around the year 2000 to date, more investigations using nickel as a target are observed. In fact, nickel plays important role not only as a source of radioisotope of medical importance, but also in nuclear technology and has thus recently been given a priority over some other metals by IAEA coordinated project on Nuclear Data Library (for Advanced Systems - Fusion Devices) (FENDL-3) (Amjed et al., 2013).

A comprehensive survey of available literature data, comprising the authors and publication year, the method used, target information and other useful experimental details have been summarised and tabulated in Table 3. Additional information on the individual element obtained in the present study has been discussed in Chapter 3 of this thesis.

Table 2.1 Literature data on deuteron irradiation of nickel

Author	Facility, Method	Target	Beam Current, monitor	Activity separations, Detection	Incident Energy (MeV)	RI reported, data points;
Blann+, 1963	Cyclotron,	Nat Ni	NS*	RadioChem Separation, NaICR	24	^{57}Ni, 24; ^{55}Co, 22;
Budzanowski+, 1963.	Cyclotron,	enrich Ni	Faraday Cup	GM counter	12.8	^{61}Cu, 1
Baron+, 1963	Cyclotron, Stack	Elemental and Comp.	Faraday Cup	GM counter	18.8	^{57}Ni, 1; ^{55}Co, 1;
			^{27}Al(d, P+A)^{24}Na			^{59}Fe, 1
			^{209}Bi(d,p)^{210}Bi			
Cogneau+ ,1967	Cyclotron, NS*	From electrolysis of NiCl, NiN03	NS*, NS*	GM counter	12	^{61}Cu, 25; ^{57}Ni, 20
Cline., 1971	Cyclotron, Stack	enriched Ni electroplated on Au	Faraday Cup	NaICR, Ge(Li)	40	Several
Coetzee+, 1972	VDG (3SAFSUN),	enriched Ni electroplated on Ta	Faraday Cup	NaICR, Ge(Li)	5.5	^{61}Cu
Brinkman+, 1977	Synchrocylo, stack	Ni foils	Faraday Cup	Ge(Li)	50.6	
Zhu Fuying, 1981	Cyclotron, stacked foils	Ni foils	Faraday cup	Ge(Li) det.	14.7	^{55,56}Co, ^{57}Ni
*P.P Dmitriev+, 1983	Cyclotron, Thick Target for Yield measurement	Thick Ni		Ge(Li) det.	22	TTY for ^{55}Fe
			^{27}Al(d,PA)^{24}Na			
Jung., 1987	Cyclotron, foils soldered on Cu bar	Ni foils and	Heating power on Cu bar		14 and 9	$^{56-58}$Co
		Alloy		NS*		
Zwait +, 1991	Cyclotron, stacked foils	Ni foils	Charge integration	Ge(Li)	18.9	^{57}Ni, $^{55-58}$Co
		enriched powered 64Ni				

Table 2.2 Literature data on deuteron irradiation of nickel (continued)

Author	Facility, Method	Target	Beam Current, monitor	Activity separations, Detection	Incident Energy (MeV)	RI reported, data points;
Takacs+, 1997	Cyclotron, stacked foils	Ni foils	Faraday cup	HPGe Det.	20.3	$^{55-58}$Co, ^{57}Ni,^{60,61}Cu
			^{27}Al(d,x)^{24}Na			
Takacs+, 2001	Cyclotron, stacked foils	Ni foils	Faraday cup	Not stated	50 and 30	^{61,64}Cu, ^{56,57}Ni,$^{55-58}$Co
			^{nat}Ti(d,x)^{23}V			
			^{27}Al(d,x)^{24}Na			
			^{27}Al(d,x)^{22}Na			
Hermanne+, 2007	Cyclotron, stacked foils	Ni foils	Faraday cup	No Chemical separation γ,	20.4	^{61,64}Cu;
			^{nat}Ti(d,x)^{48}V	HPGe Det.		
Ochiai+, 2007	Cyclotron, NS*	Ni foils	Faraday cup	HPGe Det.	47.8	$^{55-57}$Co, $^{60,\ 61}$Cu
			^{27}Al(d,x)^{24}Na			
Amjed+, 2013,	Cyclotron, stacked foils	Ni foils	Faraday cup	HPGe Det.	40	^{56,57}Ni, $^{55-58}$Co etc
		NiBSi alloy	^{27}Al(d,x)^{24}Na			
Hermanne+, 2013	Cyclotron, stacked foils	Ni foils and	^{nat}Ti(d,x)^{23}V	HPGe Det.	50 and 20	^{52,56}Mn,$^{55-58}$Co etc
		Ga-Ni Alloy electroplated on Au	^{27}Al(d,x)^{24}Na			
			^{27}Al(d,x)^{22}Na			
This work	Cyclotron, stacked foils	Ni foils	Faraday cup			
			^{nat}Ti(d,x)^{48}V			

TTY- Thick Target Yield, NS – Not Stated

2.12 Titanium Irradiations with Alpha Particles

Despite lack of commercial alpha only cyclotrons in the hospitals, the study of this production route is almost as old as nuclear physics. In particular, the study of radioisotope production via alpha irradiation of Ti metal could be traced back to as early as 1960, when Iguchi's research group (Iguchi et al., 1960) used a cyclotron in Institute of Nuclear physics, Tokyo, Japan for irradiation of 1.8 mg/cm^2 thick titanium for foil for the production of ^{51}Cr cross section. Critical observations of the work indicate that the ^{51}Cr decay data ($T_{1/2}$ =27.8 days, E_γ = 325 MeV, and I_γ=9%) used at that experimental period has been updated over the years to some new values ($T_{1/2}$ =27.7025 days, E_γ = 320.0824 keV and I_γ= 9.910%). This certainly is enough reason to cause a large discrepancy between the cross sections of this group and the recent studies, as is confirmed from graphical representations in chapter 4 of this thesis. In addition to Iguchi's group, several other groups have over the years participated in production of radionuclides using titanium target via alpha production channel and again with various discrepancies among the measured data. The use of titanium is also as a result of its recommendation by IAEA (Qaim et al., 2002) for alpha beam monitoring purpose in nuclear reactions using ^{nat}Ti(a,x)^{51}Cr reaction. The success of ^{nat}Ti(a,x)^{51}Cr reaction in beam monitoring is due to the relatively large cross sections of the ^{51}Cr via alpha production route and the excellent shape of its corresponding excitation function.

Table 2.4 represents an up to date summary of basic experimental information of all literature data on alpha particles-induced nuclear reactions on titanium targets via cyclotron. In chapter 4, each radionuclide produced was considered separately for graphical representations of the present work, the available literature data as well as the theoretical data from the TENDL-2015 library, which was based on Talys code.

Table 2.3: Summary of reviewed previous works on alpha bombardment of titanium

First Author	Facility, Method	Target	Beam Current	Activity Detection	Products RI, data points	Energy range (MeV)
Eguchi 1983	Cyclotron, Stack	Ti foils	Faraday Cup	NaICR	^{51}Cr, 13	4.8-30.3
Chang 1973	Van de Graaff, single foil	enriched ^{48}Ti	Faraday Cup	Si(Li)	^{51}Cr, 7	5.0 - 11.0
Vlieks 1974	Van de Graaff	enriched ^{46}Ti evaporated on Au-Cu disc	NS	NaICR	^{49}Cr, 11	5.89 -10.93
				Si(Li)		
Howard 1974	VDGT Tandem Accel., NS	^{nat}Ti on Ta backing	NS	NaICR	^{49}Cr, 23	4.6-10.1
Weinreich 1980	Cyclotron, Stack	^{nat}Ti foils	Faraday Cup	Ge(Li), Chemical Processing	^{51}Cr	8.98-171.5
			^{27}Al(a,x)^{24}Na		^{48}Cr	19.02-172.4
Vonach 1983	Van de Graaff	^{nat}Ti foil	*Rutherford scattering	Ge(Li)	^{51}Cr, 8	5.76-12.87
Michel 1983	ISOCyclotron, stack foils		Faraday cup	Ge(Li)	^{51}Cr, 20	21.42 - 162.18
			^{27}Al(a,x)^{22,24}Na	HPGe for 44Ti	^{48}Cr, 8;	21.42 - 171.07
					^{48}V	21.42-171.07
					^{44}Ti	43.07-171.07
					^{46}Sc, 21; ^{47}Sc, 21;	21.42-171.07
					^{44m}Sc, 20;	29.97-171.07
					^{44g}Sc, 19	36.97-171.07
					^{43}Sc, 17, etc	51.26-171.07

Table 2.4: Summary of reviewed previous works on alpha bombardment of titanium (continued)

First Author	Facility, Method	Target	Beam Current	Activity Detection	Products RI, data points	Energy range (MeV)
Tarkanyi, 1991	Cyclotron, Stack foils	^{nat}Ti foils	Faraday Cup	Ge(Li),	^{51}Cr, 28	8.58-38.42
				HPGe		
Morton 1992	Van de Graaff, Pelletron Accl., Single oil	^{48}Ti target made from TiO_2 evaporated on Au	Faraday Cup	Ge(Li)	^{51}Cr, 30	4.99-9.52
Peng 1998	Cyclotron, Stack foils	^{nat}Ti foils	Faraday Cup	HPGe	^{48}Cr, 6	17.8-26.4
					^{51}Cr, 11	4.7-26.4
Hermanne 1999	Cyclotron, Stack foils	^{nat}Ti foils	Faraday Cup	Ge(Li)	^{48}V, 31	16.04-41.84
				HPGe	^{48}Cr, 30	16.57-41.84
					^{48}Sc, 13	25.1-41.84
					^{47}Sc, 25	16.57-41.84
					$^{46(m+g)}$Sc, 30	25.1-41.84
					^{44m}Sc, 8; ^{44g}Sc, 8	33.25-41.84

Table 2.5: Summary of reviewed previous works on alpha bombardment of titanium (continued)

First Author	Facility, Method	Target	Beam Current	Activity Detection	Products RI, data points	Energy range (MeV)
Baglin 2004	Cyclotron, Stack foils	^{nat}Ti foils	Faraday Cup	Ge(Li)	^{51}Cr, 11	6.58-11.16
				HPGe		
Uddin 2016	Cyclotron, Stack foils	^{nat}Ti foils	Faraday Cup	HPGe	^{51}Cr, 21	15.5 - 39.2
			^{nat}Ti(a,x)51Cr		^{48}Cr, 21	15.5 - 39.2
					^{48}V, 21	15.5 - 39.2
					^{46}Sc, 16	15.5 - 39.2
					^{48}Sc, 11	15.5 - 39.2
This work	Cyclotron, Stack foils	^{nat}Ti foils	Faraday Cup	HPGe	See Chapter 4	See Chapter 4
			^{nat}Ti(a,x)^{51}Cr			

2.13 Review of Alpha Bombardment on Holmium

Several radionuclides of thulium (Tm) such as ^{167}Tm and ^{166}Tm have in recent years been considered for useful applications in the medical field, especially due to their relatively short half-lives and other decay properties. The ^{167}Tm has recently been proposed as a useful agent in bone studies and tumour therapy (Sadeghi et al., 2012). One of the production routes of the ^{167}Tm isotope is through bombardments of holmium (Ho) metal with alpha particles (Sadeghi et al., 2012).

There are several experimental studies in the literature for the radioisotope production through other induced reaction on holmium metals. The review of the available experimental works in the literature shows that a significant proportion of the earlier research on this subject were performed either using the oxides of holmium compound or even alloys in some cases, in contrast to the use of natural or enriched targets of most of the present-day studies. Very high purity metals are now recently more readily available from various companies with a very high level of reliability.

The first available experimental studies on production of Tm radionuclides via alpha irradiation of holmium target was reported as early as 1949 by G. Wilkinson (Wilkinson & Hicks, 1949) of the University of California, Berkeley, United State. The experimental work was reported to have been carried out using a 60-inch cyclotron of the Crocker Laboratory. Given more details of the experiment, it was learned that the authors used a holmium oxide target, which contains 15% dysprosium oxide and about 5% ytterbium oxide. The experiment involved the bombardment of holmium oxide with a 38, 30 and 20 MeV alpha particle beam in several experimental arrangement or settings, such as an initial use of the raw form of the holmium oxide, and then separated the rare-earth metals later using column method. In the subsequent irradiations, the pure

earth metals recovered in the previous stage were then used. The beam intensities were deduced from the instrumental settings of the cyclotrons.

Further details of the experiment show that the detecting set-up used by the authors were 'end-on' type Geiger-Muller counters having 3 mg/cm^2 mica windows, filled respectively with 0.5 cm and 10 cm of alcohol and argon. Also, used in the studies, was a magnetic counter, which allowed the identifications of negative and positive electrons and provided a check on the data obtained from the absorption measurements during the experiment.

The Wilkinson experiment was followed 14 years later by another research from the group of G.V.S. Rayudu (Rayudu & Yaffe, 1963) of Mc Gill University Canada, using a synchrocyclotron. The authors used a sample containing a mixture of 'spec-pure' erbium oxide and copper oxide. It was also revealed that the experiment was characterised by chemical separation of reaction products and used sodium iodide crystal (NaI) for the measurement of activity. The details of the analysis of experimental uncertainties were not explicitly stated.

The first experiment that used holmium foils instead of a compound of the element as in the previous studies was reported in 1968 by J. Sau (Sau et al., 1968), which was performed at the synchrocyclotron of University de Lyon, France. Using a stacked activation method, the stack also contained Al foils as beam degraders in addition to the high purity (99.9 %) Ho foils. Two set of Ho foils thicknesses were used: 86.0 in one experiment and 48.5 in another. The authors also used a NAI (Tl) detector during the measurement of the radioactivities.

With growing number of cyclotron facilities around the world, the interest of more research is increasing even higher with time, and therefore more explorations of

different forms of targets, irradiation techniques and activity measuring devices have been in various tests under varieties of accelerator settings by various research groups. In particular, the target forms employed ranged from Ho-oxalate in 1966 (Martin & Pilger, 1966), $HoCl_3$ (Yano, 1975) to the of Ho_2O_3 (and sediment) (Homma et al., 1980).

A particular recent study (Tarkanyi et al., 2010) have reviewed and analysed the decay properties used by some previous studies and recommended some corrections on the accessed cross sections of the Tm radionuclides by some authors, in some cases the correction is as large as a factor of 2.33.

The increasing potentials of the Tm radionuclides have recently attracted even more studies via this production route on holmium target. In this work, all previous studies through alpha production pathway on Ho have also been analysed and summarised in Table 2.3 based on targets used, activation technique, detection method and radioisotope reported.

From the review of the available literature, it can reliably be deduced that;

- The employed charge collection technique in some of the previous studies was not very reliable and could have affected the estimated beam flux value.
- The reliability of the activity measurements in several of the earlier studies is sometimes questionable.
- Since targets preparations in several of the studies used varied preparation methods of targets, the certainty in target uniformity is also unreliable.
- During the calculations of the cross sections of investigated radionuclides, the decay characteristics of such radionuclides used by different research groups were not uniform and had significantly been updated over the years.

Evidently, the above reasons are sufficient to affect the values of calculated cross sections and also the thick target yields of all studied radionuclides in the previous studies, leading to significant discrepancies among the previous measurements. Reassessment of the previous studies on many of the reported cross-sections is therefore necessary, especially in recent times when more practical uses of these radionuclides are being applied.

Most of the recent studies used metallic foils in very high purity forms as target materials and Hyper-Pure Germanium (HPGe) detectors, which offer high resolution, for the measurements of activities of irradiated targets

.

Table 2.6: Summary of reviewed previous studies on irradiation of holmium by alpha beam

Author	Method, Facility	Target	Beam Current, Monitor reaction	Activity separation, Detection	Products	Decay data used ($T_{1/2}$, E_γ, I_γ)	Energy range (MeV)
G. Wilkinson, 1949	Cyclotron (60 inch), NS	Ho oxide	NS*	Chemical separation β, GM counter	^{168}Tm;	85 d, NS*, NS*;	19 - 38
					^{167}Tm;	9.6 d, NS*, NS*;	19 - 38
					^{166}Tm	7.7 d, NS*, NS*	30 - 38
G.V.S Rayudu 1963	Synchrocyclotron, stacked foils	Ho oxide	Faraday Cup	No Chemical sepration γ, NaI (Tl)	^{168}Tm;	86d, 200, 81%.;	15-25
					^{167}Tm	9.6 d, 200, 98%.	20-39
G. C MartinJr et al, 1966	Cyclotron, stacked foils	Ho oxide	NS*	Chemical Separation γ, NaI (Tl)	^{168}Tm;	93 d,817-831, 62%;	15.9-40.1
		Ho oxalate			^{167}Tm;	9.25 d,532, 2%;	15.9-40.1
					^{166}Tm;	7.7 h,2057-2083, 48%;	24.4-40.1
					^{165}Tm	29 h,1131-1184, 5%	32.9-40.1

Table 2.7: Summary of reviewed previous studies on irradiation of holmium by alpha beam (continued)

Author	Method, Facility	Target	Beam Current, Monitor reaction	Activity separation, Detection	Products	Decay data used ($T_{1/2}$, E_γ, I_γ)	Energy range (MeV)
Y. Yano, 1975	Cyclotron,	$HoCl_3$	NS*	NS*	^{167}Tm, 1	NS*	32
	Yield measurement						
Y. Homma, 1980	Cyclotron, stacked foils	Ho_2O_3, Sediment	Beam current integrator,	No Chemical separation γ, Intrinsic Ge Det.	^{168}Tm, 5;	NS*,198.3, 53.4%;	15.6-24.8
			Iron foil		^{167}Tm, 9;	9.8 d, 207.9, 43.0%;	20.0-39.8
					^{166}Tm, 6	7.7 h, 672, 6.3%	27.8-39.8
P.P Dmitriev, 1980	Cyclotron, stacked foils	Ho foils	^{63}Cu(α,x)^{65}Zn	No Chemical separation γ, Ge(Li) Det.	^{168}Tm, 12;	93.1 d,84.26, 3.2%;	17.0-43.4
					^{167}Tm, 12;	9.24 d,207.8, 41%;	17.0-43.4
					^{166}Tm, 7;	7.7 h, 1275.3, 14.6%;	30.4-43.4
					^{165}Tm, 4	29.6 h, 296.72, 25.3%	37.7-43.4
J. Rama Rao+, 1987	Cyclotron, stacked foils	Ho foils	^{65}Cu(α,x)^{67}Ga;	No Chemical separation γ, Ge(Li) Det.; HPGe Det.	^{167}Tm, 22;	9.25 d, 208, 41%;	19.5-112.9
			^{27}Al(α,x)^{22,24}Na		^{165}Tm, 17	30.06 h, 243, 35%	35.7-112.9

NS* - Not stated

Table 2.8: Summary of reviewed previous studies on irradiation of holmium by alpha beam (continued)

Author	Method, Facility	Target	Beam Current, Monitor reaction	Activity separation, Detection	Products	Decay data used ($T_{1/2}$, E_γ, I_γ)	Energy range (MeV)
S. Mukherjee et al., 1991	Cyclotron, stacked foils	Ho foils	$^{27}Al(\alpha,x)^{22,24}Na$	No Chemical sepration γ, Ge(Li) Det.; HPGe Det.	^{168}Tm, 12;	93.1 d, 184, 16.4%,	16.8-66.5
			Faraday cup			198, 50%	
						447.5, 21.9%,	
						815.9, 46.3%;	
					^{167}Tm, 12;	9.25 d,207.8, 41%;	22.4-66.7
						532, 1.59%	
					^{166}Tm, 10;	7.7 h, 778.8, 19.7%;	29.2-71.4
					^{165}Tm, 8	30.06 h, 243, 35%	35.4-66.5
						297.3, 24.8%	
						806.8, 8.35%	

Table 2.9: Summary of reviewed previous studies on irradiation of holmium by alpha beam (continued)

Author	Method, Facility	Target	Beam Current, Monitor reaction	Activity separation, Detection	Products	Decay data used ($T_{1/2}$, E_γ, I_γ)	Energy range (MeV)
N.L Singh, 1992	Cyclotron, stacked foils	Ho foils	$^{65}Cu(\alpha,2n)^{67}Ga$;	No Chemical separation γ, Ge(Li) Det.;	^{168}Tm, 16;	93.1 d, 198, 50%,	14.8-47.2
						447.5, 21.95%,	
						815.9, 46.3%;	
					^{167}Tm, 16;	9.25 d, 207.8, 41%;	18.9-47.6
						532, 1.59%	
					^{166}Tm, 10;	7.7 h, 778.8, 19.67%;	27.9-47.6
						1176.5, 8.39%	
						1273.4, 14.41%	
					^{165}Tm, 7;	30.06 h, 243, 35%	34.0-47.1
						297.3, 24.77%	
						806.8, 8.35%	

Table 2.10: Summary of reviewed previous studies on irradiation of holmium by alpha beam (continued)

Author	Method, Facility	Target	Beam Current, Monitor reaction	Activity separation, Detection	Products	Decay data used ($T_{1/2}$, E_γ, I_γ)	Energy range (MeV)
B.P Singh 1995	Cyclotron, stacked foils	Ho foils	Faraday cup	No Chemical separation γ, Ge(Li) Det.;	^{168}Tm, 6;	93.10 d, 184, 16.1%,	15.8-33.9
						198, 49.1%	
						447, 21.3%,	
						720, 10.7%	
						741, 11.1%	
						815, 45.2%;	
					^{167}Tm, 5;	9.25 d, 208, 41%;	20.3-34.0
					^{166}Tm, 5;	7.70 h, 215, 5.3%;	27.8-39.3
						778.8, 15.1%;	
						785, 9.4%	
						1273, 14.4%	

Table 2.11: Summary of reviewed previous studies on irradiation of holmium by alpha beam (continued)

Author	Method, Facility	Target	Beam Current, Monitor reaction	Activity separation, Detection,	Products	Decay data used ($T_{1/2}$, E_γ, I_γ)	Energy range (MeV)
M.S. Gadkari, 1997	Cyclotron, stacked foils	Ho foils	Faraday cup	No Chemical separation, γ, Ge(Li) Det.;	^{168}Tm, 10;	93.1 d, 198.0, 50%,	20.0-65.8
			^{27}Al(α,α2pn)^{24}Na			447.5, 21.95%,	
						815.9, 46.3%;	
					^{167}Tm, 10;	9.25 d, 207.8, 41%;	20.0-65.8
						532.0, 1.59%	
					^{166}Tm, 8;	7.7 h, 778.8, 19.67%;	29.2-65.8
						1176.5, 8.39%	
						1273.4, 14.41%	
					^{165}Tm, 7;	30.06 h, 243.0, 35%	35.0-65.8
						297.3, 24.77%	
						806.8, 8.35%	
F. Tarkanyi, 2010	Cyclotron, stacked foils	Ho foils	Faraday cup	No Chemical separation, γ	^{168}Tm, 18;	93.1 d, 815.989, 50.03%;	12.2-38.8
			^{27}Ti(α,x)^{51}Cr	HPGe Det.	^{167}Tm, 18;	9.25 d, 207.801, 42%;	17.1-38.8
					^{166}Tm, 13;	7.70 h, 778.814, 19.1%;	26.9-38.8
					^{165}Tm, 5;	30.06 h, 242.917, 35.5%	35.4-38.8
This work	Cyclotron, stacked foils	Ho foils	Faraday cup	No Chemical separation, γ	^{168}Tm, 18;	93.1 d, 815.989, 50.03%;	Chapter 6
			^{27}Ti(α,x)^{51}Cr	HPGe Det.	^{167}Tm, 18;	9.25 d, 207.801, 42%;	
					^{166}Tm, 13;	7.70 h, 778.814, 19.1%;	
					^{165}Tm, 5;	30.06 h, 242.917, 35.5%	

CHAPTER 3: EXCITATION FUNCTIONS OF DEUTERON INDUCED REACTIONS ON NATURAL NICKEL UP TO 24 MEV

3.1 Introduction

This chapter presents the basic summary of method, findings and a short conclusion of the first objective of the present work. A comprehensive detail on the target used and irradiation technique have been provided under the material and methods section. The chapter thus presents the assessed production cross-sections of radionuclides from the bombarded natural nickel target by the 24 MeV deuteron beam.

3.2 Literature Review

The metallic nickel (Ni), its compounds or its alloys have large industrial applications which are perceived to be generally, due to its physical and chemical characteristics. This metal is corrosion-resistant, silvery-white and physically lustrous in nature. Ni has been given priority over other materials in a recently coordinated research program of IAEA FENDLE-3 (Fischer, 2009). On the other hand, Ni can be used as a target material for the production of radionuclides by accelerators leading to medical and industrial applications. Radionuclides of Co, Cu, Cr, Mn, and Ni can are producible via Ni irradiation. The productions are under optimum irradiations and measurements conditions since some of these radionuclides have very short half-lives. Co radionuclides such as ^{55,56,57}Co found potential applications in medicine and other basic research fields due to their suitable decay characteristics (Heinle et al., 1952; Lagunas-Solar & Jungerman, 1979). ^{55}Co found important applications in labelling bleomycin and the studies of cerebral and cardiac problems via PET. ^{57}Co plays a significant role as a calibration standard in γ-ray spectrometry and single photon emission computed tomography (SPECT) (Al Saleh et al., 2007). In addition to several industrial applications, the decay properties of ^{57}Ni have led to it being recently suggested as a

possible candidate in monitoring some nuclear reactions (Oblozinsky, 1997; Takács et al., 2007).

A literature survey conducted on the previous experimental data (Amjed et al., 2013; Baron & Cohen, 1963; Blann & Merkel, 1963; Brinkman et al., 1977; Budzanowski et al., 1963; Cline, 1971; Coetzee & Peisach, 1972; Cogneau et al., 1967; Fuying et al., 1983; Hermanne et al., 2013; Hermanne et al., 2007; Jung, 1992; Ochiai et al., 2007; Takács et al., 1997; Takács et al., 2001; Takács et al., 2007; Zweit et al., 1991) through deuteron irradiations on nickel indicates some considerable discrepancies among the published results, leading to the need for further analysis to minimize them. Furthermore, available experimental data via the deuteron bombardment technique are not sufficient relatively to proton route, leading to further need of enriching the database. In this study, natural Ni foil targets in the form of stack were irradiated, using an external beam of RIKEN cyclotron and measured the cross sections of the produced radionuclides. This work, thus, contributes in minimising te discrepancies of the available data and enriching the database.

3.3 Methodology

Using the well-established stacked foil activation method for irradiation and HPGe γ-ray spectrometry for activity measurement, the activation formula was used to determine the cross-sections of the $^{nat}Ni(d,x)^{55-58}Co$, ^{57}Ni, $^{52,54}Mn$ reactions for the deuteron energy range of 24 MeV down to respective thresholds. Except for some specific features relevant to the present study, the overall procedure is similar to some earlier studies (Khandaker et al., 2015; Khandaker et al., 2014; Khandaker et al., 2011).

3.3.1 Targets and Bombardments

A foil of nickel (Ni) (purity: 99.99%; thickness: 25.46-μm; Goodfellow, UK) with the natural compositions of isotopes (^{58}Ni: 68.077%; ^{60}Ni: 26.223%; ^{61}Ni: 1.140%; ^{62}Ni: 3.634%; ^{64}Ni: 0.926%) (Berglund & Wieser, 2011) was the main target material of this chapter. Some foils of other natural metals such as titanium from Goodfellow, UK company with purity 99.99% and 20.32-μm thick and platinum (from Goodfellow, UK with 9.95% purity; 10.48-μm thickness) were inserted in the first stack, while zinc (99.99 % purity; 25-μm thickness; Goodfellow, UK) and copper (99.99 % purity; 12.4-μm thickness; Goodfellow, UK) were in the second stack, in each case serving either as energy degrader or for reaction monitoring purpose. Two stacks were made from these foils, following the intermittent energy points in the deuteron energy range of 2–24 MeV.

There were nine (9) nickel foils in the first stack of 39 total foils, fashioned within the irradiated deuteron energy of 10.05 to 23.14 MeV, and in the second stack of 35 total foils, nine (9) were from nickel, covering the entire energy range from 24 down to 2.03 MeV. The thicknesses of the used foils were measured using an electronic balance. All foils, including the monitor foils, were cut in the same size (15 × 15 mm^2) following the dimension of the target container so as to ensure equal areas of the monitors and targets foils are exposed to the same beam flux. The deuteron beam was collimated to a diameter of 9-mm to the centre of the target. The bombardment of the prepared targets was done using a water-cooled target holder, serving as a Faraday cup. The first and second stacks were respectively bombarded for 2.00 h and 2.07 h, by 24-MeV deuteron beam from the AVF cyclotron of RIKEN RI Beam Factory, Japan in which about 200 nA beam current was recorded.

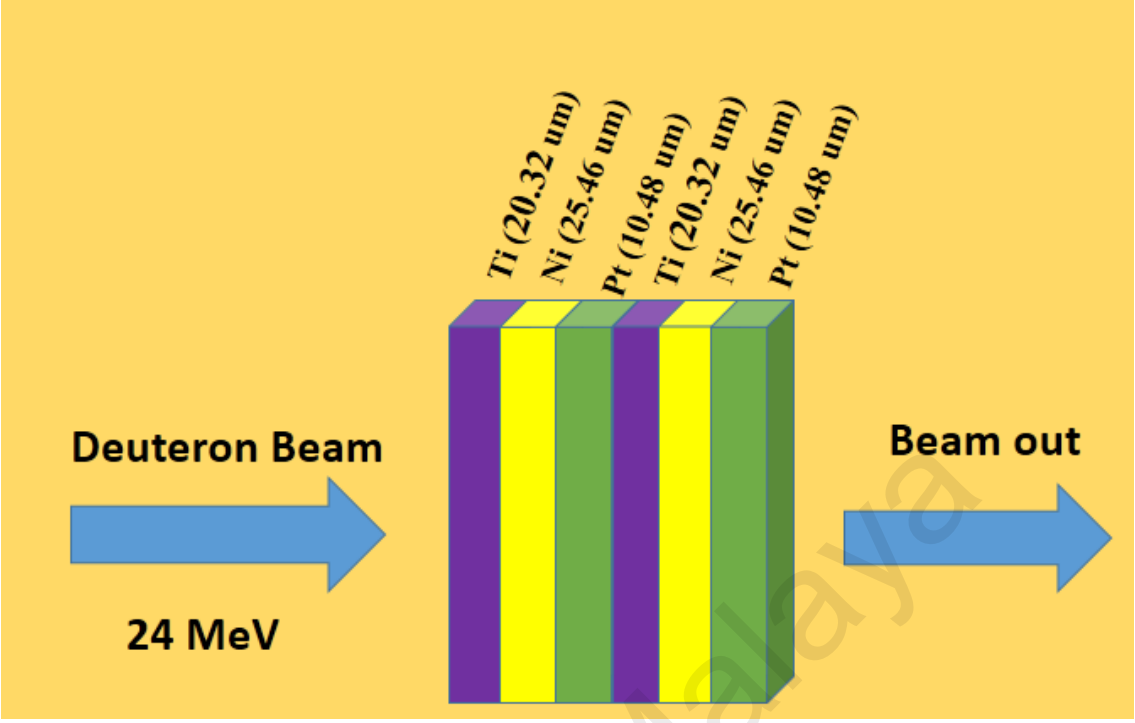

Figure 3.1: An example of Stack formation for deuteron irradiation

The computer program, SRIM-2003 (Ziegler, 2004) was used for the degradation of the deuteron energy calculations in the two prepared stacks. The uncertainty in the deuteron energy is due to the uncertainties in the initial beam energy, thickness of target, and beam straggling. The estimated uncertainties in foil energy range from ±0.43 MeV to ±1.57 MeV and they are presented together with the cross sections in Tables and Figures of this chapter.

The recommended IAEA ^{nat}Ti(d,x)^{48}V monitor reaction (σ = 217.54 mb at E_d = 23.88 MeV) (Qaim et al., 2002) was used to determine the average beam current. The beam intensity was determined from the activity of the Ti foil placed at the front of the stack and considered as a constant within the stack.

3.3.2 γ-ray Spectrometry

At the end of bombardment, the targets were transferred from the holder, for the measurements of the activation products from the activated samples. The measurements

were done with a high resolution (1.85 keV FWHM at 1332.5 keV) HPGe γ-ray spectrometer coupled to a 4096 multi-channel analyser with the associated electronics. The followings are the specifications of the detector used: ORTEC; GEM-25185P; operating voltage: +2000 V; relative efficiency: 25%. The measurements were started about eight hours after the irradiation. Detailed information of the cooling period for each series measurements have also been provided in Table 3.1. The foils have been measured at least 2-cm distances away from the detector to lessen the effects of the pile-up and dead times during the present studies. The efficiencies of the used detector at various foil-to-detector distances were determined with the help of a standard γ-ray multi-nuclide source. The Maestro version 7.0 gamma program was used for spectrum analysis (Ortec, 2012).

Table 3.1: Cooling time for different series measurements in this experiment.

1st stack		2nd stack	
Measurement series	**Cooling period**	**Measurement series**	**Cooling period**
I	8.4 - 10.7 h	I	26.7 - 27.6 h
II	10.9 - 28.5 h	II	28.7 - 29.7 h
III	1.7 - 1.8 d	III	1.7 - 1.8 d
IV	2.9 - 4.0 d	IV	2.9 - 3.1 d
V	5.2 - 5.8 d	V	5.0 - 5.8 d
VI	10.9 - 11.1 d	VI	10.8 - 10.9 d
VII	24.2 - 25.1 d	VII	23.9 - 24.2 d

The well-known activation formula (Khandaker et al., 2010; Khandaker et al., 2011; Khandaker et al., 2007) was used in the determination of the cross-sections of all the assessed radioisotopes. The decay data of the investigated reaction products were adopted from the ENSDF library (Bhat, 1998; C.D. Nesaraja et al., 2010; Huo Junde, 2008a; Huo Junde et al., 2011; Junde Huo et al., 2007; T.W. Burrows, 2006; Yang Dong & Huo Junde, 2014), assessed via the NuDat-2.6 interface (NuDat 2.6, 2011), and are presented in the Table 3.2. The threshold energies and Q-values were calculated

based on the AME mass evaluation (Audi et al., 2003) via online the Q-tool system (Qtool, 2011) and they are also presented in Table 3.2.

Table 3.2: Relevant decay data for the present work extracted from Nudat 2.6 as well as Q-values and threshold energies extracted from Q-tool

(Bold γ-lines were used in the derivation of the experimental cross-sections in the present chapter. The ^{48}V decay properties ($T_{1/2}$ = 15.9735 d, E_γ = 983.525 keV, I_γ = 99.98±0.04 %) were used for flux determination but not listed in the Table.)

Nuclide	Half-life	E_γ (keV)	I_γ (%)	Contributing reactions	Q-value (MeV)	Threshold (MeV)
^{55}Co	17.53 h	477.2	20.2	^{58}Ni($d,n+\alpha$)^{55}Co	−3.56	3.69
		931.1	75±4			
		1316.6	7.1			
		1408.5	16.9			
^{56}Co	77.236 d	**846.770**	99.9399±0.0023	^{58}Ni(d,α)^{56}Co	-6.52	0.0
		1037.843	14.05	^{60}Ni($d,2n+\alpha$)^{56}Co	−13.86	14.33
		1238.288	66.46	^{61}Ni($d,3n+\alpha$)^{56}Co	−21.69	22.40
		1771.357	15.41			
^{57}Co	271.74 d	**122.0607**	85.60 ±0.17	^{58}Ni($d,n+2p$)^{57}Co	−10.40	10.76
				^{60}Ni($d,n+\alpha$)^{57}Co	−2.49	2.57
		136.47356	10.68	^{61}Ni($d,2n+\alpha$)^{57}Co	−10.31	10.65
				^{62}Ni($d,3n+\alpha$)^{57}Co	−20.90	21.58
^{58g}Co	70.86 d	**810.7593**	99.450 ±0.010	^{60}Ni(d,α)^{58}Co	-6.08	0.0
				^{61}Ni($d,n+\alpha$)^{58}Co	−1.74	1.79
				^{62}Ni($d,2n+\alpha$)^{58}CoIT(100%) decay of ^{58m}Co($T_{1/2}$=9.10 h)	−12.33	12.73
^{60g}Co	1925 d	**1173.228**	99.85 ±0.03	^{60}Ni($d,2p$)^{60}Co	-4.27	4.41
		1332.492	99.9826	^{61}Ni($d,n+2p$)^{60}Co	-12.09	12.48
				^{62}Ni(d,α)^{60}Co	-5.6	0.0
				^{64}Ni($d,2n+\alpha$)^{60}Co	-10.88	11.22
				IT(99.75%) decay of ^{60m}Co($T_{1/2}$=10.467 min)		
^{57}Ni	35.60 h	127.164	16.7	^{58}Ni($d,2n+p$)^{57}Ni	−14.44	14.94
		1377.63	81.7±2.4			
		1919.52	12.3			
^{52g}Mn	5.591 d	744.233	90.0	^{60}Ni($d,2n+2\alpha$)^{52}Mn	−21.62	22.34
		935.544	94.5	IT(1.75%) decay of ^{52m}Mn($T_{1/2}$=21.1 min)		
		1434.06	98.3±5.0	^{58}Ni($d,2\alpha$)^{52}Mn	−1.24	1.28
^{54}Mn	312.12 d	**834.848**	99.9760 ±0.0010	^{58}Ni($d,2p+\alpha$)^{54}Mn	−8.54	8.84
				^{60}Ni($d,2\alpha$)^{54}Mn	−0.63	0.65
				^{61}Ni($d,n+2\alpha$)^{54}Mn	−8.45	8.73
				^{62}Ni($d,2n+2\alpha$)^{54}Mn	−19.05	19.67
^{61}Cu	3.333 h	**656.008**	10.8±2.0	^{60}Ni(d,n)^{61}Cu	-2.58	0.0
				^{62}Ni($d,3n$)^{61}Cu	-15.84	16.36

The followings were the major sources of uncertainties considered during this experiment: (0.3-10%) for γ-ray counting statistics, (~1%) for target thickness, (~5%) for beam intensity, efficiency of detector as (~4%), and (~1%) for γ-ray intensity. All

the above uncertainties were added quadratically to obtain the cumulative uncertainty of 6.6-11.9%. The uncertainties in γ-ray counting statistics were determined in this work and those of γ-ray intensities were taken from the literatures (Bhat, 1998; Browne & Tuli, 2013; Burrows, 2006; Huo Junde, 2008b; Huo Junde et al., 2011; Junde Huo et al., 2007; Nesaraja et al., 2010; Yang Dong & Huo Junde, 2014). Other uncertainties such as for efficiency of the detector, target thickness, and so on, have been evaluated based on the experimental conditions of the present study and are presented together with the other uncertainties in Table 3.3. The uncertainties related to the monitor reaction such as statistics of γ-ray counting, γ-ray intensity, etc., have not been included in the table.

Table 3.3: Fractional (%) partial uncertainties in the cross-sections
(The fractional partial uncertainties have been quadratically added to obtain the cumulative uncertainties in the cross-sections. Other uncertainties were assumed).

Nuclide	γ-ray counting statistics of the nuclide	beam intensity	detector efficiency	target thickness	γ-ray intensity of the nuclide	Cumulative uncertainty
^{55}Co	0.8-33.9	5	4	1	5.333	8.4-34.9
^{56}Co	0.4-2.9				0.002	6.5-7.1
^{57}Co	0.3-9.3				0.199	6.5-11.4
^{58}Co	0.2-1.3				0.010	6.5-6.6
^{60}Co	8.7-16.1				0.030	10.9-17.3
^{57}Ni	0.8-13.0				2.938	7.2-14.8
^{52g}Mn	3.2-11.8				5.086	8.8-14.36
^{54}Mn	9.8-31.6				0.001	11.8-32.3
^{61}Cu	1.5-4.9				18.519	19.7-20.2

3.3.3 Theoretical Models

The experimental work is preceded with a clear understanding of the theoretical knowledge of the nuclear reactions under consideration. Nuclear reaction codes are therefore designed to serve this purpose. Modelling of the nuclear reaction mechanism can predict even the energy regions where experiments may not be achievable or

reliable. The models can give information on direct particle interaction, pre-equilibrium and cumulative or compound nucleus contributions of the interacting nuclei. Several models have so far been developed by several research groups. Some of the popularly known codes include ALICE, EMPIRE, and TALYS.

3.3.3.1 Talys code and TENDL library

One of the most widely known nuclear reaction codes is TALYS. It has been developed by the nuclear research and consultancy group, Netherlands. The TALYS code is capable of calculating nuclear reaction cross-sections at 1 keV-200 MeV. It is characterized as efficient, flexible and user-friendly, capable of simulating most of the known nuclear reactions on all isotopes using proton, deuteron, gamma, alpha, neutron, triton, or helium-3 as projectiles. The TALYS code has been upgraded and modified from the first version, TALYS 1.0 on December 2007, to the most current version, TALYS 1.6 on December 2014. Recently, many research groups on this field use TALYS-based evaluated nuclear data Library (TENDL). The 8th version is currently the latest (TENDL-2015). The measured data of the ^{nat}Ni(*d*,*x*) processes were compared with theoretical values extracted from TENDL-2014 library, which was entirely calculated using default and adjustable TALYS code.

3.4 Results and Discussions

The newly measured production cross sections from the bombarded nickel by the 24 Mev deutron energy are presented in Tables 3.4 and 3.5 of this chapter. The plotted excitation functions of the assessed $^{55\text{-}58(g+m)}$Co, $^{60(g+m)}$Co, ^{57}Ni and ^{52,54g}Mn radionuclides are in the Figs. 3.3 – 3.11 of this chapter where they have been compared with the previously reported experimental data extracted from the EXFOR database (Otuka et al., 2014). On the other hand, the output of the theoretical Talys code values (Koning & Rochman, 2012) were taken from the TENDL-2014 library (Koning et al.,

2014a). Some of the previous measurements on enriched targets (Baron & Cohen, 1963; Blann & Merkel, 1963; Brinkman et al., 1977; Budzanowski et al., 1963; Cline, 1971; Cogneau et al., 1967; Fuying et al., 1983) have been normalized to elemental cross sections before plotting. More so, the data of (Takács et al., 1997) were adjusted by a factor of 1/1.18 following the recommendation of the authors in (Takács et al., 2007). The presented cross sections have been used to calculate the integral thick target yields of some selected radionuclides by integrating over the whole energy region.

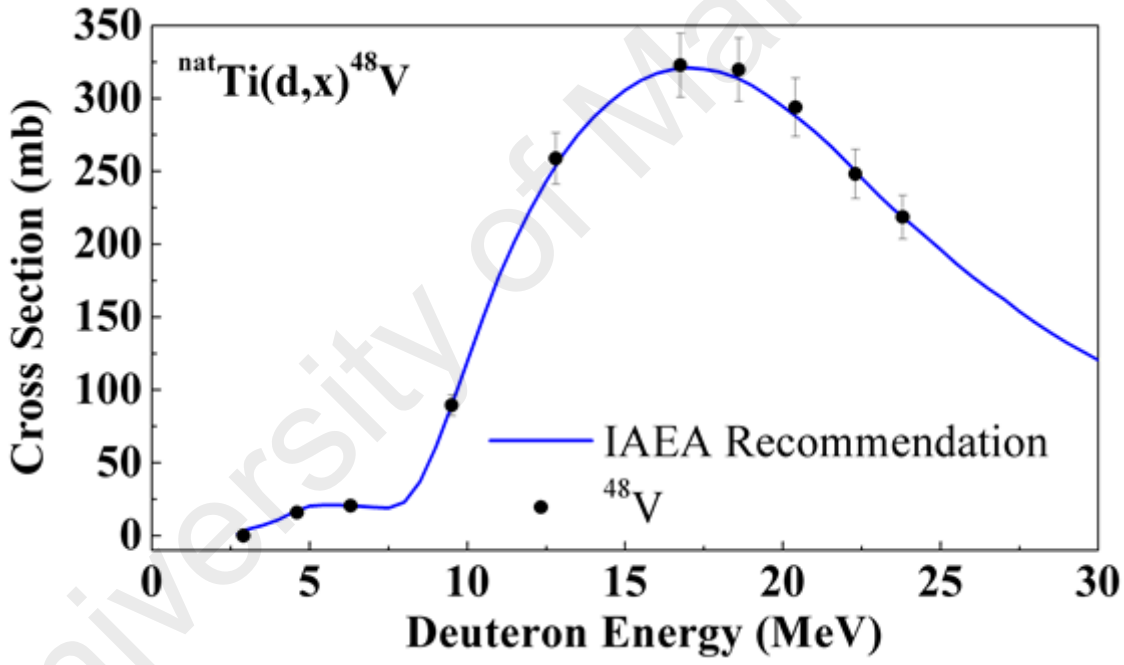

Figure 3.2: Excitation function of the ^{nat}Ti(*d,x*)^{48}V monitor reaction cross-sections.

Table 3.4: Measured production cross-sections for ^{55,56,57,58,60}Co radionuclides.

Energy (MeV)	Cross-sections (mb)				
	^{nat}Ni(d,x)^{55}Co	^{nat}Ni(d,x)^{56}Co	^{nat}Ni(d,x)^{57}Co	^{nat}Ni(d,x)$^{58g+m}$Co	^{nat}Ni(d,x)$^{60g+m}$Co
23.71 ± 0.49	22.7 ± 1.71	7.19 ± 0.53	243 ± 16	183 ± 12	14.5 ± 1.3
23.04 ± 0.48	21.5 ± 1.5	7.29 ± 0.53	219 ±15	192 ± 13	13.2 ± 0.9
21.94 ± 0.51	23.6 ± 1.6	6.83 ± 0.50	164 ± 11	195 ± 13	12.6 ± 0.7
21.75 ± 0.51	21.6 ± 1.5	8.10 ± 0.59	166 ± 11	212 ± 14	08.29 ± 1.30
20.67 ± 0.51	20.7 ± 1.4	8.09 ± 0.58	134 ± 9	223 ± 15	11.83 ± 1.10
19.31 ± 0.33	18.0 ± 1.2	9.28 ± 0.66	86.1 ± 5.9	226 ± 15	09.51 ± 0.80
18.10 ± 0.54	17.0 ± 1.2	10.4 ± 0.7	49.2 ±3.4	217 ± 15	
17.45 ± 0.54	14.3 ± 1.0	11.7 ± 0.8	46.9 ± 3.2	229 ±16	
15.48 ± 0.57	10.2 ± 0.7	16.0 ± 1.1	28.6 ± 2.0	215 ± 16	
14.67 ± 0.61	8.17 ± 0.56	17.4 ± 1.2	21.2 ± 1.5	183 ± 12	
14.15 ± 0.60	7.36 ± 0.51	20.7 ±1.4	21.7 ±1.5	202 ± 14	
12.77 ± 0.65	2.95 ± 0.20	26.4 ± 1.8	11.0 ± 0.8	154 ± 10	
11.35 ± 0.66	0.82 ± 0.08	33.4 ± 2.3	6.10 ±0.46	137 ± 9	
9.82 ± 0.54	0.03 ± 0.01	33.2 ± 2.3	0.86 ±0.07	67.2 ± 4.6	
9.15 ± 0.74		31.7 ± 2.2	0.55 ±0.05	60.3 ± 4.1	
7.17 ± 0.86		18.3 ± 1.2	0.21 ±0.02	12.7 ± 0.9	
4.43 ± 0.97		3.10 ± 0.21	0.18 ±0.02	2.68 ±0.18	
1.79 ± 1.11			0.19 ±0.01	1.25 ±0.09	

Table 3.5: Measured production cross-sections for ^{57}Ni, ^{52g,54}Mn and ^{61}Cu radionuclides.

(The reported cross-section of ^{52g}Mn includes the IT decayed 1.75 % of ^{52m}Mn.)

Energy (MeV)	Cross-sections (mb)			
	^{nat}Ni(d,x)^{57}Ni	^{nat}Ni(d,x)^{52g}Mn	^{nat}Ni(d,x)^{54}Mn	^{nat}Ni(d,x)^{61}Cu
23.71 ± 0.49	20.9 ± 1.4	1.60 ± 0.12	2.04 ± 0.24	
23.04 ± 0.48	18.6 ± 1.3	1.60 ± 0.12	1.51 ± 0.23	13.7 ± 2.8
21.94 ± 0.51	17.9 ± 2.7	1.24 ± 0.10	1.09 ± 0.19	
21.75 ± 0.51	13.8 ± 1.0	1.17 ± 0.09	1.16 ± 0.24	12.9 ± 2.6
20.67 ± 0.51	10.3 ± 0.7	0.92 ± 0.07	0.75 ± 0.19	14.6 ± 2.9
19.31 ± 0.33	6.87 ± 0.49	0.58 ± 0.05	0.57 ± 0.18	15.1 ± 3.0
18.10 ± 0.54	4.89 ± 0.35	0.25 ± 0.03		
17.45 ± 0.54	4.64 ± 0.33	0.18 ± 0.02		16.6 ± 3.3
15.48 ± 0.57	3.42 ± 0.25			20.6 ± 4.1
14.67 ± 0.61	2.34 ± 0.17			
14.15 ± 0.60	2.49 ± 0.20			23.4 ± 4.6
12.77 ± 0.65	0.14 ± 0.02			
11.35 ± 0.66	0.53 ± 0.06			33.9 ± 6.7
9.82 ± 0.54	0.08 ± 0.01			
9.15 ± 0.74				
7.17 ± 0.86				
4.43 ± 0.97				
1.79 ± 1.11				

3.4.1 Production Cross-sections of ^{55}Co

With its relatively long half-life of $T_{1/2}$ =17.53 h, ^{55}Co was measured after a few hours of bombardment via its most distinct and abundant γ line of E_γ = 931.3 keV (I_γ = 75%). As shown in Table 3.2, two reaction channels are possible for the formation of ^{55}Co within the investigated energy region: the nuclear reaction processes via the ^{58}Ni(d,$n\alpha$)^{55}Co (E_{th}=3.694 MeV) and the possible contribution of ^{60}Ni(d,$3n\alpha$)^{55}Co reaction (E_{th}=24.75 MeV). The measured cross-sections are in agreement with some recently measured data (Amjed et al., 2013; Fuying et al., 1983; Hermanne et al., 2013; Ochiai et al., 2007; Takács et al., 2007), while a few earlier results show either large (Blann & Merkel, 1963) and slight (Cline, 1971; Zweit et al., 1991) discrepancies. The data reported by Cline (Cline, 1971) were scattered. Specifically, the excitation

functions reported by Amjed et al. (Amjed et al., 2013) appeared to be slightly lower above 18 MeV, while those by (Ochiai et al., 2007) are slightly higher in the same energy region. The experimental cross-sections show higher values when compared to the TENDL 2014 library particularly at 12 MeV and above.

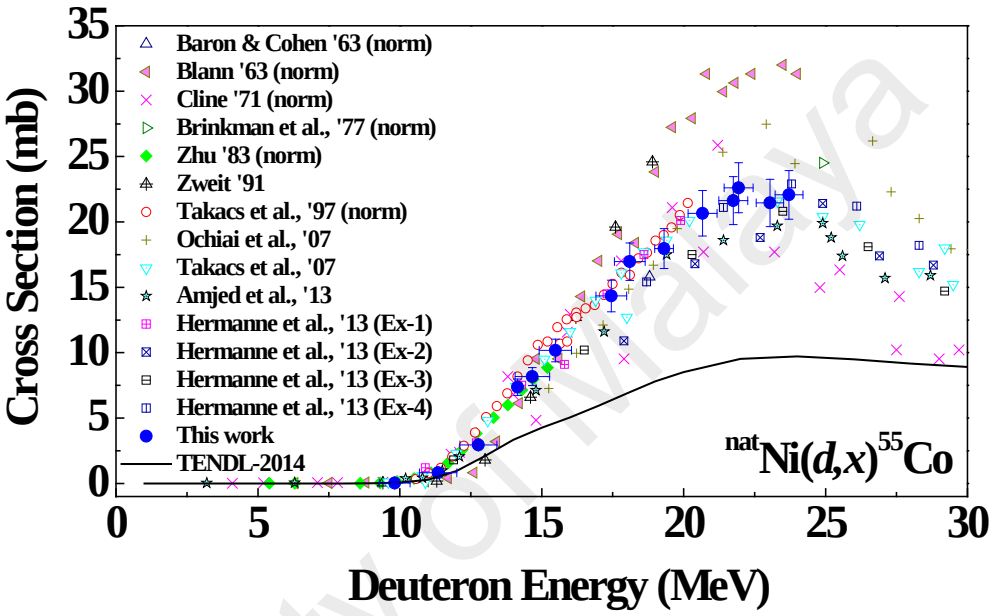

Figure 3.3: Excitation function of ^{nat}Ni(d,x)^{55}Co independent cross-sections

3.4.2 Production Cross-sections of ^{56}Co

The radionuclide ^{56}Co ($T_{1/2}$ = 77.27 d) can be measured from any of its four intense γ lines listed in the Table. 3.2 (E_γ = 846.770, 1037.843, 1238.288, and 1771.357 keV). Since ^{56}Co is formed by only the direct reactions of ^{58}Ni(d,α)^{56}Co (E_{th} = 0 MeV), ^{60}Ni(d,2$n\alpha$)^{56}Co (E_{th} = 14.33 MeV), and ^{61}Ni(d,3$n\alpha$)^{56}Co (E_{th} = 22.4 MeV), the measured cross-sections are independent. The measured excitation function shows clear discrepancies with the some previous measured cross-sections from Zweit et al. (Zweit et al., 1991) and Blann and Merkel (Blann & Merkel, 1963). Although the shape of the present excitation function is maintained by that of Takacs et. al., however, the cross-

sections reported by the Takacs et al. (Takács et al., 1997) presents somewhat higher magnitude as compared in the Figure below, especially around 10 MeV. The measured cross-sections agree well with the reported data by some other groups (Amjed et al., 2013; Fuying et al., 1983; Hermanne et al., 2013; Takács et al., 2007). The predictions of the TENDL-2014 library, on the other hand, presents lower values compared to the present measured cross-sections.

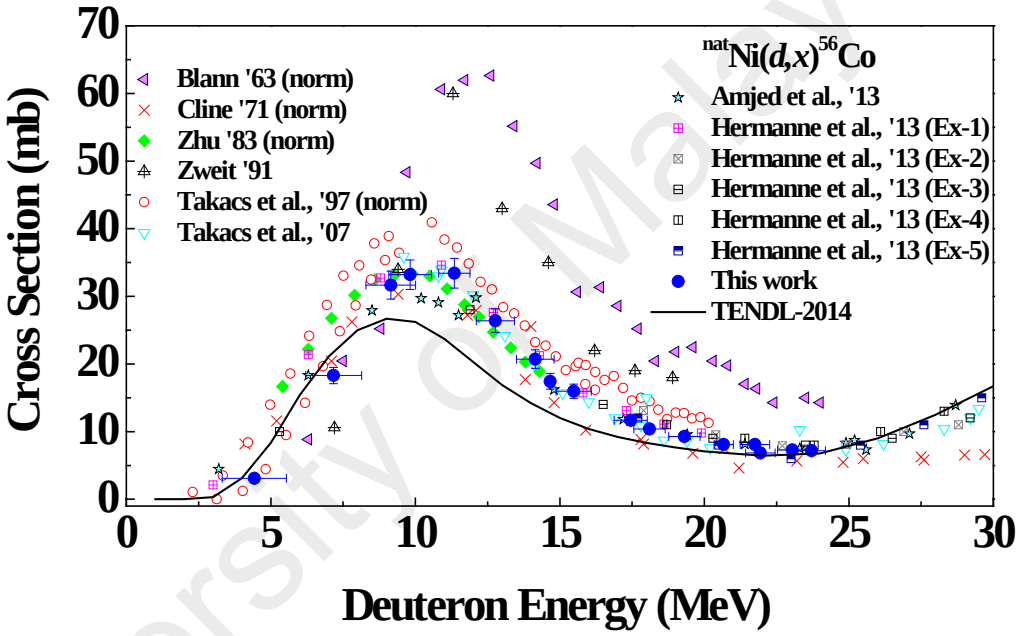

Figure 3.4: Excitation function of the ^{nat}Ni(d,x)^{56}Co reaction.

3.4.3 Production Cross-sections of ^{57}Co

^{57}Co was identified through one of its intense γ lines (E_γ = 122.1 keV). The cross-sections of the long-lived ^{57}Co ($T_{1/2}$ = 271.79 d) could be contributed by all the other stable nickel isotopes via the following direct reactions: ^{58}Ni(d,$n2p$)^{57}Co (E_{th} = 10.40 MeV), ^{60}Ni(d,$n\alpha$)^{57}Co (E_{th} = 2.75 MeV), ^{61}Ni(d,$2n\alpha$)^{57}Co (E_{th} = 10.65 MeV), and ^{62}Ni(d,$3n\alpha$)^{57}Co (E_{th} = 21.58 MeV). As a result of the indirect contribution to the formation of ^{57}Co through the ^{57}Ni ($T_{1/2}$ = 35.5 h) positron decay, the presented cross-

sections of this long-lived isotope (^{57}Co) are therefore cumulative. This is because the measurements of this radionuclide were made with a long cooling period after irradiation, long enough for this contribution to happen.

Eight previous investigations have been seen in the literatures (Amjed et al., 2013; Blann & Merkel, 1963; Cline, 1971; Hermanne et al., 2013; Ochiai et al., 2007; Takács et al., 1997; Takács et al., 2007; Zweit et al., 1991) and most of them agree with one another up to about 19 MeV. Beyond this region, Blann and Merkel (Blann & Merkel, 1963) presented relatively larger magnitude of the cross-sections while Cline (Cline, 1971) reported lower values in comparison with the present investigation. The present cross-sections of ^{57}Co indicate agreement with some other reported cross-sections (Amjed et al., 2013; Ochiai et al., 2007; Takács et al., 2007), even beyond the 19 MeV. On the other hand, the evaluated TENDL-2014 library data show higher cross-sections than those presented by the current experiment here, at 18 MeV and beyond.

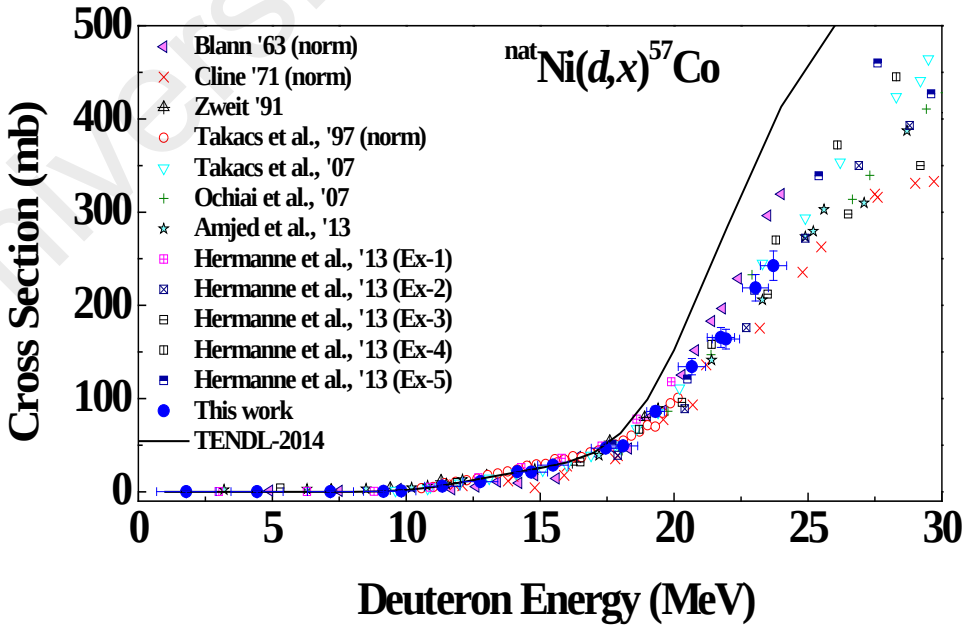

Figure 3.5: Excitation function of the ^{nat}Ni(d,x)^{57}Co reaction cross-sections.

3.4.4 Production Cross-sections of $^{58g+m}$Co

^{58}Co exist in states: the relatively short-lived metastable state ^{58m}Co ($T_{1/2}$ = 9.10 h, with low energy and low transition probability of E_γ = 25 keV, and I_γ = 0.04% respectively) which is known to decays through IT (100%) to the ground state, and the long-lived ground state, ^{58g}Co ($T_{1/2}$ = 70.86 d, E_γ = 810.7793 keV, with intensity, I_γ = 99.45%). Because of the extreme low gamma energy (25-keV) and intensity of the gamma line, the metastable state could not be measured under the experimental conditions of the present work. However, a long waiting time allowed ^{58m}Co to decay to ^{58g}Co, and thus the measured cross section of ^{58g}Co is the sum of the meta-stable and ground-states cross-sections, $^{58m+g}$Co. It is worth noting that there is likely an interference in the characteristic 810.7793-keV γ line of ^{58}Co by the characteristic 811.85-keV γ line of the simultaneously produced ^{56}Ni, which must be considered by correcting its measured photopeak area. In Fig. 3.6, the presents cross sections have been compared with the earlier experimental data as well as the evaluated data taken from the TENDL-2014 library. Most of the previous results, especially the data of (Amjed et al., 2013; Hermanne et al., 2013; Jung, 1992; Takács et al., 2007) show consistency with the present study via the observed relative similarity in magnitude and shape. On the other hand, the data presented by Cline (Cline, 1971) show the lower cross-sections at the peak energy region of the excitation function and looks scatted. Similarly the reported data by Zweit (Zweit et al., 1991) presented the lowest cross-sections especially from about 11 MeV and above. The extracted data of TENDL-2014 show rather higher values for $^{58g+m}$Co radionuclide as compared to the present experimental data, especially within the investigated energy region of 10 – 25 MeV.

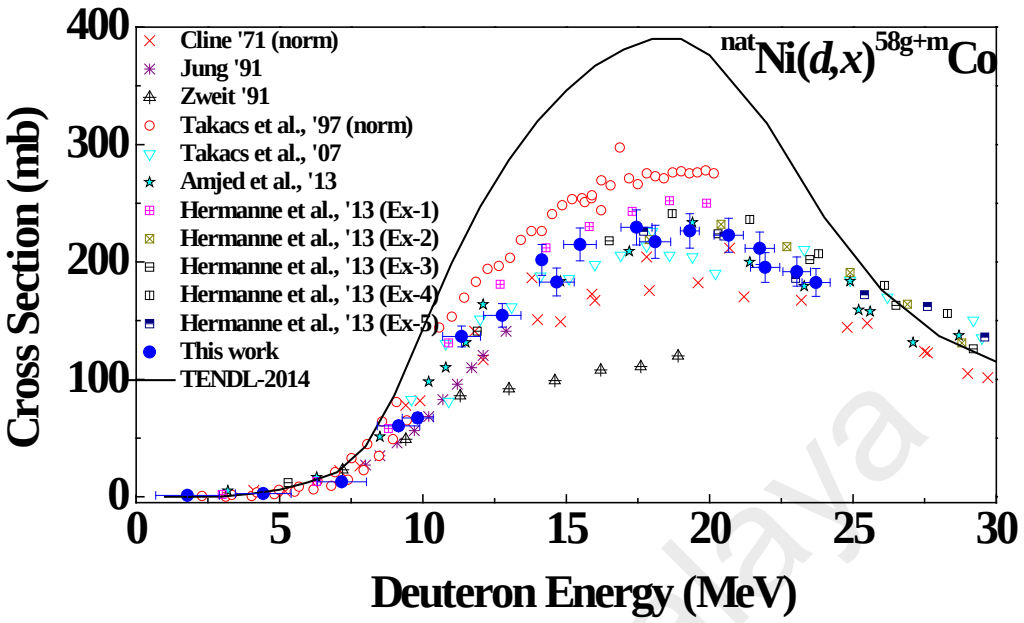

Figure 3.6: Excitation function of the ^{nat}Ni(d,x)$^{58g+m}$Co reaction cross-sections

3.4.5 Production Cross-sections of ^{60}Co

The cross-sections of the long-lived ^{60}Co ($T_{1/2}$ = 5.27 y) are normally be measured by either of its two abundant γ lines (E_γ =1173.228 keV and 1332.492 keV). Production cross-sections for ^{60}Co in the present study are cumulative due to the decay of its metastable state, ^{60m}Co ($T_{1/2}$ =10.467 min) via isomeric transition to the ground state (IT = 99.75%). To evaluate the cross-section of ^{60}Co, sufficient measurement time may be helpful due its long half-life. Only two earlier studies (Hermanne et al., 2013; Takács et al., 2007) reported the cross-sections of ^{60}Co, and they are inconsistent with each other as shown in Fig. 3.7. The present data are consistent to those reported by Hermanne exp. 2 and 4 (Hermanne et al., 2013). The TENDL-2014 library presented higher cross-sections than the present experimental measurements. A separate experiment based on the optimized experimental condition for ^{60}Co could help to measure a more consistent and reliable cross sections of the ^{nat}Ni(d,x)^{60}Co process.

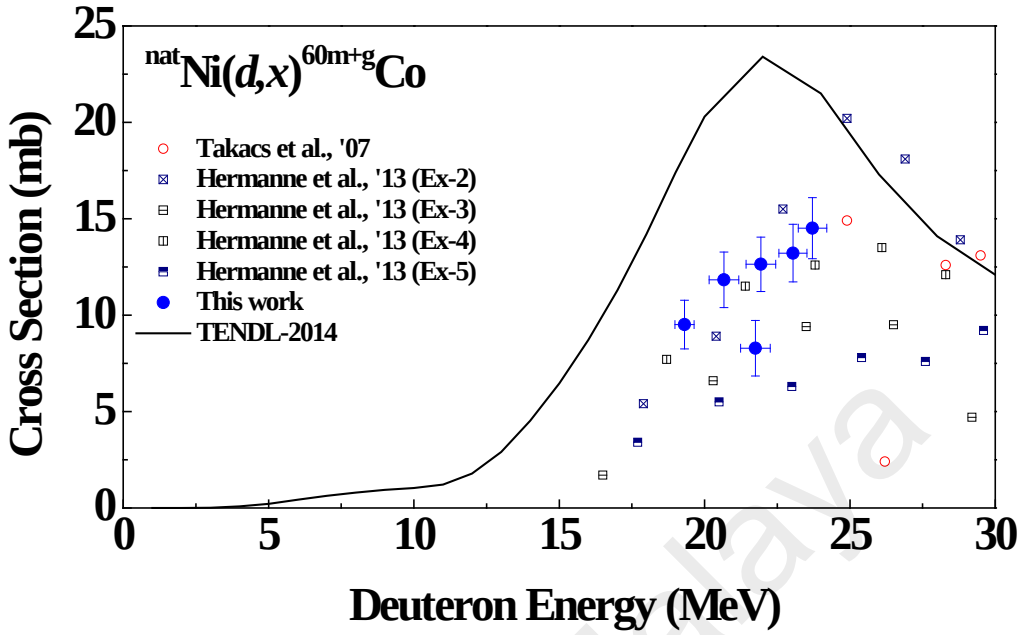

Figure 3.7: Excitation function of the ^{nat}Ni(d,x)$^{60g+m}$Co reaction cross-sections.

3.4.6 Production Cross-sections of ^{57}Ni

The ^{57}Ni cross-sections ($T_{1/2}$ = 35.6 h) presented here is independent. The cross-sections were mainly contributed by the ^{58}Ni(d,2np)^{57}Ni (E_{th} = 14.94 MeV) reaction within the investigated energy region. There may, however, be likely a contribution from an EC decay of the short-lived meta-stable state ^{57}Cu ($T_{1/2}$ = 196.4 min) via the ^{58}Ni(d,3n)^{57}Cu (E_{th} = 24.8 MeV) reaction toward the maximum of the energy interval used. Identification and analysis of ^{57}Ni were aided by its strong (E_γ = 1377.63 keV; I_γ = 81.7%) and weak (E_γ = 127.16 keV; I_γ = 16.7%) γ lines. The measured excitation function shows a excellent agreement with the earlier ones (Amjed et al., 2013; Hermanne et al., 2013; Takács et al., 1997; Takács et al., 2007). There exist, however, an obvious disagreement with the reported data (Cogneau et al., 1967; Fuying et al., 1983). The data reported here is scanty because, the nearest possible contribution reaction threshold is about 15 MeV within the energy interval considered, thereby

limiting the number of contributing reactions. The obtained cross-sections generally show a good agreement with the data extracted from the TENDL-2014 library.

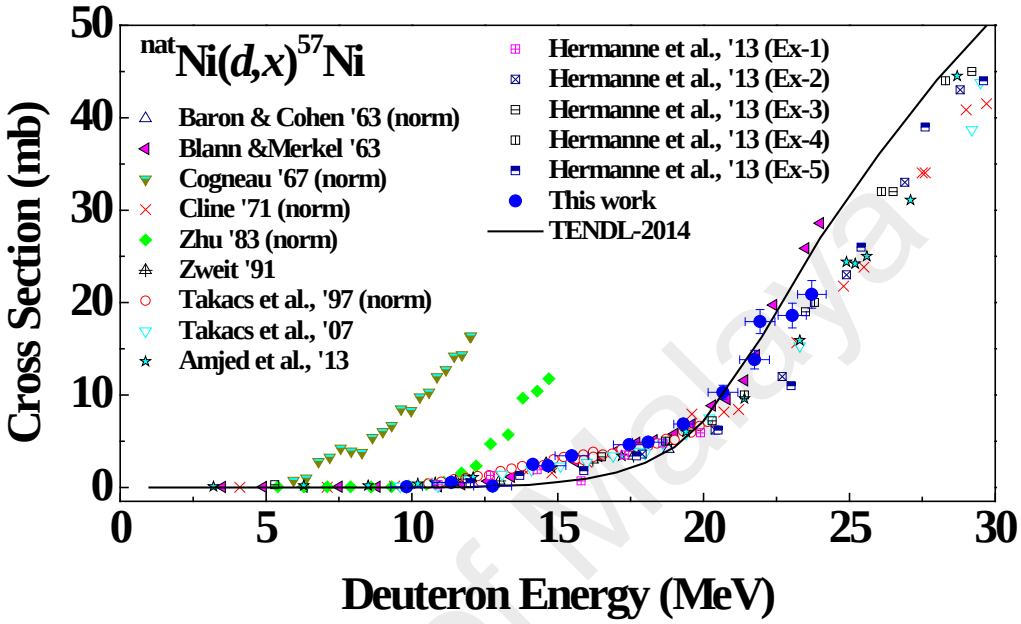

Figure 3.8: Excitation function of the ^{nat}Ni(d,x)^{57}Ni independent reaction.

3.4.7 Production Cross-sections of ^{52}Mn

Since the measurements considered for this radionuclide was about four days after bombardment, the meta-stable state of ^{52m}Mn ($T_{1/2}$ = 21.1 min) was not detected. The present study was, therefore, interested in the ground state of ^{52g}Mn ($T_{1/2}$ = 5.59 d; decay 100% by the β^- particle). ^{52g}Mn was produced most likely by the ^{58}Ni(d,2α)^{52}Mn and ^{60}Ni(d,2α2n)^{52}Mn reactions. The present calculations were made using the strongest 935.544-keV (I_γ = 94.5%) γ line of ^{52}Mn except for some special cases where other γ line in Table 3.2 was used. The present results are presented in Fig. 3.9 together with some prior experimental studies (Amjed et al., 2013; Cline, 1971; Hermanne et al., 2013; Takács et al., 2007) and the theoretical data taken from the TENDL-2014 library. The cross-sections presented here agree with some earlier reported experimental values

(Amjed et al., 2013; Hermanne et al., 2013; Takács et al., 2007) within the considered energy interval of this study. The cross-sections reported by Cline (Cline, 1971) were found to be slightly higher and scattered near the upper energy region. Figure 3.9 below indicates that the TENDL-2014 library data could not reproduce the present experimental data correctly, possibly due to its shortcomings when predicting composite particle emission phenomena. The predicted TENDL-library data thus, show lower cross sections as compared to the present measured cross-sections.

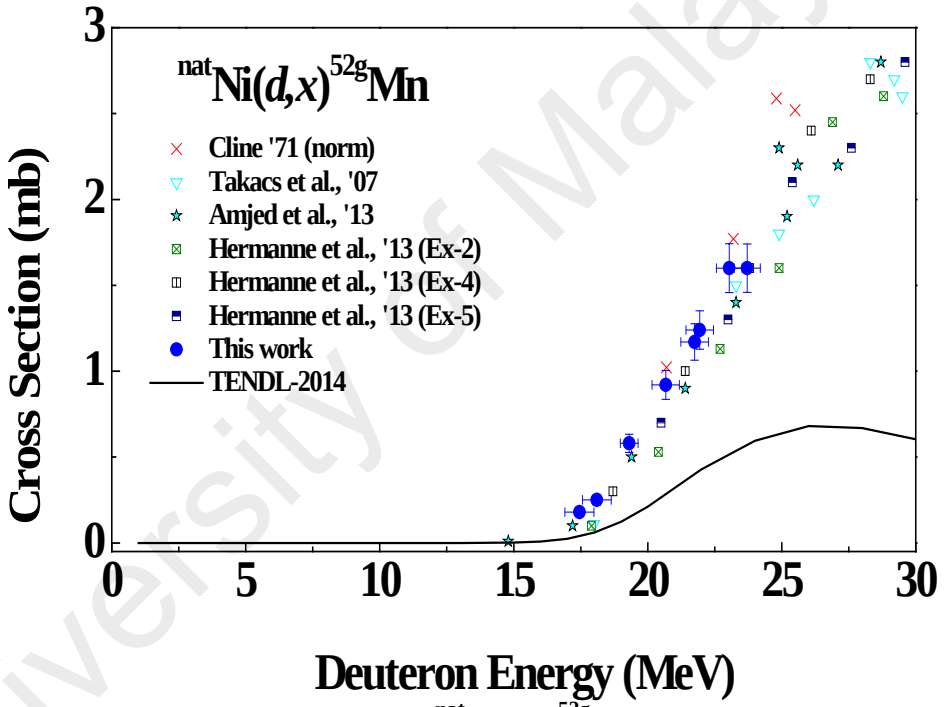

Figure 3.9: Excitation function of the ^{nat}Ni(d,x)^{52g}Mn cumulative reaction cross-sections.

3.4.8 Production Cross-sections of ^{54}Mn

^{54}Mn ($T_{1/2}$ = 312.3 d) has a very strong and high-intensity γ line of E_γ = 834.848 keV (I_γ = 99.9760%) which was used for identification and radioactivity assessment of this isotope. The possible reactions to form ^{54}Mn are ^{58}Ni(d,2$p\alpha$)^{52}Mn (E_{th} = 8.84 MeV), ^{60}Ni(d,2α)^{52}Mn (E_{th} = 0.65 MeV), ^{61}Ni(d,n2α)^{52}Mn (E_{th} = 8.75 MeV) and ^{62}Ni(d,2n2α)^{52}Mn (E_{th} = 19.67 MeV) within the investigated energy region. Amid

some possible reaction channels to produce this radioisotope, such that the emission of some combinations of single and composite particles are much likely to occur, the excitation curve gives one simple rising shape beginning from 20 MeV and continues under the investigated energy region. Present measured cross sections are compared in Fig. 3.10 together with four earlier investigations (Amjed et al., 2013; Cline, 1971; Hermanne et al., 2013; Takács et al., 2007) and the TENDL-2014 library. While the observed shape of the measured excitation function confirmed an overall agreement of this study to the earlier reported results, but Hermanne Exp.-2 (Hermanne et al., 2013) and Cline (Cline, 1971) cross sections presents slightly lower cross-sections within the investigated energy region. The TENDL-2014 predicts the shape of the measured excitation function rather well, except for the slightly lower absolute values.

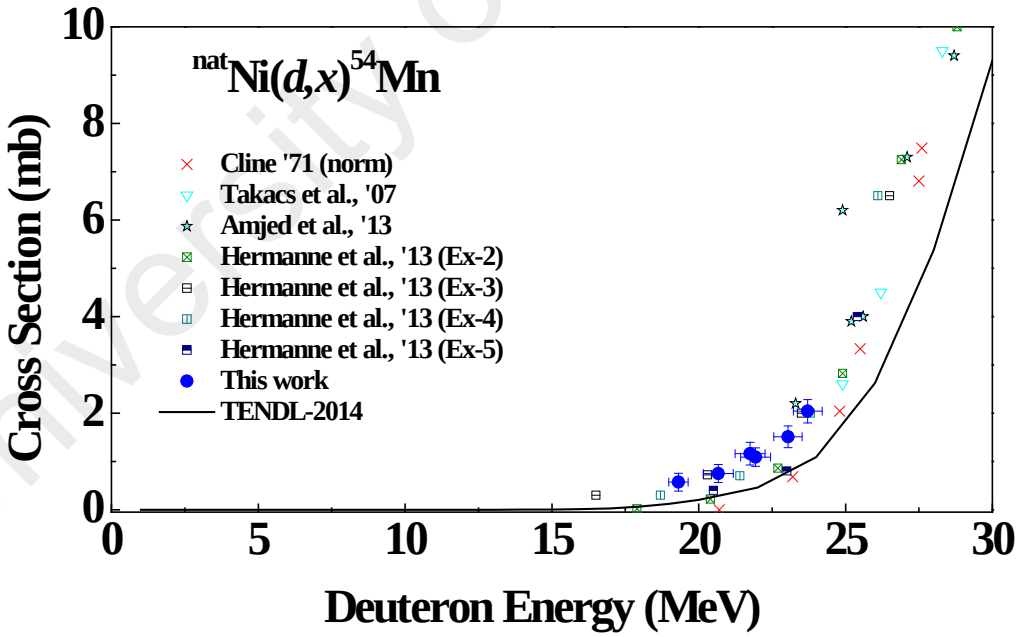

Figure 3.10: Excitation function of the $^{nat}Ni(d,x)^{54}Mn$ independent reaction cross-sections.

3.4.9 Production Cross-sections of ^{61}Cu

Sd ^{61}Cu ($T_{1/2}$ = 3.333 h) was measured via its γ line E_γ = 656.008 keV (I_γ = 10.8%). ^{61}Cu has a half-life of $T_{1/2}$ = 3.333 h and decays to ^{61}Ni. The major contribution reaction for the production of ^{61}Cu is ^{60}Ni(d,n)^{61}Cu (Q- value = +2.58 MeV) as a result of little abundance of other stable Ni isotopes with higher mass numbers. Since the target foils were measured about 2 to 3 half-lives after the bombardment, in the first target stack and much later in the second stack, the cross-sections for ^{61}Cu of the second stack were accompanied with large errors, necessitating the exclusion of the data from the stack in the reported cross-sections of this study. There exist 10 earlier measurements on the production cross sections of ^{61}Cu (Budzanowski et al., 1963; Coetzee & Peisach, 1972; Cogneau et al., 1967; Hermanne et al., 2013; Hermanne et al., 2007; Ochiai et al., 2007; Takacs et al., 1997; Takács et al., 2001; Takács et al., 2007; Zweit et al., 1991). As shown in the Fig. 3.11, the cross-sections of (Zweit et al., 1991) and (Cogneau et al., 1967) are larger than the present data and other earlier data at around 5 to 12 MeV. Other experimental data agree with each other. The TENDL-2014 library reproduces the shape of the excitation function but slightly underestimates the absolute values above 7 MeV. The (Takács et al., 2007) proposed a renormalization of their cross-sections in (Takács et al., 1997) by a factor of 1/1.18. However, present work found that the IAEA-recommended cross-sections (IAEA, 2007) reproduce the original ones (Takács et al., 1997) before the renormalization. Furthermore, the IAEA-recommended cross-sections overestimate the recent experimental cross-sections (Hermanne et al., 2013; Hermanne et al., 2007; Takács et al., 2007) at the peak region around 7 MeV. Therefore, upgrade of the recommended cross-sections must be considered.

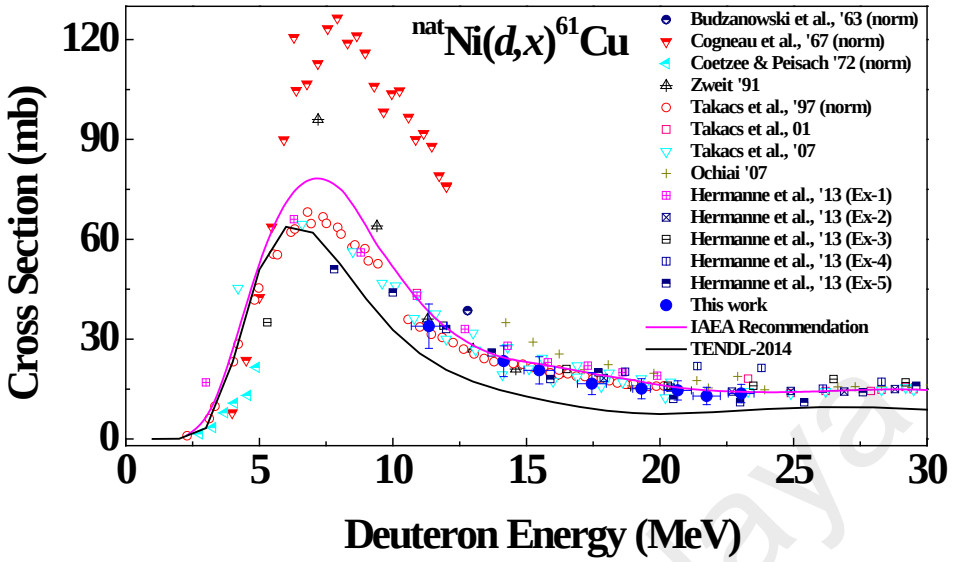

Figure 3.11: Excitation function of the ^{nat}Ni(d,x)^{61}Cu independent cross-sections.

3.5 Integral Thick Target Yield

The integral thick target yields for ^{55}Co, ^{57}Co, and ^{58}Co radionuclides have been calculated and compared with the previous calculations by Amjed (Amjed et al., 2013). The numeral values of the calculated thick target yields, at some selected higher energy portion of the investigated energy region, are presented in Table 3.6. The calculated values also presented together with the literature values in Figure 3.12. Among the calculated TTYs, the ^{55}Co radionuclide has the highest (15.6 MBq/μA-hr) at 23.7 MeV while 57Co has the least value (3.2 MBq/μA-hr) at the same energy. The calculated values have been compared with the literature values calculated by Amjed group (Amjed et al., 2013). The present calculated yields of ^{55}Co are very comparable to the value reported by Amjed et al. (2013) at the same energy region. On the other hand, the present calculated values for ^{58}Co are higher than the corresponding value reported by the same authors (Amjed et al., 2013).

Table 3.6: Integral Thick Target Yields, TTY (MBq/μA-hr) for ^{55}Co, ^{57}Co and ^{58}Co radionuclides

En(MeV)	^{55}Co	^{57}Co	^{58}Co
	TTY (MBq/μA-hr)	TTY (MBq/μA-hr)	TTY (MBq/μA-hr)
15.5	2.0	0.2	2.5
17.5	4.2	0.4	3.6
18.1	5.1	0.5	4.0
19.3	6.9	0.8	4.7
20.7	9.4	1.3	5.6
21.8	11.5	1.9	6.3
21.9	11.9	1.9	6.4
23.0	14.1	2.7	7.0
23.7	15.6	3.2	7.4

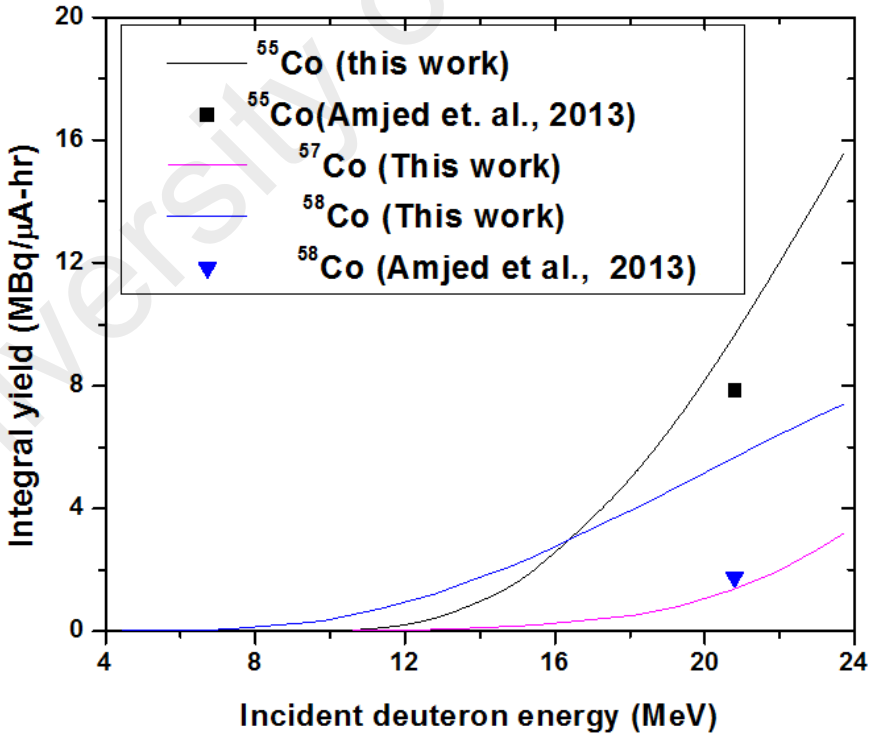

Figure 3.12: Integral thick target yields for ^{55}Co, ^{57}Co and ^{58}Co radionuclides

3.6 Conclusion

The present studies present new experimental cross-sections on the nuclear processes of $^{nat}Ni(d,x)^{55-58,60}Co$, ^{57}Ni $^{52,54}Mn$ and ^{61}Cu within the deuteron energy 1.79 – 24 MeV. The measured excitation functions were compared with the earlier experimental data as well as the extracted theoretical data from TENDL-2014 library. The presents newly measured cross-sections enriched the current database and further confirmed some of the earlier reported measurements with added insights. Some of the literature data reported much earlier showed larger discrepancies to the present cross-sections. Some discrepancies (either in amplitude difference or energy shift etc.) between the experiments and the TENDL-2014 library are found for several reaction cross-sections, especially for $^{55,57,58,60}Co$ and ^{52}Mn. Therefore, in addition to previous measurements, the present result could play a major role for improvements of the TALYS code.

On the production of ^{60}Co, the EXFOR library indicated an extensive report on the experimental production of this radionuclide via proton and neutron bombardments in contrast via deuteron. Since the production of ^{60}Co radionuclide is possible via deuteron beam bombardment on Ni, the present study, therefore, recommends further enrichment of the EXFOR database on the production of ^{60}Co radionuclide via this production route, with more dedicated experimental conditions such as a sufficient irradiation time, cooling period and periodic measurements. These would reduce the observed discrepancies and in turn, a better understanding of its excitation function. On the other hand, the excellent shapes of the excitation functions observed from some of the cobalt radionuclides show greater reliance of their cross-sections at different intermittent energies. Thus, the measured cross-sections (also influenced by the decay characteristics) of some cobalt radionuclides, $^{56-58}Co$ could be considered as possible candidates for the beam monitoring in deuteron bombardments. Present study observed

also that the $^{nat}Ni(d,x)^{61}Cu$ cross-sections recommended by the IAEA overestimate the recent measured data, and their upgrade must be considered.

CHAPTER 4: EXCITATION FUNCTIONS OF ALPHA-INDUCED REACTIONS ON NATURAL TITANIUM UP TO 50.2 MEV

4.1 Introduction

This chapter presents the experimental procedures and results obtained from the bombardment of natural titanium metal by 50.4 MeV alpha beam. One of the main purposes of using titanium in the stack was for beam monitoring purpose via ^{nat}Ti(a,x)^{51}Cr monitor reaction recommended by IAEA. However, titanium as a target also serves as an important source of several radionuclides with potential applications in nuclear medicine and other various scientific usage. For this reason, therefore, an extensive analysis of the measured activities of titanium after bombardment are paramount so as to explore these radionuclides, especially that there has been some recent increasing interest in several radioisotopes of scandium.

Efforts have been made to report several radionuclides and their respective excitation functions. To this end, some chromium and potassium radionuclides have been investigated and reported. The chapter also reported some scandium radionuclides of reported significance in the literature. The thick target yields of the investigated radionuclides have been calculated and plotted, together with some previous literature data, in some Figures of this chapter.

4.2 Literature Review

Applications of some radionuclides such as ^{131}I and ^{99m}Tc in diagnostic procedures and treatments of ailments are well established. Advancement in nuclear technology provides the basis for the production of many potential radionuclides that can reduce additional dose to patients and produce better images of tissues during medical procedures. Cyclotron-based radionuclides production is one of the most sophisticated

technologies that allow producing a range of potential radionuclides to be used in the medical field.

Titanium (Ti) shows various applications due to its desirable physical and chemical characteristics. Charged particle irradiation of metallic titanium is an important production pathway of some few vital radionuclides of technological and medical applications. As an example, the relatively long-lived ^{47}Sc ($T_{1/2}$ = 3.3492 d) is a potential radionuclide for radiotherapy whereas ^{43}Sc and ^{44}Sc are good candidates for PET imaging (Duchemin et al., 2015). The ^{44m}Sc radionuclide attracts interest to many researchers as its relatively long half-life ($T_{1/2}$ = 58.61 h) allows ample time in imaging and thus greater accuracy in assessment of distribution and absorbed doses to an affected organ (Alliot et al., 2015). Also, the emission of a low energy gamma-ray of ^{47}Sc (E_γ = 159.381 keV, I_γ = 68.3%) made it suitable for *in vivo* studies targeted imaging, documenting of a status of a disease or even therapeutic efficacy (Mamtimin et al., 2015). Due to the suitable decay characteristics, ^{46g}Sc ($T_{1/2}$ = 83.79 d; E_γ = 889.277 keV, I_γ = 99.9840%; E_γ = 1120.545 keV, I_γ = 99.987%) could be used in monitoring of medium energy alpha beam (Hermanne et al., 2014). The increasing explorations of more applications of scandium radionuclides go in phase with the continuous search for alternative production routes. Recently, some groups have reported such alternative production pathways with a sole aim of production improvement or reduction in the cost of production (Deilami-nezhad et al., 2016; Hoehr et al., 2014; Szkliniarz et al., 2016; Valdovinos et al., 2015; van der Meulen et al., 2015).

Apart from this, the ^{48}V has been found suitable as a diagnostic agent in life-science (Xuan Tham et al., 2001) and material (Rorat et al., 2005) studies, as well as for therapeutic functions during renal artery brachytherapy (Arbabi et al., 2009). Moreover, the ^{48}V have also been reported to exhibit some very useful biochemical characteristics

like its anti-carcinogenic effect, and thus became a good candidate for labelling compounds for *in vivo* studies (De Cremer et al., 2002). Also, a study searching an alternative radionuclide to the conventional use of ^{68}Ge ($T_{1/2}$ =271 d) in PET for improvement of the quality of images has prioritised the use of ^{48}V as a transmission source for correction of attenuation in PET (Hichwa et al., 1995). On the other hand, ^{51}Cr draws special attention to monitoring alpha particles beams due to its excellent decay characteristics and fine shape of its excitation function (IAEA, 2007). The ^{51}Cr is also used to label red blood cells for measurements of mass and volume of blood (Al-Abyad et al., 2010; Vimalnath et al., 2014). It is also useful in labelling platelets to determine their survival period as well as in diagnosis of gastrointestinal bleeding through sequestration studies (Vimalnath et al., 2014). In the same way, studies of ^{48}Cr cross-sections are of interest due to its consideration as a substitute for the medically important ^{51}Cr radionuclide (Weinreich et al., 1980).

A detailed survey of the literature revealed that production cross-sections of residual radionuclides, especially ^{43,44m,44g}Sc, were extensively reported via proton and deuteron irradiations on titanium targets but scarcely reported via alpha irradiation. Furthermore, the available literature data for the chromium radionuclides via the (α,x) reactions show significant discrepancies among them. Recognising the aforementioned drawbacks, this thesis aimed to minimise or remove the existing discrepancies for the Cr radionuclides, and also reports new cross-sections for the scandium and other useful radionuclides via the (α,x) nuclear processes.

4.3 Materials and Method

Based on some previous basic experimental procedures (Khandaker et al., 2015; Khandaker et al., 2014; Khandaker et al., 2011; Usman et al., 2016a), the well-established stacked-foil activation technique and an offline HPGe γ-ray spectrometry

were employed for the determinations of the production cross-sections. The excitation functions of several radionuclides with half-lives of more than 30 min have been studied herein, and details of the experimental procedure are given below.

4.3.1 Targets, Stack Formation and Bombardment

A metallic Ti foil (purity: >99.6%, nominal thickness: 10.40 μm, supplier: Goodfellow, UK) with natural isotopic abundances (^{46}Ti: 8.25%; ^{47}Ti: 7.44%; ^{48}Ti: 73.72%; ^{49}Ti: 5.41%; ^{50}Ti: 5.18%) (Berglund & Wieser, 2011) was used as a target material. For degradation of the beam energy, several other natural metallic foils of Cu (purity: 99.9%, nominal thickness: 9.71 μm, supplier: Nilaco, Japan) and Ho (purity: 99%, nominal thickness: 12.29 μm, supplier: Goodfellow, UK) were inserted in between the Ti foils in the stack. The stack was arranged such that the Ho foils succeeding the Ti foils also served as recoil catcher. All used foils were weighed using a high precision electronic balance for an accurate thickness determination. The stack was prepared as the same foil area of 15 × 15 mm^2 following the dimension of the target holder, which ensured the focusing of the incident beam to the centre of all foils in the stack. The irradiation of the stacked samples was performed using the beam line of the AVF cyclotron of the RI Beam Factory, Nishina Centre for Accelerator-Based Science, RIKEN, Japan. Through a tantalum slit in the particle exit channel of the cyclotron, the beam was collimated to 9-mm diameter onto the target foils. The stacked samples were mounted on a water-cooled target holder, which serves as a Faraday cup, and then bombarded for 2.0 h using the 50.4 MeV α beam with an average beam current of 194 nA. The 50.4 MeV initial alpha beam energy of the RIKEN AVF cyclotron was determined by a recent precise measurement using time of flight (TOF) measurement system (Watanabe et al., 2014), with reported spread and uncertainty as 0.28% (±0.14

MeV) and 0.24% (±0.12 MeV), respectively. Thus, the initial beam energy is considered as 50.4±0.2 MeV.

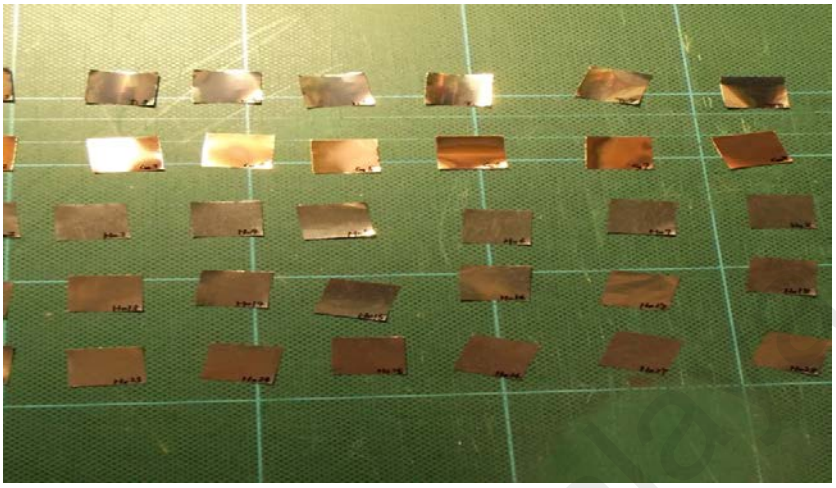

Figure 4.1: Sample of target cutting and preparation

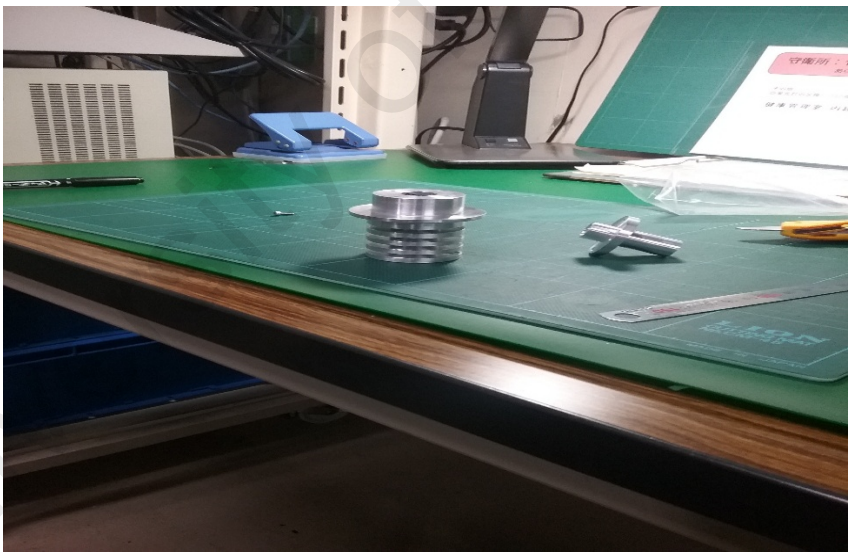

Figure 4.2: The target holder for irradiating the prepared foils.

4.3.2 Spectrometry of Activation Products

After the irradiation, the activated foils were dismantled from the target holder and taken to an offline gamma ray spectrometry laboratory for activity measurements. The emitted γ-rays were measured non-destructively with a high resolution HPGe γ-ray spectrometer (ORTEC; GEM-25185P; 55.1-mm crystal diameter and 52.0-mm thickness; operating voltage: +2000 V; relative efficiency: 25%) which was coupled to a 4096-multi-channel analyser and other associated electronics. Since the half-lives of the studied radionuclides vary from few minutes to tens of days, the activity measurements were repeatedly continued for several days after the end of irradiation (EOI) to ensure optimum counting with reduced dead times. Accurate activity measurements of various short and long-lived radionuclides were ascertained through progressive reduction of source-to-detector distances from 15 cm down to 1 cm. However, to minimise pile-up effect and coincidence loss, a 3-cm minimum source-to-detector distance was considered during the activity measurements of longer-lived radionuclides. Similarly, all measurements were done with dead times less than 10% by adjusting the source-to-detector distances. The first measurement was started about 3.6 hours after the EOI and was continuously repeated to follow the decay of the produced radionuclides. Table 4.1 shows the details of the measurement periods for each assessed radionuclide. The gamma spectrum analysis was performed using the Maestro (Ver. 7.01; ORTEC) gamma vision program (Ortec, 2012).

Table 4.1: Cooling periods for the accessed radionuclides

Measurement series	Cooling period	Radionuclide
I	3.6 - 4.2 h	^{49}Cr, ^{43}Sc and ^{44g}Sc
III	15.8 - 17.0 h	^{48}Cr
IV	1.7 - 1.8 d	^{48}Sc, ^{44m}Sc
V	7.3 - 7.5 d	^{51}Cr, ^{48}V, ^{46}Sc and ^{47}Sc

The detector efficiencies at various source-to-detector distances were determined with a standard multi-nuclide γ-ray source from DBA Isotopes Products Laboratories (USA). Details of complete procedure of the calculations of these efficiencies at various source-to-detector-distances were reported in chapter five and in (Usman et al., 2016b).

4.3.3 Determination of Beam Intensity, Foil Energies and Cross-sections

The beam intensity was calculated by placing a Ti foil at the front position of the stack so as to receive the initial alpha energy delivered by the cyclotron. The IAEA recommended ^{nat}Ti(α,x)^{51}Cr monitor reaction (σ = 26.4 mb at E_α = 50 MeV) and the corresponding counts of ^{51}Cr from the first Ti foil (E_α = 50.16) MeV) were used to determine the α beam intensity (Qaim et al., 2002). The intensity was considered as a constant in the stack and was used to deduce cross-sections for each foil in the stack. The uniformity of the beam intensity along the stack was confirmed by obtaining the cross-sections of ^{51}Cr from the activities of all Ti foils in the stack and then comparing the cross-sections with the ^{nat}Ti(α,x)^{51}Cr cross sections recommended by the IAEA (Qaim et al., 2002). The use of other metallic foils of different densities and thicknesses helped in slowing down the incident alpha beam along the stack. The SRIM-2003 (Ziegler, 2004) computer program was used for the calculation of the degradation of initial incident 50.4 MeV alpha beam energy along the stacked foils, without any further adjustment (correction) of the energy for the fitting of the recommended cross-section.

The average (incident) alpha-energy on each foil has been reported as the representative energy value for the foils during the calculation of the cross-sections.

The cross-sections for the assessed radionuclide $\sigma(E_i)$ were computed using the well-known activation formula (Khandaker et al., 2010; Khandaker et al., 2011; Usman et al., 2016b):

$$\sigma\,(E_i) = \frac{\lambda C(E_i)}{\varepsilon_\gamma I_\gamma t_h \rho \varphi (1- e^{-\lambda t_{\mathrm{irr}}})(e^{-\lambda t_{\mathrm{coo}}})(1- e^{-\lambda t_{\mathrm{mea}}})}, \qquad (4.1)$$

where λ is the decay constant of the radionuclide, $C(E_i)$ represent the net counts of the characteristic gamma-lines of the radionuclide under the photo-peak area at the i-th foil, ε_γ stands for the efficiency of detection for the gamma-line at a particular source-to-detector distance, I_γ is the emission probability of the gamma-line, t_h is the thickness of the Ti foil while ρ is the atomic density of the Ti foil (5.71×10^{22} atoms/cm^3). Other symbols in the equation are φ for the intensity of the α beam (5.45×10^{11} particle/s), whereas t_{irr}, t_{coo} and t_{mea} are irradiation, cooling and measurement times, respectively.

The adopted decay data of the investigated reaction products were from the ENSDF library (Burrows, 2006, 2007, 2008; Chen et al., 2011; Singh & Chen, 2015; Wu, 2000; Xiaolong, 2006) and retrieved via the interface of Live Chart of Nuclides (IAEA, 2009b). The Q-values and threshold energies were calculated based on the AME mass evaluation (Audi et al., 2003), assessed through the Q-tool system (Qtool, 2011), and they are also presented in Table 4.2. In the table, symbol ε stands for EC and β^+ decay while the italicised numbers refer to the last digits of the value (e.g., 99.9840 *10* means 99.9840±0.0010).

Table 4.2: Adopted decay data for the assessed radionuclides based on the decay data evaluated in the ENSDF library*

Nuclide	Half-life	Decay mode (%)	E_γ (keV)	I_γ (%)	Contributing reactions	Q-Value (MeV)	Threshold (MeV)
^{51}Cr	27.7010 d	ε:100	**320.0824**	**9.910 *10***	^{47}Ti(α,γ)^{51}Cr	8.94	0.00
					^{48}Ti(α,n)^{51}Cr	-2.69	2.911
					^{49}Ti(α,2n)^{51}Cr	-10.83	11.71
					^{50}Ti(α,3n)^{51}Cr	-21.77	23.51
^{49}Cr	42.3 m	ε:100	62.289	16.4 *6*	^{46}Ti(α,n)^{49}Cr	-4.44	4.83
			90.639	**53.2 *19***	^{47}Ti(α,2n)^{49}Cr	-13.32	14.46
			152.928	30.3 *11*	^{48}Ti(α,3n)^{49}Cr	-24.95	27.03
					^{49}Ti(α,4n)^{49}Cr	-33.09	35.80
					^{50}Ti(α,5n)^{49}Cr	-44.03	47.56
^{48}Cr	21.56 h	ε:100	112.31	96.0 *20*	^{46}Ti(α,2n)^{48}Cr	-15.02	16.33
			308.24	**100.0 *20***	^{47}Ti(α,3n)^{48}Cr	-23.90	25.94
					^{48}Ti(α,4n)^{48}Cr	-35.53	38.50
					^{49}Ti(α,5n)^{48}Cr	-43.67	47.24
^{48}V	15.9735 d	ε:100	**944.130**	**7.870 *7***	^{46}Ti(α,d)^{48}V	-10.36	11.26
			983.525	99.98 *4*	^{47}Ti(α,t)^{48}V	-12.98	14.09
			1312.106	98.2 3	^{48}Ti(α,d2n)^{48}V	-30.87	33.45
					^{49}Ti(α,d3n)^{48}V	-39.01	42.20
					EC (100%) decay of ^{48}Cr		
^{43}K	22.3 h		**372.760**	**86.80 *20***	^{46}Ti(α,α3p)^{43}K	-29.42	31.98
			617.490	**79.2 *6***	^{47}Ti(α,p^{3}Heα)^{43}K	-30.58	33.19
					^{48}Ti(α,p2α)^{43}K	-21.63	23.44
					^{49}Ti(α,d2α)^{43}K	-27.55	29.80
					^{50}Ti(α,t2α)^{43}K	-32.23	34.81

*See Table 4.3

Table 4.3: Adopted decay data for the assessed scandium radionuclides based on the decay data evaluated in the ENSDF library*

Nuclide	Half-life	Decay mode (%)	E_γ (keV)	I_γ (%)	Contributing reactions	Q-Value (MeV)	Threshold (MeV)
^{43}Sc	3.891 h	ε: 100	**372.9**	**22.5** ***7***	^{46}Ti(α,ndα)^{43}Sc	-29.15	31.68
					^{47}Ti(α,dα2n)^{43}Sc	-38.03	41.27
					^{48}Ti(α,tα2n)^{43}Sc	-43.40	47.02
					EC and β^+ (100%) decay of ^{43}Ti		
^{44m}Sc	58.61 h	IT: 98.80	**271.241**	**86.7** ***3***	^{46}Ti(α,dα)^{44}Sc	-19.72	21.41
		ε: 1.20	1157.002	1.20	^{47}Ti(α,ndα)^{44}Sc	-28.60	31.01
					^{48}Ti(α,dα2n)^{44}Sc	-40.22	43.56
					^{49}Ti(α,tα2n)^{44}Sc	-42.10	45.53
^{44g}Sc	3.97 h	ε: 100	**1157.020**	**99.9** ***4***	^{46}Ti(α,dα)^{44}Sc	-19.45	21.14
					^{47}Ti(α,ndα)^{44}Sc	-28.33	30.74
					^{48}Ti(α,dα2n)^{44}Sc	-39.95	43.29
					^{49}Ti(α,tα2n)^{44}Sc	-41.83	45.26
					IT decay (98.80%) of ^{44m}Sc (58.61 h)		
^{46g}Sc	83.79 d	β^-: 100	**889.277**	**99.9840** ***10***	^{47}Ti(α,pα)^{46}Sc	-10.47	11.36
			1120.545	99.987 10	^{48}Ti(α,dα)^{46}Sc	-19.87	21.53
					^{49}Ti(α,ndα)^{46}Sc	-28.01	30.30
					^{50}Ti(α,dα2n)^{46}Sc	-38.95	42.07
					IT decay (100%) of ^{46m}Sc (18.75 s)		
^{47}Sc	3.3492 d	β^-: 100	**159.381**	**68.3** ***4***	^{46}Ti(α,3p)^{47}Sc	-19.23	20.91
					^{47}Ti(α,p^{3}He)^{47}Sc	-20.39	22.13
					^{47}Ti(α,d2p)^{47}Sc	-25.89	28.10
					^{48}Ti(α,pα)^{47}Sc	-11.44	12.40
					^{49}Ti(α,dα)^{47}Sc	-17.36	18.78
					^{50}Ti(α,ndα)^{47}Sc	-28.30	30.57
^{48}Sc	43.67 h	β^-: 100	175.361	7.48 *10*	^{47}Ti(α,3p)^{48}Sc	-19.88	21.57
			983.526	100.1 *6*	^{48}Ti(α,d2p)^{48}Sc	-29.28	31.72
			1037.522	**97.6** ***7***	^{49}Ti(α,pα)^{48}Sc	-11.35	12.28
			1312.120	100.1 *7*	^{50}Ti(α,dα)^{48}Sc	-20.06	21.67

ENSDF library*(Burrows, 2006, 2007, 2008; Chen et al., 2011; Singh & Chen, 2015; Wu, 2000; Xiaolong, 2006) as extracted from the interface of Live Chart of Nuclides of the IAEA (IAEA, 2009b) while the threshold energies and Q-values (Audi et al., 2003) were retrieved through the Qtool system (Qtool, 2011). The symbol ε stands for EC and/or β^+ decay. The italicised numbers refer to the last digits of the value (e.g., 99.9840 *10* means 99.9840±0.0010).

4.3.4 General Evaluation of Uncertainties

The uncertainties on cross-sections were evaluated in the standard error propagation approach. From the following quadrature equation, the uncertainties in the cross-sections were evaluated based on various relative independent sources following the experimental conditions of this work. The fractional uncertainties were thus analysed and quadratically summed to obtain cumulative uncertainties, and they are presented together with the cross-sections in Table 4.5 and 4.6 and Figs. 4.4 – 4.14 of this chapter.

$$\left(\frac{\Delta\sigma\,(E_i)}{\sigma}\right)^2 = \left(\frac{\Delta \mathrm{C}(E_i)}{\mathrm{C}(E_i)}\right)^2 + \left(\frac{\Delta\varphi}{\varphi}\right)^2 + \left(\frac{\Delta\varepsilon_\gamma}{\varepsilon_\gamma}\right)^2 + \left(\frac{\Delta \mathrm{I}_\gamma}{\mathrm{I}_\gamma}\right)^2 + \left(\frac{\Delta \mathrm{t_h}}{\mathrm{t_h}}\right)^2. \quad (4.2)$$

In which $\mathrm{C}(E_i)$, is defined as γ-ray counts of assessed radionuclides as a function of gamma energy E_i, $\Delta\mathrm{C}(E_i)$ represents γ-ray counting statistical uncertainty, while other symbols maintained their earlier definitions.

However, the above equation is not applicable for the uncertainty calculations of the ^{44g}Sc cross-sections due to the interfering gamma lines discussed in the Tables 4.3 and 4.4, Fig 4.3 and section 4.3.5 of this chapter. The following more suitable equation (Usman et al., 2017) was therefore used for the propagation of the ^{44g}Sc uncertainty on the cross-section:

$$\left(\Delta\sigma(E_i)\right)^2 = \left(\sum_{i=1}^{10} \frac{\partial\sigma(E_i)}{\partial x_i}\Delta x_i\right)^2 \quad (4.3)$$

Where the x_i runs from 1 to 10 and represents all the contributing factors such as flux, gamma intensities of the shared gamma lines, and so on which have effects on the cross-sections of the ^{44g}Sc

The uncertainties presented in Table 4.4 were based on the following assumed fractional partial uncertainties: uncertainties due to beam intensity (5%), γ-ray detection

efficiency of the detector (4%) and target thickness (2%). The retrieved uncertainty due to γ-ray intensities of the investigated radionuclides (0.001 to 5.833%) was adopted from the ENSDF library (Burrows, 2006, 2007, 2008; Chen et al., 2011; Singh & Chen, 2015; Wu, 2000; Xiaolong, 2006). As indicated in the same Table, the uncertainty due to γ-ray counting statistics ranged from 0.2 to 41.4%. Uncertainties due to time scale during sample irradiation and measurements were not considered in the cross-section calculations as their effects are quite negligible, especially for long-lived radionuclides.

Table 4.4: Uncertainties in cross-sections. The uncertainties in the γ-ray intensities were taken from the ENSDF library via Live-chart

(The ENSDF library data source (Burrows, 2006, 2007, 2008; Chen et al., 2011; Singh & Chen, 2015; Wu, 2000; Xiaolong, 2006). The uncertainties in the counting statistics were determined experimentally. Other sources were given some assumed uncertainties.)

Nuclide of interest	Uncertainties (%)					
	γ-ray intensity (ΔIγ/ Iγ)	beam intensity	detector efficiency	Target thickness	γ-ray counting statistics	Total uncertainty
^{51}Cr	0.101	5	4	2	0.2 – 28.8	6.7 – 29.6
^{49}Cr	3.571				0.8 – 25.9	7.6 – 27.0
^{48}Cr	2.000				1.0 – 2.9	7.1 – 7.6
^{48}V	0.089				1.1 – 11.7	6.8 – 13.5
^{43}K (373 keV)	0.230				11.4 – 12.77	13.3 – 14.4
^{43}K (617 keV)	0.758				16.19 – 27.97	17.5 – 28.8
^{43}Sc	3.111				12.1 – 22.3	14.2 – 23.5
^{44m}Sc	0.346				0.5 – 23.7	6.7 – 24.6
^{44g}Sc	0.400 ($I_{1157,g}$) 5.833 ($I_{1157,m}$) 0.346 (I_{271}) 0.071 (b_{IT})				1.1 – 2.6 (1157 keV), 1.2 – 2.6 (271 keV)	6.8 – 7.3
$^{46g+m}$Sc	0.001				0.9 – 39.5	6.8 – 40.1

On the other hand, the uncertainty in the beam energy spread on each foil solely depends on the foil location in the stack. This was due to a beam straggling effect, the uncertainties due to thickness of target (~2%) and the initial beam energy (~2.5%). Thus, the uncertainty of the average alpha energy on the first Ti foil (the first foil facing the beam) was initially estimated as ±0.5 MeV but eventually increased along the stack to ±1.3 MeV until it reached on the final Ti foil. The estimated uncertainties in the α-beam energy for all energy points are indicated in Tables 4.5 and 4.6 and Figs. 4.5 – 4.15.

4.3.5 Correction for Interfering Gamma Lines

During decay process of radionuclides, some radionuclides share certain (common) gamma lines, and this has an inference effect on the cross section. The counts in such situation are cumulative for the radionuclides which shared the same gamma line energy. Two phenomena related to the present studies in which such gamma line interferences are seen, firstly, when one or more radionuclide in a Metastable state decays to its corresponding ground state. The second possibility is when two or more radionuclides decay to the same final radionuclides, such as the case of ^{48}Sc and ^{48}V, both decaying to stable ^{48}Ti. A computational technique may be necessary to separate the gamma lines, especially if their half-lives are very close.

Gamma counts C_γ contributed by both metastable (with properties λ_m, f_m, I_m, σ_m) and ground state (with properties λ_g, f_g, I_g, σ_g) of a particular radionuclide from a specific shared gamma line can be separated computationally by considering all contributing processes, as in the following equation (Otuka et al., 2017).

$$C_\gamma = n\varphi\varepsilon_\gamma(A_{\mathrm{gs}} + A_{\mathrm{ms}} + A_{\mathrm{msIT}}), \tag{4.4}$$

Where *n* is the areal atom number density and;

$$A_{\mathrm{gs}} = \sigma_g I_g \frac{f_g}{\lambda_g}, \tag{4.5}$$

$$A_{\mathrm{ms}} = \sigma_m I_m \frac{f_m}{\lambda_m}, \tag{4.6}$$

and

$$A_{\mathrm{msIT}} = \sigma_m I_{\mathrm{IT}} I_g \frac{\lambda_m}{\lambda_m - \lambda_g}\left(\frac{f_g}{\lambda_g} - \frac{\lambda_g}{\lambda_m}\frac{f_m}{\lambda_m}\right), \tag{4.7}$$

And the time related factors f_m and f_g are defined as follows;

$$f_m = [1 - \exp(-\lambda_m t_i)]\exp(-\lambda_m t_c)[1 - \exp(-\lambda_m t_m)], \tag{4.8}$$

and

$$f_g = \left[1 - \exp\left(-\lambda_g t_i\right)\right]\exp\left(-\lambda_g t_c\right)\left[1 - \exp\left(-\lambda_g t_m\right)\right], \tag{4.9}$$

Rearranging the above equations, a single formula is obtained. For the computation of the independent production cross-section of ^{44g}Sc as an example, the equation below is obtained. Using C_{1157} for the net counts via 1157 keV gamma line (with ε_{1157} as its detection efficiency) and C_{271} as the net counts via the 271 keV gamma line (with ε_{271} as its detection efficiency), the independent ^{44g}Sc production cross-section (without the shared ^{44m}Sc cross sections) can be calculated by the following equation (Usman et al., 2017);

$$\sigma\,(E_i) = \frac{\lambda_g}{t_{\mathrm{h}}\rho\varphi(1-e^{-\lambda g t_{irr}})(e^{-\lambda g t_{coo}})(1-e^{-\lambda g t_{mea}})}\left[\frac{C_{1157}(E_i)}{\varepsilon_{1157}} - \frac{C_{271}(E_i)}{\varepsilon_{271}}\frac{I_{1157,m}}{I_{271}} - \frac{C_{271}(E_i)}{\varepsilon_{271}} b_{IT}\frac{I_{1157,g}}{I_{271}}\frac{{\lambda_m}^2\lambda_g}{\lambda_m-\lambda_g}\left(\frac{1}{{\lambda_g}^2}\frac{(1-e^{-\lambda g t_{irr}})(e^{-\lambda g t_{coo}})(1-e^{-\lambda g t_{mea}})}{(1-e^{-\lambda m t_{irr}})(e^{-\lambda m t_{coo}})(1-e^{-\lambda m t_{mea}})} - \frac{1}{{\lambda_m}^2}\right)\right] \tag{4.10}$$

Where λ_g and λ_m are the decay constants of ^{44g}Sc and ^{44m}Sc, respectively, $I_{1157,g}$ and $I_{1157,m}$ are the emission probabilities of the 1157 keV gamma-lines directly from ^{44g}Sc and ^{44m}Sc, respectively, I_{271} is the emission probability of the 271 keV gamma line, and b_{IT} is the isomeric transition probability of ^{44m}Sc (Otuka et al., 2017). All other symbols maintain their previous definitions.

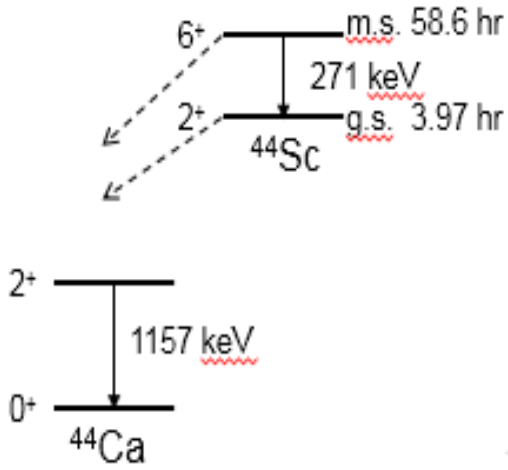

Figure 4.3 A Sketch of Decay Scheme of ^{44g}Sc (adopted from Otsuka et al. 2016)

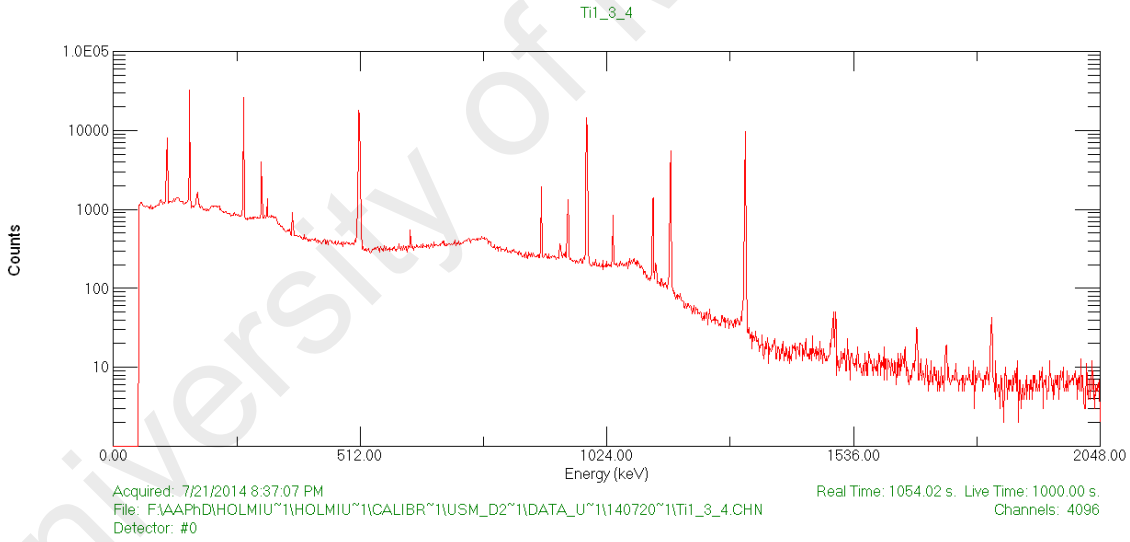

Figure 4.4: A spectrum of titanium foil showing peaks of gamma lines

4.3.6 Thick Target Yield Calculation

Excitation functions and experimental thick target yields are an essential tool in nuclear reaction processes and their knowledge in every production route on specific metallic targets are very essential for optimisation of the nuclear processes. One of such applications of such tools is seen in the processes of developing a high current large-scale medical system (Otuka & Takacs, 2015). The practical (routine) thick target production yields are usually lower than the corresponding measurements made under more monitored conditions (the nominal yields).

The calculation of the integral thick target yield for the assessed radionuclides was deduced using the measured cross-sections. Also, the stopping power of ^{nat}Ti within the investigated energy region of alpha particles from the threshold of each reaction process to the 50.2 MeV maximum energy, such that the total energy is assumed to be absorbed in the target. The integral thick target yield was thus calculated using the following equation (Bonardi et al., 2002; Shahid et al., 2015a);

$$Y = I_{\alpha}\rho\lambda \int_{E_{th}}^{E_{in}} \left(\frac{\sigma(E_i)}{(dE/dx)_E}\right) dE, \quad (4.11)$$

where the integral runs from the threshold energy (E_{th}) to the initial α particle energy (E_{in}), I_{α} represents the number of incident α particles per electronic charge corresponding to 1 μA×1 h, and $(-1/\rho)(dE/dx)_E$ is the stoping power of an α particle at the energy *E*. The other parameters in the equation maintain their previous definitions.

4.4 Results and Discussions

The measured production cross-sections of ^{43}K,^{43,44m,44g,46,47,48}Sc, ^{48}V and ^{48,49,51}Cr radionuclides are tabulated in Tables 4.5 and 4.6 while the corresponding excitation functions were shown in Figs. 4.5 – 4.15 together with those in the earlier experimental

measurements from the EXFOR library (Otuka et al., 2014) and the evaluated data in the TENDL-2014 library (Koning et al., 2014b) which provides the output of the TALYS code (Koning & Rochman, 2012). In some cases, the reported isotopic cross-sections from some the earlier measurements (Baglin et al., 2004; Chang et al., 1973; Howard et al., 1974; Iguchi et al., 1960; Levkovskij, 1991; Morton et al., 1992; Vlieks et al., 1974; Vonach et al., 1983) were normalized by multiplying by their natural isotopic abundances for comparison with the present elemental cross-sections. The isotopic cross-sections reported by Levkovskij (Levkovskij, 1991) often cover an energy range where several Ti target isotopes may contribute to the production of the radionuclide of interest, and their isotopic cross-sections are often not directly comparable with our elemental cross-sections. Nevertheless, the Levkovskij's isotopic cross-sections are plotted together with our new data after the above-mentioned normalisation but without further discussion. Correction to the recoil loss due to the high energy α beam irradiation was considered, except in some few cases where the gamma lines could not be seen, because of the complete decay of the short-lived nuclides before the measurements of the catcher foils. In the frame of irradiation of our very thin Ti target (10.40 μm) by the 50.4 MeV, we observed and corrected an average of 10 % recoil loss in most of the studied radionuclides. Specifically, the gamma lines of ^{43}Sc, ^{44g}Sc, and ^{48}Sc radionuclides were not observed on catcher foils, and thus no recoil corrections were made on their cross-sections.

Table 4.5: Measured cross-sections for $^{nat}Ti(\alpha,x)^{51,49,48}Cr$, ^{48}V and ^{43}K nuclear processes

Energy (MeV)	Cross-sections (mb)					
	$^{nat}Ti(\alpha,x)^{51}Cr$	$^{nat}Ti(\alpha,x)^{49}Cr$	$^{nat}Ti(\alpha,x)^{48}Cr$	$^{nat}Ti(\alpha,x)^{48}V$	$^{nat}Ti(\alpha,x)^{43}K$ (372.760keV)	$^{nat}Ti(\alpha,x)^{43}K$ (617.490 keV)
50.2 ± 0.5	26.4 ± 2.2	40.2 ± 3.2	1.8 ± 0.1	133 ± 10	0.29 ± 0.03	0.28 ±0.13
47.4 ± 0.5	34.3 ± 3.7	50.1 ± 3.9	1.7 ± 0.1	109 ± 08	0.17 ± 0.02	0.13 ± 0.04
42.9 ± 0.5	35.8 ± 2.4	58.2 ± 4.5	1.6 ± 0.1	58.2 ± 4.6		
38.1 ± 0.6	46.4 ± 3.1	42.4 ± 3.2	2.1 ± 0.2	53.7 ± 4.1		
32.8 ± 0.7	61.8 ± 4.6	28.1 ± 2.3	3.0 ± 0.2	59.1 ± 4.4		
26.8 ± 0.8	72.8 ± 5.2	16.2 ± 1.3	2.9 ± 0.2	56.8 ± 4.1		
19.7 ± 1.0	209.0 ± 14.08	19.6 ± 2.2	1.1 ± 0.1	32.4 ± 2.3		
10.4 ± 1.5	412.6 ± 27.7	17.3 ± 1.3				

Table 4.6: Measured cross-sections for $^{nat}Ti(\alpha,x)^{43,44m,44g,46g+m,47,48}Sc$ nuclear processes

Energy (MeV)	Cross-sections (mb)					
	$^{nat}Ti(\alpha,x)^{43}Sc$	$^{nat}Ti(\alpha,x)^{44m}Sc$	$^{nat}Ti(\alpha,x)^{44g}Sc$	$^{nat}Ti(\alpha,x)^{46g+m}Sc$	$^{nat}Ti(\alpha,x)^{47}Sc$	$^{nat}Ti(\alpha,x)^{48}Sc$
50.2 ± 0.5	0.95 ±0.13	16.0 ± 1.2	7.04 ± 0.52	76.8 ± 5.3	16.8 ± 1.1	1.4 ± 0.1
47.4 ± 0.5	0.45 ± 0.11	15.0 ± 1.2	6.25 ± 0.46	69.7 ± 4.9	17.5 ± 1.2	1.0 ± 0.1
42.9 ± 0.5		10.2 ± 0.9	4.00 ± 0.30	42.4 ± 3.0	18.1 ± 1.3	0.81 ± 0.07
38.1 ± 0.6		3.0 ± 0.2	1.04 ± 0.08	16.3 ± 1.2	18.3 ± 1.3	0.38 ± 0.03
32.8 ± 0.7		0.08 ± 0.02		4.4 ± 0.5	10.6 ± 0.7	0.19 ± 0.03
26.8 ± 0.8				2.1 ± 0.2	3.0 ± 0.2	0.01 ± 0.00
19.7 ± 1.0					0.04 ± 0.01	
10.4 ± 1.5					0.04 ± 0.01	

4.4.1 Production of ^{51}Cr

^{51}Cr ($T_{1/2}$ = 27.7025 d) decays via an EC (100%) process to ^{51}V. The radionuclide was measured through its relatively intense gamma-line of E_γ = 320.0824 keV (I_γ = 9.910%). Several groups previously reported the excitation function of this monitor reaction (Baglin et al., 2004; Chang et al., 1973; Hermanne et al., 1999b; Howard et al., 1974; Iguchi et al., 1960; Levkovskij, 1991; Michel et al., 1983; Morton et al., 1992; Peng et al., 1998; Uddin & Scholten, 2016; Vonach et al., 1983; Weinreich et al., 1980). The present excitation function is consistent with the recommended IAEA ^{51}Cr monitor cross sections and with those by some other research groups as in the Fig. 4.5. The two data sets from the Levkoskij group (Levkovskij, 1991) on the enriched samples show lower cross-sections from 30 MeV and beyond. The extracted data from the TENDL-2014 show lower values, especially in the peak region than most of the experimental data.

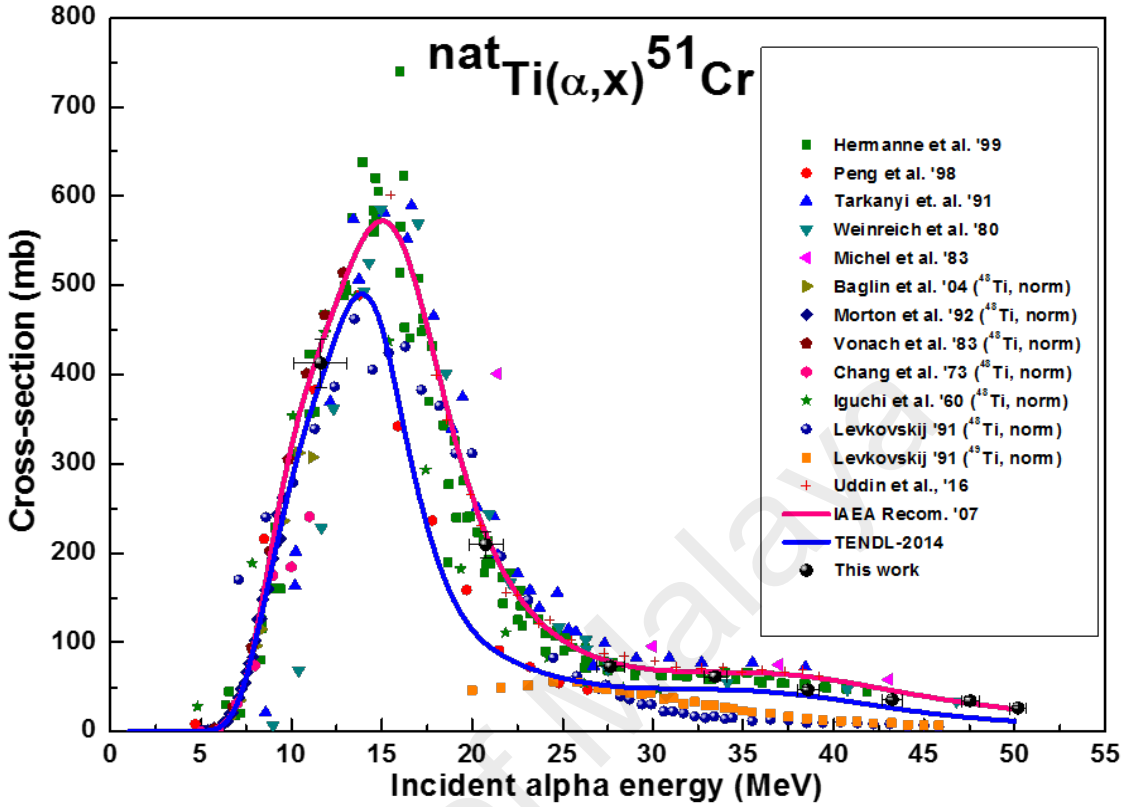

Figure 4.5: Excitation function of ^{nat}Ti(α,x)^{51}Cr reaction.

4.4.2 Production of ^{49}Cr

^{49}Cr ($T_{1/2}$ = 42.3 min) usually decays to ^{49}V via an EC+β^+ (100%) process. Among the three characteristic gamma lines of ^{49}Cr shown in Table 4.2, the most intense E_γ =90.639 keV (I_γ = 53.2%) was used to determine its cross-sections. Figure 4.6 shows the present new measured cross-sections in comparison with the available previous experimental data (Howard et al., 1974; Levkovskij, 1991; Vlieks et al., 1974) and also the theoretical data in the TENDL-2014 library. Below 30 MeV, the present cross-sections show consistency with the previous experimental data and TENDL-2014. In the high-energy region, there are considerable discrepancies among the experimental data and also with the theoretical data.

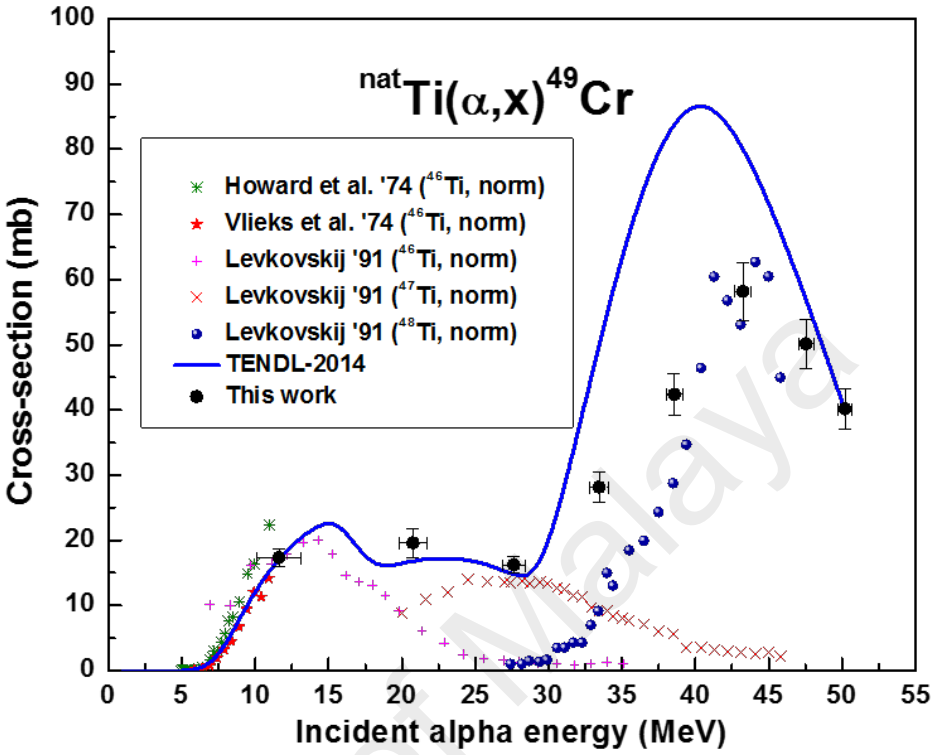

Figure 4.6: Excitation function of ^{nat}Ti(α,x)^{49}Cr reaction

4.4.3 Production of ^{48}Cr

The formation and the characteristic gamma lines of ^{48}Cr ($T_{1/2}$ = 21.56 h) are presented in Table 4.2. The production cross-sections of ^{48}Cr were calculated using its intense gamma line of E_γ = 308.24 keV (I_γ = 100%). The measured data are compared with the available experimental data (Hermanne et al., 1999b; Levkovskij, 1991; Michel et al., 1983; Peng et al., 1998; Uddin & Scholten, 2016; Weinreich et al., 1980) and the theoretical data in Fig 4.7. The present results show a good agreement with some of the earlier measurements (Hermanne et al., 1999b; Michel et al., 1983; Uddin & Scholten, 2016). The normalised cross-sections for the enriched isotopes of ^{46,47,48}Ti (Levkovskij, 1991) show very low cross-sections. TENDL-2014 presents a shape like the present experimental excitation function but not in magnitude.

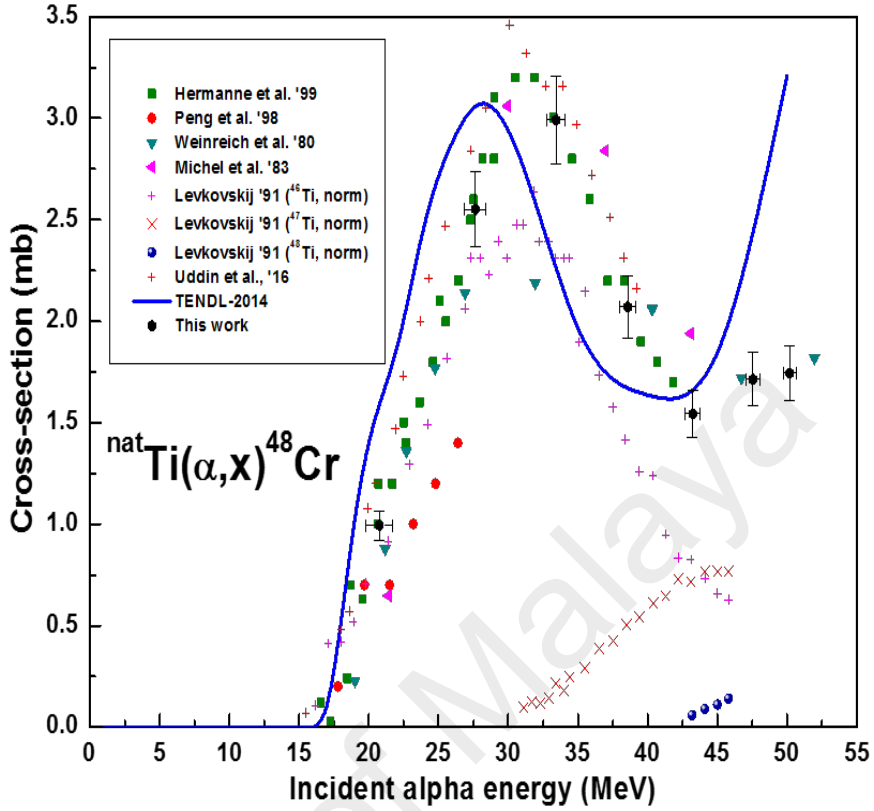

Figure 4.7: Excitation function of ^{nat}Ti(α,x)^{48}Cr reaction.

4.4.4 Production of ^{48}V

As ^{48}V ($T_{1/2}$ = 15.9735 d) and ^{48}Sc ($T_{1/2}$ = 43.67 h,) decay to the same stable nuclide ^{48}Ti, some of their gamma lines are common as shown in Table 4.2. Thus, in this work, a weak but independent gamma line of E_γ = 944.130 keV (I_γ = 7.870%) was adopted to determine the activity of ^{48}V. The main contributing reactions to form ^{48}V are presented in Table 4.2, including the contribution of ^{48}Cr via an EC decay (100%). Four experimental studies (Hermanne et al., 1999b; Levkovskij, 1991; Michel et al., 1983; Uddin & Scholten, 2016) are available in the literature. In Fig. 4.8, all experimental data are not in good agreement with one another. Also, there are three sets of the experimental data by (Levkovskij, 1991) on different isotopes of ^{46,47,48}Ti but all

show lower values when compared with the present measurement. On the other hand, TENDL-2014 presents higher values compared to the present data above 40 MeV.

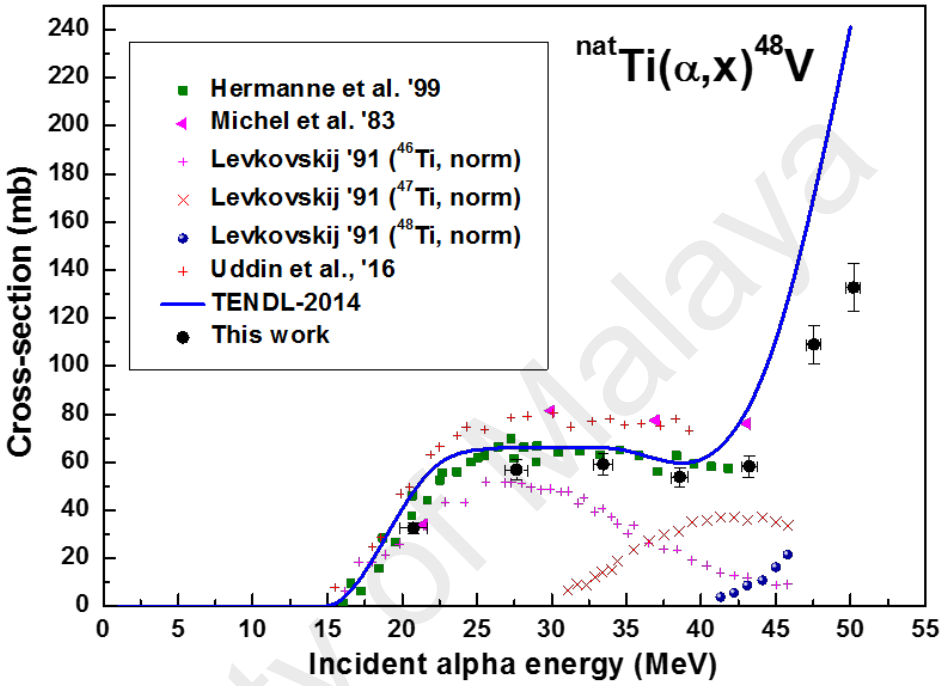

Figure 4.8: Excitation function of ^{nat}Ti(α,x)^{48}V reaction.

4.4.5 Production of ^{43}K

The cross-sections of ^{43}K ($T_{1/2}$ = 22.3 h) radionuclide are contributed by all the stable Ti isotopes via various reaction Q-values listed in Table 4.2. The ^{43}K has a gamma line (E_γ = 372.760 keV) very close to that of ^{43}Sc. Thus, to avoid possible contamination of the ^{43}K cross-sections by ^{43}Sc, a longer cooling period of over 40 hours were ensured before its measurement, as reported in Table 4.1 of this chapter. There was only one previous experimental data for comparison in the literature. Two most intense gamma lines, E_γ = 372.760 keV, (I_γ = 86.80%) and E_γ = 617.490 keV (I_γ = 79.2%) of this radionuclide were both used separately for the calculations of the cross-sections. Both results from the gamma lines agree with each other. The new numeral cross-sections for both gamma lines have been reported in Table 4.5 while Fig. 4.9 presents the excitation

functions for both gamma lines and the literature data. As seen in the Figure, the evaluated TALYS code via both the TENDL-2014 (Koning et al., 2014b) and TENDL-2015 (Koning et al., 2015) have been used for comparison with the present study. Although the two libraries agree with each other, however, both the theoretical results from the two gamma lines show some deviations to the present experimental cross sections. The theoretical results are largely discrepant to the previously reported literature data, especially at higher energy. A slight improvement could be seen in the prediction capability of the TENDL-2015 library over its older version, the TENDL-2014.

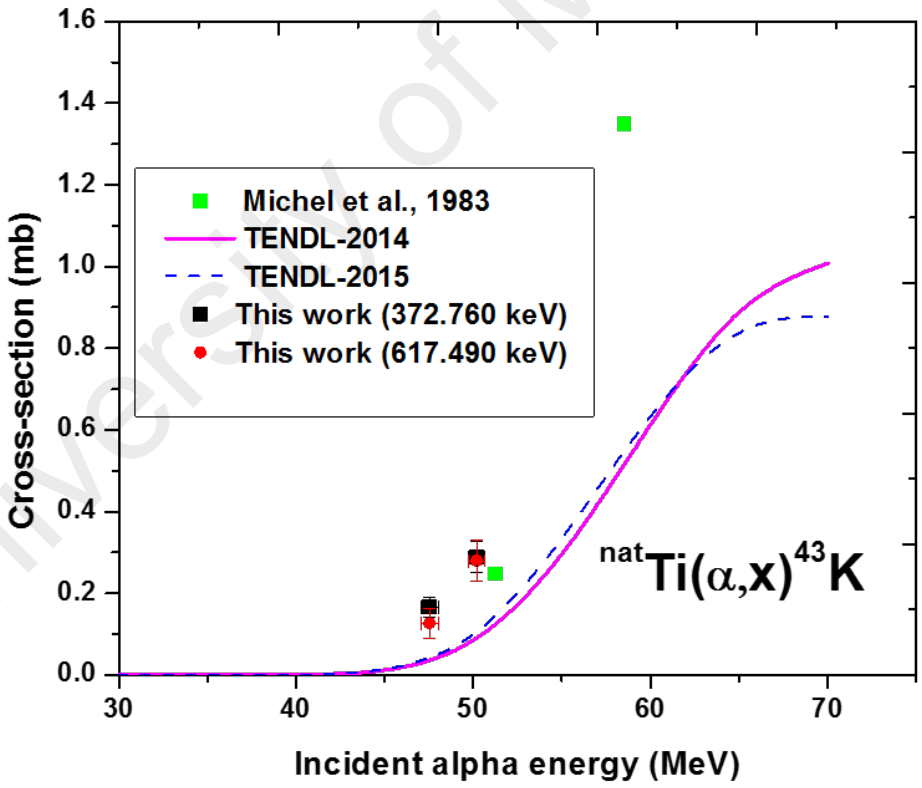

Figure 4.9: Excitation functions of $^{nat}Ti(\alpha,x)^{43}K$ reaction.

4.4.6 Production of ^{43}Sc

^{43}Sc ($T_{1/2}$ = 3.891 h) decays to the stable ^{43}Ca via an EC decay (100%). The cross-section of this radionuclide was determined using the only available intense and

interference free gamma line (E_γ = 372.9 keV, I_γ = 22.5%). Table 4.6 contains the numeral cross-sections of this radionuclides. Figure 4.10 shows the present excitation function together with the literature data and the evaluated data of TENDL-2014 library. There is only one previous study (Michel et al., 1983) but above the present investigated energy region. The consistency of the TENDL-2014 with the present data gradually deviates as the energy increases.

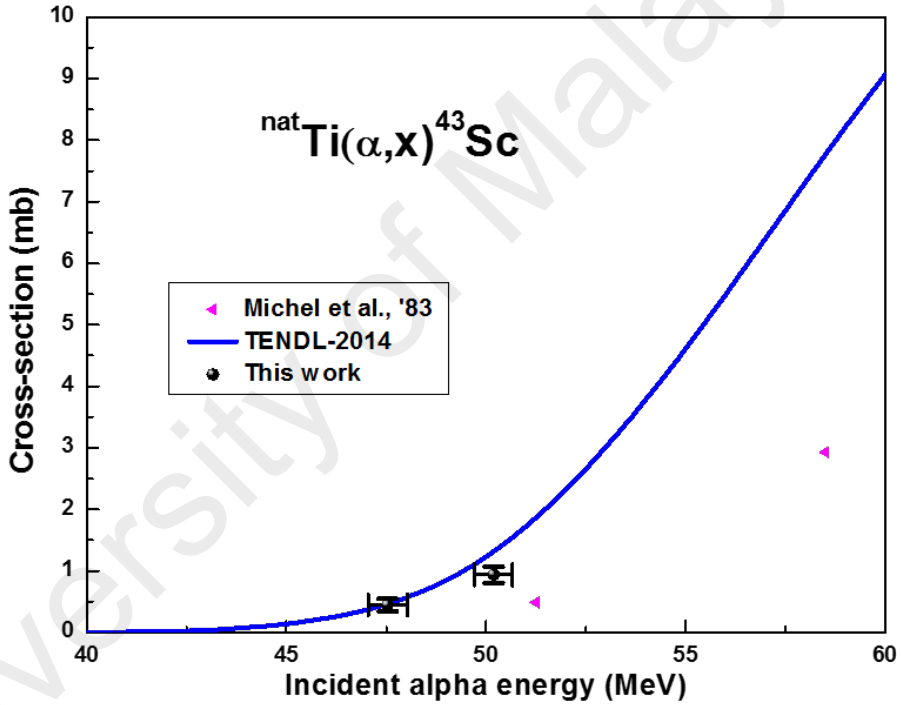

Figure 4.10: Excitation function of ^{nat}Ti(α,x)^{43}Sc reaction.

4.4.7 Production of ^{44m}Sc

The formation of ^{44m}Sc ($T_{1/2}$ = 58.61 h) cross sections follows the direct reactions mentioned in Table 4.2. The radionuclide decays partly to the stable ^{44}Ca through an EC (1.20%) decay process and mostly to ^{44g}Sc via an IT (98.80%) process. The cross-sections of this radionuclide were determined using the high intensity and interference free gamma line 271.241 keV (I_γ = 86.7%). The available literature data (Hermanne et

al., 1999b; Levkovskij, 1991; Michel et al., 1983), as well as the theoretical evaluated data extracted from the TENDL-2014 library, are compared with the present results in Fig. 4.11, and show consistency among one another.

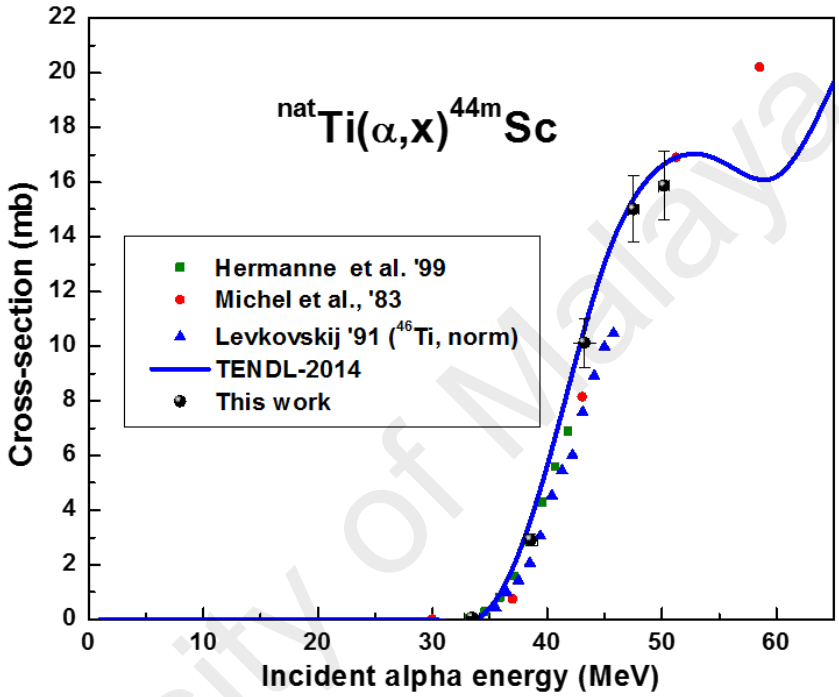

Figure 4.11: Excitation function of ^{nat}Ti(α,x)^{44m}Sc reaction.

4.4.8 Production of ^{44g}Sc

^{44g}Sc ($T_{1/2}$ = 3.97 h) decays to the stable ^{44}Ca via an EC process (100%). Principally, two nuclear processes contribute to the formation of the ^{44g}Sc cross-sections: the direct nuclear reactions listed in Table 4.3 and the IT decay (98.80%) of ^{44m}Sc ($T_{1/2}$ = 58.61 h). From net counts of both 271 and 1157 keV gamma lines in the same spectrum, the cross-sections of the ^{44g}Sc can be determined by the equation 4.9. With the help of this equations, the contributions of ^{44m}Sc via the 1157 keV gamma line as well as through the isomeric transition to ^{44g}Sc were removed. The presented results here are thus independent cross-sections of ^{44g}Sc, measured within its first half-life and are presented

in the Fig. 4.12 and Table 4.6 of this chapter. Note that the measurement of ^{44g}Sc within the first half-life helped to minimise the possible slow contribution of ^{44}Ti ($T_{1/2}$ = 60 y) through its gradual decay (EC = 100%) to ^{44g}Sc.

As shown in Fig. 4.12, the present data show reasonable agreement with the previous experimental studies (Hermanne et al., 1999b; Levkovskij, 1991; Michel et al., 1983) as well as with the theoretical TENDL-2014 data.

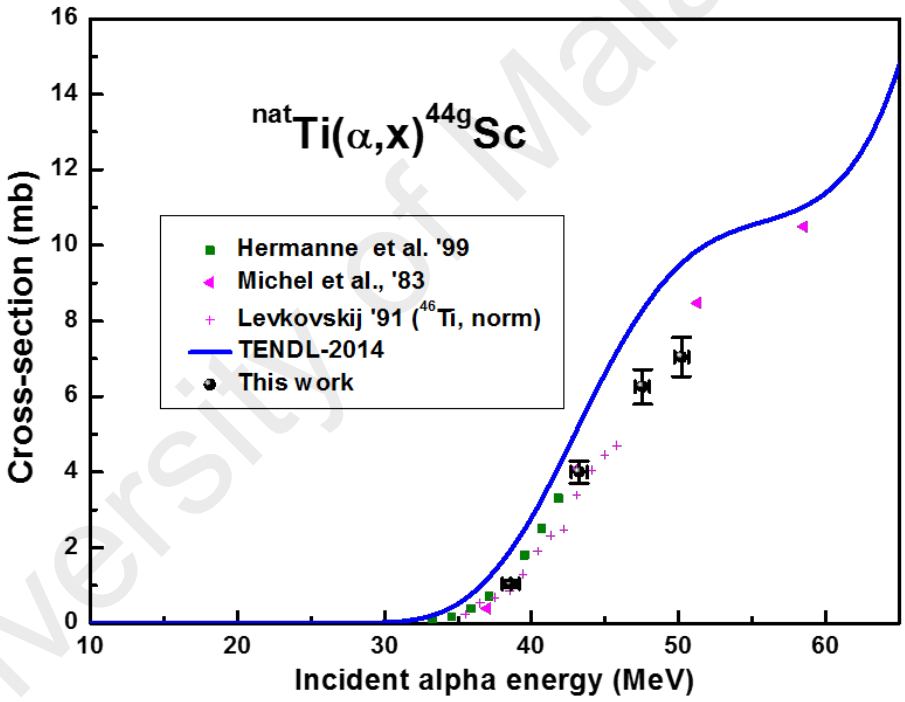

Figure 4.12: Excitation function of ^{nat}Ti(α,x)^{44g}Sc reaction.

4.4.9 Production of $^{46m+g}$Sc

The ^{46}Sc has an isomeric state (^{46m}Sc) of very short half-life ($T_{1/2}$ =18.75 s) which could not be measured in the present experimental conditions and eventually decayed within five mins of EOI to ^{46g}Sc ($T_{1/2}$ =83.79 d) via an IT (100 %) process. Thus, the measured data are the total cross-sections of $^{46g+m}$Sc. The ^{46g}Sc decays to the stable ^{46}Ti via an emission of a β^- (100%) particle. Identification and analysis of activities of ^{46g}Sc

were done through its high intensity and interference free gamma line of E_γ = 889.277 keV (I_γ = 99.9840%). The possible contributing reactions for the formation of ^{46g}Sc radionuclide are listed in Table 4.6. In Fig. 4.13, the present data are compared with those in literature (Hermanne et al., 1999b; Levkovskij, 1991; Uddin & Scholten, 2016) and the TENDL-2014 library data. They agree with one another, except for the isotopic data normalised from ^{47}Ti given in Levkovskij (Levkovskij, 1991).

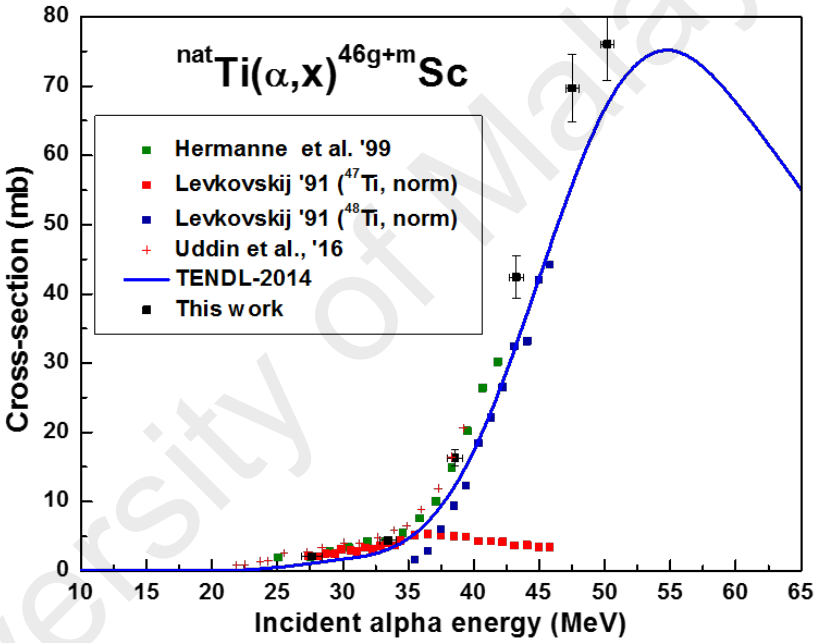

Figure 4.13: Excitation function of ^{nat}Ti(α,x) $^{46g+m}$Sc reaction.

4.4.10 Production of ^{47}Sc

The relatively long-lived ^{47}Sc ($T_{1/2}$ =3.3492 d) was formed via the direct reactions given in Table 4.3, and decays to the stable ^{47}Ti via an emission of a β^- (100%) particle. The activity of ^{47}Sc was determined using its characteristic intense gamma line of 159.381 keV (I_γ = 68.3%). There exist three previous studies (Hermanne et al., 1999b; Levkovskij, 1991; Michel et al., 1983) in the literature, whereas (Hermanne et al., 1999a) is a preliminary report of the experiment published in (Hermanne et al., 1999b).

As shown in Fig. 4.14, the new data show consistency with those reported by (Hermanne et al., 1999b; Levkovskij, 1991; Michel et al., 1983) except for the normalised data of (Levkovskij, 1991) from the ^{49}Ti target nuclide. TENDL-2014 overestimated the present cross-sections almost for the whole energy region.

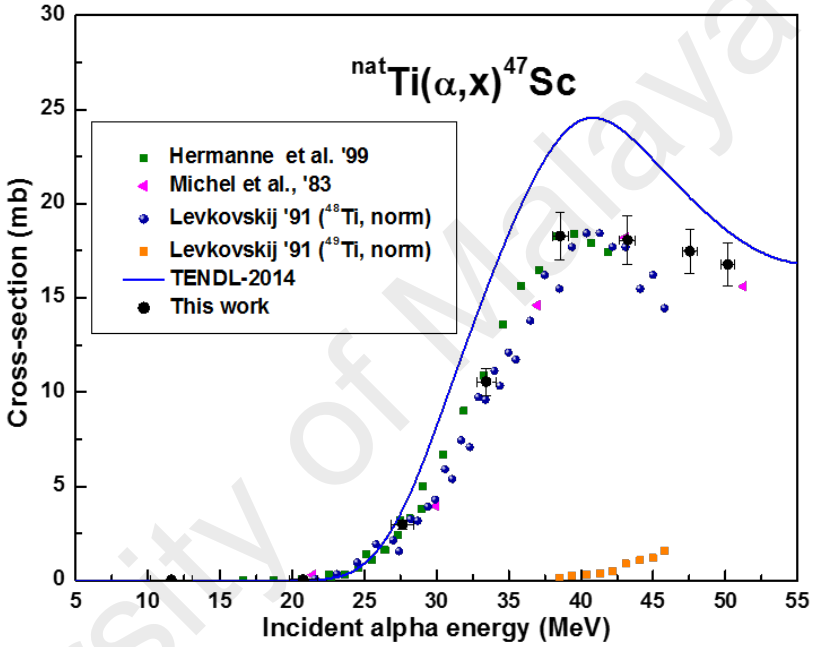

Figure 4.14: Excitation function of ^{nat}Ti(α,x)^{47}Sc reaction.

4.4.11 Production of ^{48}Sc

^{48}Sc ($T_{1/2}$ = 43.67 h) was formed via the contributing reactions shown in Table 4.3 and decays via a β^- (100%) particle emission to the stable ^{48}Ti. Several gamma lines of this radionuclide (see Table 4.3) are shared with ^{48}V. Present cross-sections were measured using the independent gamma line of 1037.522 keV (I_γ = 97.6 %). Four earlier studies (Hermanne et al., 1999b; Levkovskij, 1991; Michel et al., 1983; Uddin & Scholten, 2016) were found in the database. In Fig. 4.15, the present data are compared with the earlier measurements as well as TENDL-2014 which slightly overestimates the

cross-sections of the present study but agree with those reported in Ref. (Uddin & Scholten, 2016).

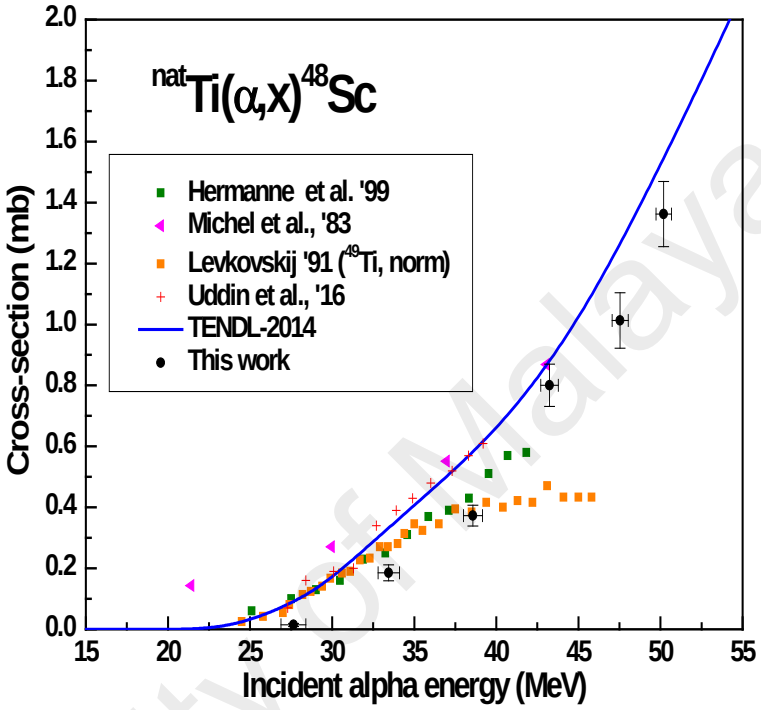

Figure 4.15: Excitation function of ^{nat}Ti(α,x)^{48}Sc reaction.

4.4.12 Thick Target Yield Calculations

The thick target yields have been deduced for all the investigated radionuclides. There is only one direct measurement of thick target yield in the literature for ^{51,49,48}Cr and ^{48}V productions by one group (Abe et al., 1984). The present calculated values have been compared with their directly measured thick target yields in Figs. 4.16 and 4.17. The discrepancy seen in the ^{51}Cr production is probably due to lack of our experimental data point around the peak region of the excitation function (~15 MeV). Figs. 4.18 and 4.19 show the thick target yields of ^{43}K, ^{43,44g,44m,66,47,48}Sc for which direct measurements are not seen in the EXFOR library. From the irradiation of the ^{nat}Ti target with 50.2-MeV α beam, the calculated yields indicate that ^{49}Cr (363.45 MBq/μA-hr) has the

highest production yield among all the studied radioactive isotopes. Generally, the scandium radionuclides have demonstrated very low integral yields, although their corresponding cross sections via the present investigated production route are also very low. Therefore, for the scandium radionuclides, the ^{44g}Sc has the highest yield (3.35 MBq/μA-hr) among them radionuclides. Similarly, the observed low integral yield of ^{46g}Sc (0.080 MBq/μA-hr.) could be attributed to its long half-life (83.79 d).

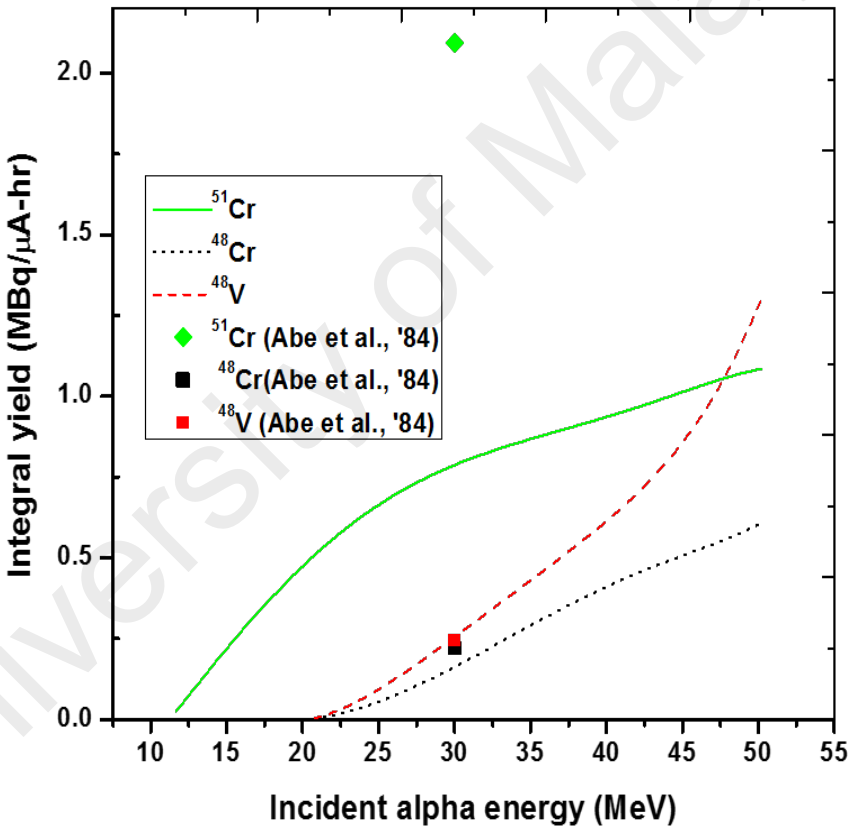

Figure 4.16: Integral thick target yield for ^{51,48Cr,48}V

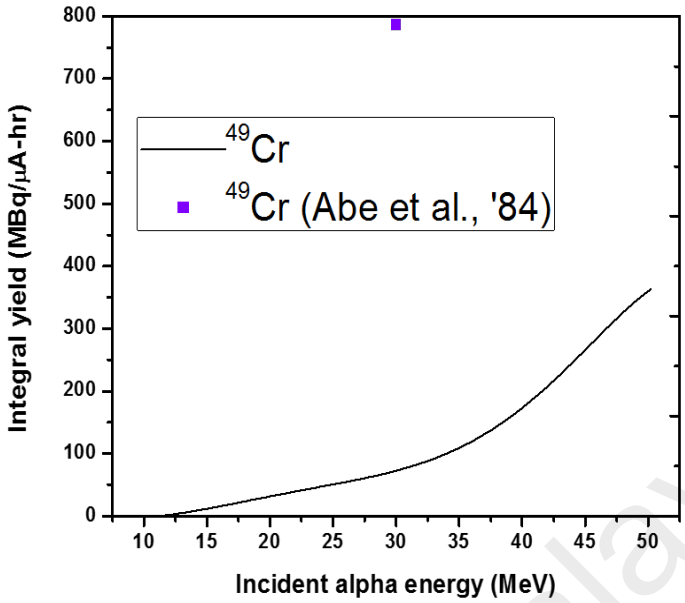

Figure 4.17: Integral thick target yield for ^{49}Cr

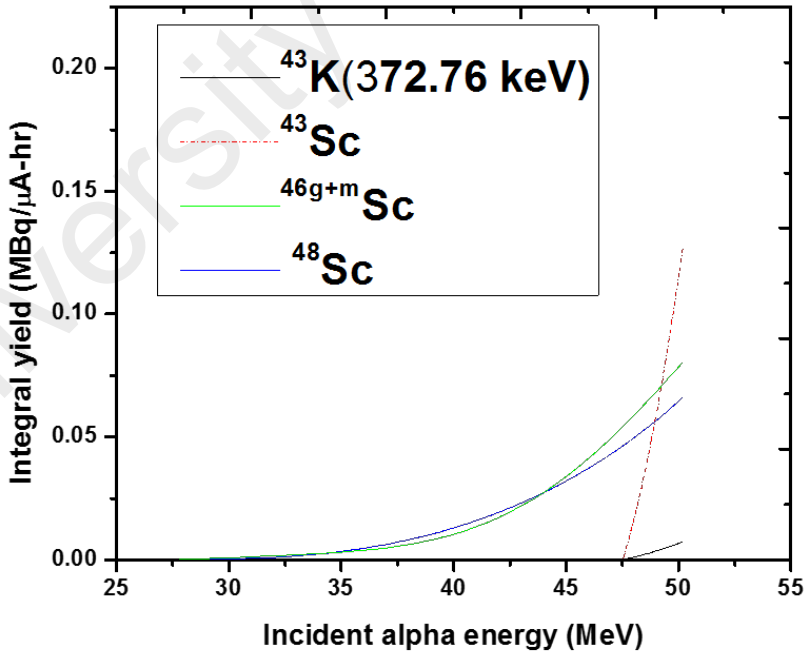

Figure 4.18: Integral thick target yields for ^{43}K,$^{43, 46g+m, 48}$Sc

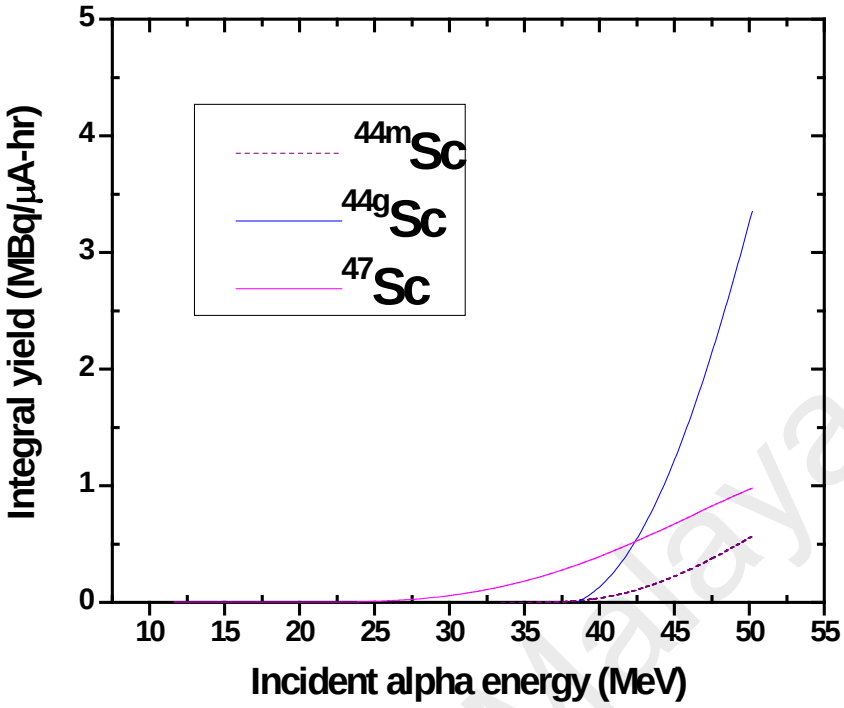

Figure 4.19: Integral thick target yields for $^{44m,\ 44g,\ 47}$Sc

4.5 Conclusions

In this chapter production cross-sections for, $^{48,47,46g+m,44g,44m,43}$Sc, ^{51,49,48}Cr, ^{48}V, ^{43}K and radionuclides are reported via α particles bombardment on natural titanium in the region of 10. – 50.2 MeV. Apart from this, the integral thick target yields were calculated for all the reported radionuclides using the measured cross-sections, assuming total energy was absorbed. For the production of $^{46g+m,48}$Sc radionuclide, there exist only one previous work in the high-energy region and another for the ^{48}V and ^{48,49}Cr production in the same high energy region before the present work. There is one direct measurement for the thick target yields of ^{51,49,48}Cr and ^{48}V radionuclides in the literature, but none for the ^{43,44m,44g,46,47,48}Sc and ^{43}K radionuclides before the present study. The newly measured cross-sections were compared with the earlier experimental data and with the evaluated data taken from the TENDL-2014 library. Some of the literature data showed discrepancies to the present results.

Similarly, discrepancies between the experiments and the TENDL-2014 library are found for several reaction cross-sections of the investigated radionuclides. Therefore, the new cross-sections might be useful to remove the discrepancy among the previous measurements and to enrich the database on this aspect. The present result could also play an important role to enhance the prediction capacity of the TALYS nuclear reaction code.

CHAPTER 5: EXCITATION FUNCTIONS OF ALPHA-INDUCED REACTIONS ON NATURAL COPPER

5.1 Introduction

This chapter presents the experimental components and findings based on bombarded natural copper metal by the alpha beam. The theoretical contributing reactions for the formation of each assessed radionuclide have been retrieved via relevant online interfaces. The excitation functions of radionuclides are presented along with available literature data for comparison, as well as the theoretical prediction of Talys code.

The metallic copper was used in the stack on the one hand as an energy degrader, and on the other hand, it also serves as an excellent source of gallium, zinc and some other radionuclides. The excellent production cross-sections of several useful radionuclides from the metal are too good to be overlooked.

5.2 Literature Review

Production of radioactive isotopes (RIs) through the bombardment of metallic targets by light charged particles has attracted huge attention, especially as they find increasing applications in different fields such as nuclear medicine, environmental science, agriculture and various industrial procedures. The multitude of RIs demand is leading to more quests for greater accuracy of data, optimised production and alternative production routes. Despite increasing number of variable energy cyclotrons in the world, production of some radionuclides, especially via α irradiation, has not yet been optimised. Studies on production of RIs via (*p,x*) route are relatively active compared to other light charged particle irradiation routes, though (*d,x*) and (α,x) routes are sometimes more effective than the (*p,x*) route for the production of the same RIs.

Natural and enriched isotopes of copper (Cu) have both been used as target materials to produce medically and technologically significant RIs such as ^{66,67}Ga, ^{65}Zn, ^{64}Cu, ^{57}Co, etc. Among them, in addition to the increasing use of gallium (Ga) RIs for beam monitoring, ^{66}Ga has recently been tested as ^{66}Ga-labeled nano-graphene in an in vivo study and found to have high potentials for PET imaging of vasculature (Hong et al., 2012). The proposal of the positron emitting ^{66}Ga($T_{1/2}$ = 9.49 h) as a potential substitute to ^{68}Ga ($T_{1/2}$ = 67.71 min) in PET is partly attributed to the longer half-life of the ^{66}Ga (Lopez-Rodriguez et al., 2015). Moreover, the suitable decay characteristics of ^{66}Ga (EC: 43.5%; β^+: 56.5%), symbolized by its abundant unique high energy β^+ particle (4.15 MeV) emission, is considered to be very useful in therapy (mean range in human tissue: 7.6 mm) (Lopez-Rodriguez et al., 2015). It is also useful as a tracer in a long-term study of physiological processes and labelling of macromolecules with slow pharmacokinetics (Lopez-Rodriguez et al., 2015; Ugur et al., 2002). The Auger-electron-emitting radionuclides such as ^{67}Ga and ^{125}I have cancer therapeutic potentials because of their short-range tissue penetration and high level of cytotoxicity (Koumarianou et al., 2014; O'Donoghue & Wheldon, 1996), leading to less collateral damage to the neighbouring normal tissues of the cancerous cells. The short half-life of ^{67}Ga ($T_{1/2}$ = 3.2617 d) and its emission of 4.7 Auger and Coster-Kronig electrons per decay makes ^{67}Ga-labeled compounds clinically more suitable to patients than the prototype ^{125}I ($T_{1/2}$ = 59.4 d) counterpart (Koumarianou et al., 2014). Additionally, besides its popularity as a source in Mössbauer spectroscopy (Adler & Ghosh, 2003; Schröder et al., 2006; Tsoncheva et al., 2015), ^{57}Co is similarly used as a standard in γ-ray spectrometry calibration as well as single photon emission computed tomography (SPECT) (Al Saleh et al., 2007). ^{60}Co radionuclide, with its relatively long half-life, is also a popular radionuclide for γ-ray calibration as well as a source for γ-ray during simple irradiations of biological samples.

A critical review of the vast experimental literature shows that both natural and enriched copper isotopes have been employed in the past as targets for the cross-section measurements. As an example, a large part of the previous studies focused mostly on the production cross-sections of ^{66,67}Ga and ^{65}Zn for monitoring α beam. However, large discrepancies exist among the reported data, despite employing similar basic experimental procedures. More so, the ongoing Coordinated Research Project by IAEA on "Nuclear Data for Charged-particle Monitor Reactions and Medical Isotope Production" also concludes that re-examination of α-induced ^{66,67}Ga and ^{65}Zn production cross-sections is compulsory (Nichols & Capote Noy, 2013). Furthermore, the data on production cross-sections of radionuclides of cobalt through this production route are quite scarce. In the present work, new data of the α-particle induced reaction cross-sections on natural Cu have been measured hoping to reduce the observed large variations among the experimental literature and to also enrich the database, more especially for the productions of cobalt radionuclides.

5.3 Materials and Method

The experimental procedures are related to those in the previous chapters as well as in some previous articles of this group (Khandaker et al., 2015; Khandaker et al., 2014; Usman et al., 2016a). The well-established stacked foil activation technique was employed together with HPGe γ-ray spectrometry.

5.3.1 Targets Details and Irradiation

High purity foils of copper metal (purity: 99.9%; thickness: 9.71 μm; company: Nilaco, Japan) with its natural isotopic abundance (^{63}Cu: 69.15%; ^{65}Cu: 30.85%) (Berglund & Wieser, 2011) were the main target materials to be presented in this chapter. Several other foils of natural titanium (purity: >99.6%; thickness: 10.40 μm; company: Goodfellow, UK) and holmium (purity: 99%; thickness: 12.29 μm; company:

Goodfellow, UK) were inserted as intermittent fashion in the stack, serving in each case either as energy degraders or beam intensity monitors. For beam monitoring purpose, the stack was arranged in such a way that a Ti foil took the front position of the stack so as to receive the initial beam energy while the subsequent foils received the degraded energy along the stack. Accurate determination of thicknesses of the used metallic foils was ensured by mass measurements using a high precision electronic balance. For the assurance of equal beam to all foils of the targets and monitor, the used foils were prepared with equal size of 15 × 15 mm^2. The stack prepared was then placed in a (water-cooled) target holder that served as a Faraday cup. The targets in the holder were then irradiated for 2.0 h by a 51.2-MeV α beam from the AVF cyclotron of the RIKEN RI Beam Factory, Japan. The beam was collimated to 9-mm diameter via a tantalum slit. A 194 nA average beam current was recorded during the irradiation.

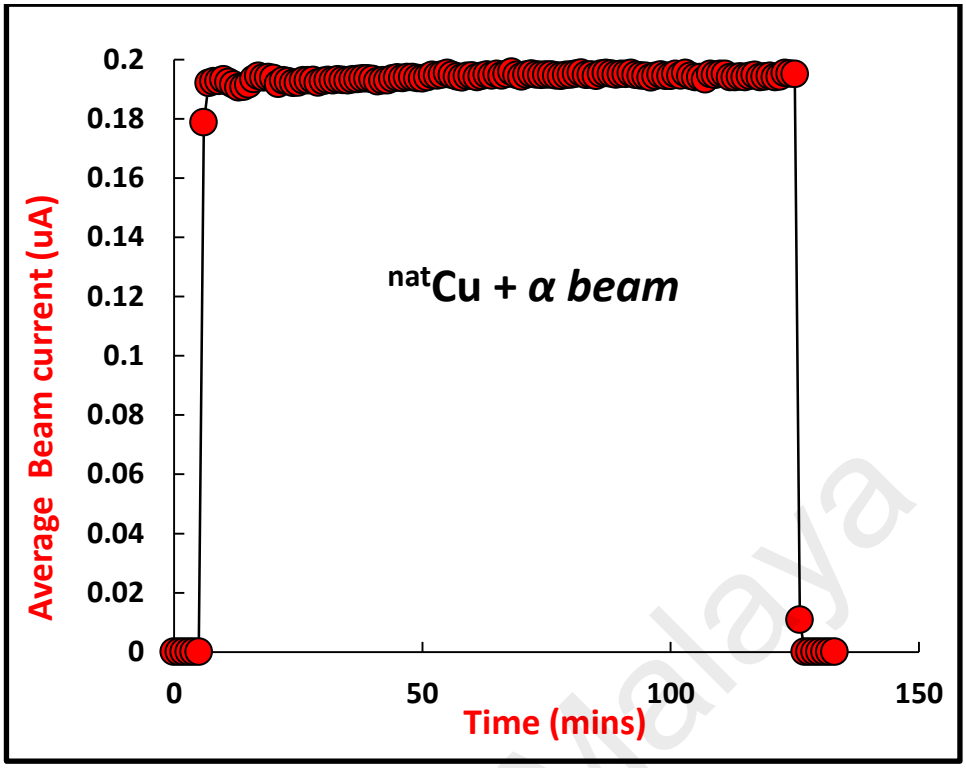

Figure 5.1: Beam current recorded by the Faraday-cup-like target holder

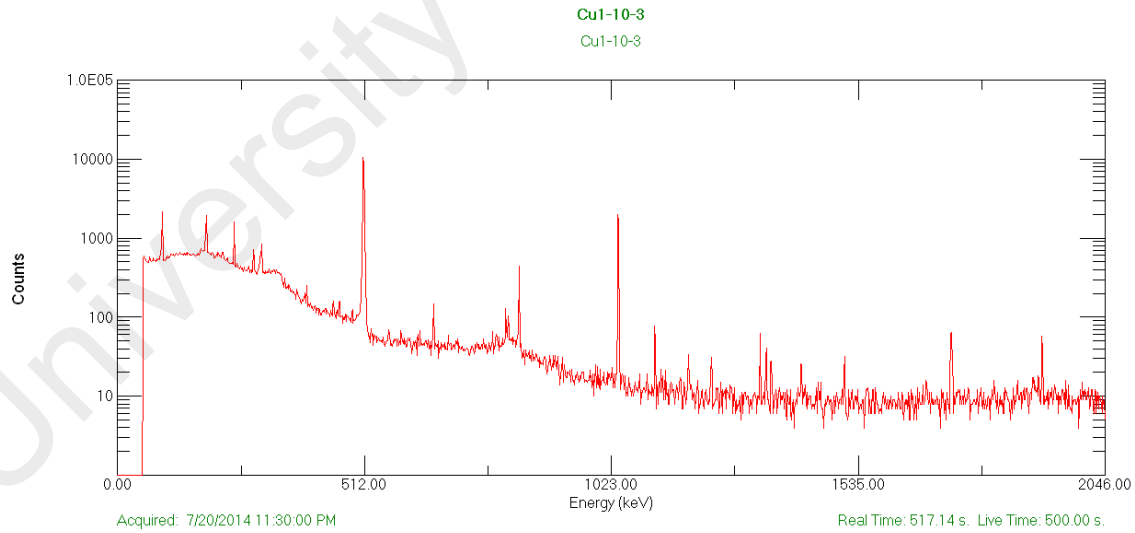

Figure 5.2: A spectrum of copper foil showing gamma peaks

5.3.2 Analysis of γ-ray Spectra

At the end of the stack bombardment, all the irradiated foils were transferred to the hot laboratory for the measurement of γ-rays from the activated foils. The measurements were done using a high resolution (1.85 keV FWHM at 1332.5 keV) HPGe γ-ray spectrometer (ORTEC; GEM-25185P and 52.0-mm thickness; operating voltage: +2000 V; relative efficiency: 25%) coupled to a 4096 multi-channel analyser with the associated electronics. The measured gamma activities from the irradiated Cu metals were started approximately 20 hours after their bombardment. The analysis of the γ lines of the assessed nuclides was done by using some cooling times of 20.9 h to 22.3 h for ^{66}Ga, 1.8 d to 2.4 d for ^{67}Ga and 22.4 d to 23.9 d for ^{65}Zn, ^{57,58g}Co and ^{60g}Co radionuclides. The measurements of the gamma activities were continuously repeated for several times to follow the pattern of the assessed radionuclides decay curves. The measurements were performed using the 1-, 3-, 5-, 10- and 15-cm sample-to-detector positions from the detector cap. The 3-cm minimum sample-to-detector distance was, however, the most chosen for the measurements of activities of the long-lived radionuclides so as to reduce the dead times and pile-up effect. To determine efficiencies of the HPGe detector used, a standard multiple γ-ray emitting point sources at each source-to-detector distance. The source comprises of the several radionuclides as follows: ^{241}Am, ^{139}Cs, ^{113}Sn, ^{57}Co,^{109}Cd, ^{203}Hg, ^{137}Cs, ^{88}Y, ^{85}Sr and ^{60}Co. The calibration mixed standard source was obtained from DBA Isotopes Products Laboratories (USA). The use of fifth order polynomial fitting (Khandaker et al., 2013; Nikolic et al., 2015; Osae et al., 1999) allowed determination of efficiencies for the γ-energies of interest:

$$\ln(\varepsilon) = \sum_{j=0}^{5} a_{\mathrm{j}} \left(\ln(E)\right)^{j} \qquad (5.1)$$

(ε: photo-peak efficiency of the detector, E: emitted γ energy of the radionuclide and a_j fitting coefficient).

The values in Table 5.1 represent the coefficients (a_j) for the fitting of the efficiency response of each photon energy from the standard multiple γ-ray emitting point source in the detector up to 15-cm distance. The fitted efficiency curves for various source-to-detector distances are shown in Fig. 5.3.

Table 5.1: The coefficients of the polynomial fitting for efficiency of the HPGe detector

Source to detector distances (cm)	Coefficients of the polynomial fitting						Fitting Parameter (R^2)
	a_0	a_1	a_2	a_3	a_4	a_5	
1.0	-8.27E+02	6.85E+02	-2.27E+02	3.75E+01	-3.09E+00	1.02E-01	0.54
3.0	-5.78E+02	4.64E+02	-1.49E+02	2.38E+01	-1.89E+00	6.00E-02	0.66
5.0	-5.52E+02	4.42E+02	-1.42E+02	2.26E+01	-1.80E+00	5.72E-02	0.65
10.0	-5.44E+02	4.33E+02	-1.38E+02	2.21E+01	-1.75E+00	5.56E-02	0.60
15.0	-4.32E+02	3.34E+02	-1.04E+02	1.62E+01	-1.26E+00	3.90E-02	0.61

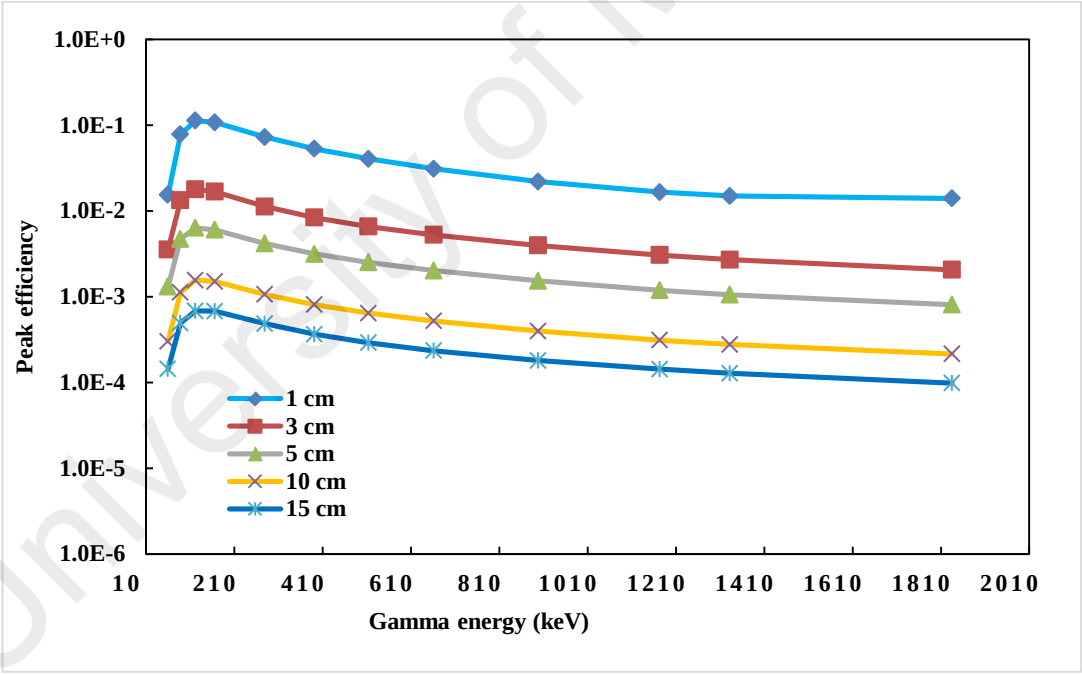

Figure 5.3: Efficiency response of the HPGe detector as a function of gamma energy.

5.3.3 Determination of Initial Beam Energy and Intensity and Estimation of foil Energies

As discussed in chapter four, the initial beam energy was determined using the recently installed TOF system at the Nishina Centre. The degradation of the initial 50-MeV alpha energy along the stack of the foils was calculated by the code SRIM-2003 (Ziegler, 2004), a popular computer program for energy degradation in metallic layers. Throughout the stack, foil location is the major cause of the overall beam span and uncertainty on each foil. The uncertainty of the incident α energy has thus been calculated at ±0.75 MeV for the first Cu foil facing the beam. Alon the stack, the initial uncertainty value eventually increased to ±1.90 MeV on the last Copper foil. The increase was attributed to the effect of beam straggling, the (~1%) uncertainties surrounding the initial alpha beam (MeV) as well as (~1%) uncertainties in target thickness. The sum of estimated α-beam energy span and uncertainty for all data points are indicated in tables and figures of this chapter. A separate section has discussed the uncertainties on cross-sections from all possible contributions.

The intensity of the alpha beam was calculated from the measured activities of the Ti foil made to take the front position of the stack. The IAEA recommended ^{nat}Ti(α,x)^{51}Cr monitor reaction (σ = 26.4 mb at E_α = 50 MeV) (Qaim et al., 2002) was used during the calculation of the beam intensity. The calculated intensity from the first foil was then considered to be constant throughout the stack for the calculation of the cross-sections from other foils within the stack. The ^{51}Cr radionuclide cross-sections from the other Ti metals of the irradiated stack were also calculated and plotted against the incident energies to ascertain further that the beam intensity was constant throughout the stack.

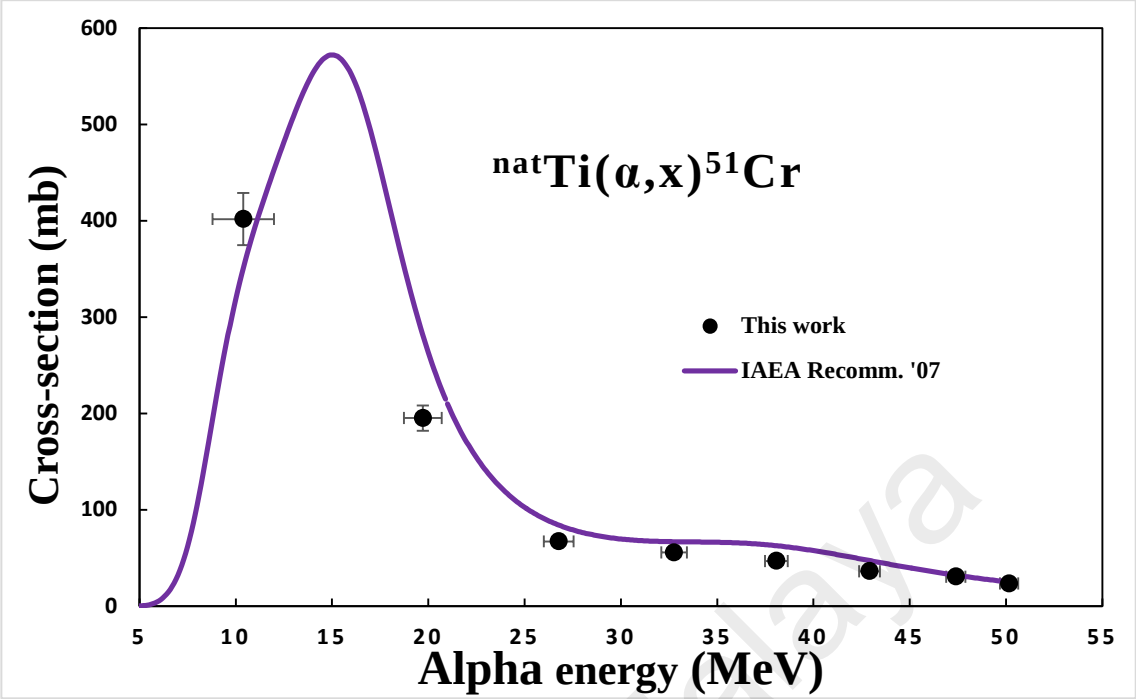

Figure 5.4: Excitation function of the ^{nat}Ti(α,x)^{51}Cr reactions for beam monitoring.

5.3.4 Computation of Cross-sections of the Assessed Radionuclides

In the present work, the following popularly known activation equation (Khandaker et al., 2010; Khandaker et al., 2011) for cross-section evaluation was employed to calculate the cross-sections of the assessed radionuclides:

$$\sigma\,(E_i) = \frac{\lambda C(E_i)}{\varepsilon_\gamma I_\gamma t_h \rho\varphi(1-e^{-\lambda t_{irr}})(e^{-\lambda t_{coo}})(1-e^{-\lambda t_{mea}})}, \qquad (5.2)$$

From which $C(E_i)$ stands for the net gamma activities (counts) of a photo-peak area under consideration, at an i-th position of a foil, λ is the decay constant ($\lambda = \ln 2/T_{\frac{1}{2}}$) of the assessed radioisotupe and ε_γ is for the gamma ray efficiency of detection at certain sample location in the detector. The I_γ stands for the (absolute) γ intensity of the used γ energy, t_h for the thickness of the bombarded metallic foil and ρ represents the target (foil) atomic density (8.49×10^{22} atoms/cm^3). Also, the other symbols and signs

used in the formula are φ for the calculated α beam intensity (5.45×10^{11} partc./s) whereas the t_{irr}, t_{mea} and t_{coo} respectively represent the times for irradiation, measurement and cooling,.

The gamma computer program by ORTEC (Maestro; Ver. 7.01) (Ortec, 2012) was employed during the spectral analysis. The relevant decay data for the assessed radionuclide productions are presented in Table 5.2 and were extracted from the ENSDF library (Bhat, 1998; Browne & Tuli, 2010a, 2010b, 2013; Junde et al., 2005; Nesaraja et al., 2010). The data was accessed via the NuDat 2.6 interface (NuDat 2.6, 2011). The Q-values and threshold energies presented in Table 5.2 were computed following the atomic mass evaluation (Audi et al., 2003) and accessed via the Q-tool system (Qtool, 2011).

Table 5.2: The extracted evaluated decay data of the assessed radionuclides accessed via the ENSDF library

(The ENSDF library (Bhat, 1998; Browne & Tuli, 2010a, 2010b, 2013; Junde et al., 2005; Nesaraja et al., 2010) data were extracted from the Nudat (NuDat 2.6, 2011) while the Q-values and threshold energies (Audi et al., 2003) extracted from the Qtool system (Qtool, 2011)).

Nuclide	Half-life	E_γ(keV)	I_γ (%)	Contributing reaction	Q-value (MeV)	Threshold (MeV)
^{66}Ga	9.49 h	833.5324	5.9	^{63}Cu(α,n)^{66}Ga	-7.50	7.98
		1039.220	**37.0 ± 2.0**	^{65}Cu(α, 3n)^{66}Ga	-25.33	26.89
^{67}Ga	3.2617 d	93.31	38.81	^{63}Cu(α,γ)^{67}Ga	3.72	0
		184.576	21.41	^{65}Cu (α,2n)^{67}Ga	-14.10	14.97
		300.217	**16.64 ± 0.12**			
		393.527	4.56			
^{65}Zn	243.93 d	**1115.54**	**50.04 ± 0.10**	^{63}Cu(α,d)^{65}Zn	-10.38	11.04
				^{63}Cu(α,n + p)^{65}Zn	-12.60	13.40
				^{65}Cu(α,n + t)^{65}Zn	-21.95	23.30
				^{65}Cu(α,2n + d)^{65}Zn	-28.21	29.94
				^{65}Cu(α,3n + p)^{65}Zn	-30.43	32.31
				EC+β^+decay (100%) of ^{65}Ga (15.2 min)		
^{57}Co	271.74 d	**122.0607**	**85.60 ± 0.17**	^{63}Cu(α,2n+ 2α)^{57}Co	-24.81	26.38
		136.47356	10.68	^{63}Cu(α,2t + α)^{57}Co	-36.13	38.43
				^{63}Cu(α,2n+p+t+ α)^{57}Co	-44.62	47.45
				^{63}Cu(α,3n+^{3}He+ α)^{57}Co	-45.38	48.27
				^{63}Cu(α,n + d + t + α)^{57}Co	-42.39	45.09
				^{65}Cu(α,4n+2α)^{57}Co	-42.63	45.26
^{58g}Co	70.86 d	**810.7593**	**99.450± 0.010**	^{63}Cu(α,n + 2α)^{58}Co	-16.23	17.26
				^{63}Cu(α,d + t + α)^{58}Co	-33.82	35.97
				^{63}Cu(α,n + p + t + α)^{58}Co	-36.04	38.34
				^{63}Cu(α,2n+^{3}He+α)^{58} Co	-36.81	39.15
				^{63}Cu(α,n + 2d+α)^{58}Co	-40.08	42.62
				^{63}Cu(α,2n+p+d+α)^{58} Co	-42.30	44.99
				^{63}Cu(α,3n+2p+α)^{58}C o	-44.52	47.36
				^{65}Cu(α,3n+2α)^{58}Co	-34.06	36.16
				^{65}Cu(α,n+2t+α)^{58}Co	-45.39	48.19
				IT decay (100%) of ^{58m}Co (9.10 h)		

Table 5.3: Decay data of the radionuclides adopted in this studies (continued)

Nuclide	Half-life	E_γ(keV)	I_γ (%)	Contributing reaction	Q-value (MeV)	Threshold (MeV)
^{60g}Co	1925 d	**1173.228**	**99.85 ± 0.03**	^{63}Cu(α,3He+α)^{60}Co	-18.86	20.06
		1332.492	99.9826	^{63}Cu(α,p+d+α)^{60}Co	-24.35	25.90
				^{63}Cu(α,n+2p+α)^{60}Co	-26.58	28.27
				^{63}Cu(α,p+t+^{3}He)^{60}Co	-38.67	41.13
				^{63}Cu(α,n+2^{3}He)^{60}Co	-39.44	41.95
				^{63}Cu(α,2d+^{3}He)^{60}Co	-42.71	45.42
				^{63}Cu(α,d+t+2p)^{60}Co	-44.17	46.98
				^{63}Cu(α,n+p+d+^{3}He)^{60}Co	-44.93	47.79
				^{63}Cu(α,n+3p+t)^{60}Co	-46.39	49.34
				^{65}Cu(α,n2α)^{60}Co	-16.11	17.10
				IT decay (99.75%) of ^{60m}Co (10.467 min)		

5.3.5 Computation of Uncertainties on Cross-sections

The present work has evaluated and quadratically summed all the possible uncertainties from several sources, following the experimental conditions of the present work, to get the total uncertainties. These uncertainties have been exclusively reported (Table 5.4), and they have also been presented with the cross-sections in Table 5.5 and Figs. 5.5 – 5.10. The assumed fractional uncertainties during the evaluation are as follows: the (5%) uncertainties from beam intensity, (4%) for detector efficiency and (1%) for the thickness of target. The uncertainties for the intensities (0.01 to 5.41%) of the assessed γ-ray of the studied nuclides were accessed from the ENSDF library (Bhat, 1998; Browne & Tuli, 2010a, 2010b, 2013; Junde et al., 2005; Nesaraja et al., 2010). Additionally, the uncertainties due to the statistics of γ-ray counting (0.12 to 16.3 %) have also been evaluated.

Table 5.4: Uncertainties (%) propagated to the total uncertainty in the cross-sections

(The uncertainties in beam intensity, detector efficiency and thickness of target were assumed based on the present experimental conditions while the uncertainty in γ-ray intensity was taken from the ENSDF library (Bhat, 1998; Browne & Tuli, 2010a, 2010b, 2013; Junde et al., 2005; Nesaraja et al., 2010).

Product Nuclide	Uncertainties (%)					
	γ-ray intensity (ΔIγ/ Iγ)	beam intensity	detector efficiency	Target thickness	γ-ray counting statistics	Total uncertainty
^{66}Ga	5.41	5	4	1	0.8 - 9.0	8.5-12.3
^{67}Ga	0.72				0.3 - 16.3	6.5-17.6
^{65}Zn	0.20				0.1 - 0.6	6.5-6.5
^{57}Co	0.20				1.3 - 6.1	6.6-8.9
^{58g}Co	0.01				0.3 - 1.3	6.5-6.6
^{60g}Co	0.03				4.9 - 10.5	8.1-12.3

5.4 Results and Discussions

The reported production cross-sections for the ^{66,67}Ga, ^{57,58,60}Co and ^{65}Zn have been presented with their corresponding uncertainties in Table 5.5. The corresponding excitation functions of these radionuclides are presented in the Figs. 5.5–5.10 together with the prior reported literature experimental data obtained from EXFOR database (Otuka et al., 2014) and the theoretical data of TENDL-2014 library (Koning et al., 2014). The TENDL-2014 is the database for the compiled evaluated output data of the TALYS nuclear reaction code (Koning & Rochman, 2012). The cross-sections reported in some works from the isotopes of copper (Bhardwaj et al., 1988; Bryant et al., 1963; Didik et al., 1994; Graf & Münzel, 1974; Hille et al., 1972; Houck & Miller, 1961; Lebowitz & Greene, 1970; Levkovskij, 1991; Lin & Alexander, 1977; Mukherjee et al., 1997; Navin et al., 2004; Porges, 1956; Porile & Morrison, 1959; Rao et al., 1991; Rizvi et al., 1987; Ruddy & Pate, 1969; Singh et al., 1994; Stelson & McGowan, 1964; Watson et al., 1973; Zhukova et al., 1970; Zweit et al., 1987) have been renormalized by multiplying their production cross-sections with the corresponding natural

abundances of the corresponding target isotopes (copper has two stable isotopes: ^{63}Cu and ^{65}Cu) employed. The "cumulative cross-sections" defined by the CNEA group (Bonesso et al., 1991; Nassiff, 1983; Ozafrán et al., 1989) in their original publications have been converted (normalized) in to the corresponding elemental cross-sections by multiplying the cross-sections in those publications with the atomic weight (63.5 g/mol) of natural copper. Following this conversion and some other renormalization procedures performed on the experimental literature data, some definitions are made in the text and Figures of this chapter as follows;

- norm: The reported isotopic cross-sections are multiplied by natural isotopic abundances of target nuclides;
- norm,+: The reported isotopic cross-sections are multiplied by their natural abundances and summed over two target nuclides (as a result of two or more reports of the same work such that a uniform symbol could be used to represent both data sets);
- norm,*: The reported CNEA "cumulative cross-sections" are multiplied by the atomic weight of natural copper.

The Figure 5.4 indicates that the currently measured monitor reaction, the ^{nat}Ti(α,x)^{51}Cr cross-sections, renormalized to the IAEA recommended cross-sections (Qaim et al., 2002) are in agreement with the IAEA cross-sections below 50 MeV.

Table 5.5: Cross-sections for $^{nat}Cu(\alpha,x)^{66,67}Ga$, ^{65}Zn and $^{57,58,60}Co$ reactions

Energy (MeV)	Cross-sections (mb)					
	$^{nat}Cu(\alpha,x)^{66}Ga$	$^{nat}Cu(\alpha,x)^{67}Ga$	$^{nat}Cu(\alpha,x)^{65}Zn$	$^{nat}Cu(\alpha,x)^{57}Co$	$^{nat}Cu(\alpha,x)^{58g+m}Co$	$^{nat}Cu(\alpha,x)^{60g+m}Co$
48.8 ± 0.8	86.6 ±7.1	37.9 ± 3.6	245.7 ± 16.1	2.9 ± 0.2	25.2 ± 1.6	3.7 ± 0.3
45.2 ± 0.9	114.9 ± 9.4	48.6 ± 4.6	236.2 ± 15.5	0.36 ± 0.03	22.1 ± 1.4	2.4 ± 0.2
40.5 ± 0.9	128.8 ± 10.6	78.3 ± 7.3	311.2 ± 20.4		13.5 ± 0.9	0.86 ± 0.10
36.0 ± 1.0	86.7 ± 7.1	147.1 ± 13.8	566.0 ± 37.0		2.5 ± 0.2	
30.0 ± 1.2	28.1 ± 2.4	271.5 ± 25.4	813.9 ± 53.3			
23.4 ± 1.4	117.8 ± 9.7	281.4 ±26.3	411.0 ± 26.9			
16.4 ± 1.9	435.6 ± 35.6	22.9 ± 2.2	29.1 ± 1.9			

5.4.1 Independent Production Cross-sections of ^{66}Ga

The formation of ^{66}Ga ($T_{1/2}$ = 9.49 h) was only possible via the $^{63}Cu(\alpha,n)^{66}Ga$ (E_{th} = 7.98 MeV) and $^{65}Cu(\alpha,3n)^{66}Ga$ (E_{th} = 26.89 MeV) reactions. Identification and analysis of this radionuclide were done via its intense γ line of E_γ = 1039.22 keV (I_γ = 37.0 %). In Fig. 5.5, the present cross-sections of ^{66}Ga are compared with those in the previous experimental studies as well as the TENDL-2014 library. A large amount of the literature (Bhardwaj et al., 1988; Bonesso et al., 1991; Bryant et al., 1963; Didik et al., 1994; Hille et al., 1972; Levkovskij, 1991; Nassiff, 1983; Navin et al., 2004; Porges, 1956; Porile & Morrison, 1959; Rao et al., 1991; Rattan et al., 1986; Rizvi et al., 1987; Shahid et al., 2015b; Singh et al., 1994; Sonck et al., 1996; Stelson & McGowan, 1964; Szelecsényi et al., 2012; Szelecsényi et al., 2001; Tárkányi et al., 1992; Tárkányi et al., 2000; Zhukova et al., 1970; Zweit et al., 1987) is available for this radionuclide, and they show obvious differences among them. The cross-sections reported in some previous studies (Porges, 1956; Porile & Morrison, 1959; Rizvi et al., 1987; Zhukova et al., 1970) are generally much lower than the present work. As pointed in (Tárkányi et al., 2000), cross-sections reported in the literature are sometimes not clear whether elemental or isotopic, especially when they are reported as $^{63}Cu(\alpha,n)^{66}Ga+^{65}Cu(\alpha,3n)^{66}Ga$ cross-section. At around 30 MeV and beyond, the reported data of some groups (Bonesso et al., 1991; Levkovskij, 1991; Porges, 1956;

Zhukova et al., 1970) are very low compared to the present cross-sections and those recommended by the IAEA (Qaim et al., 2002). The too low cross-sections from the first data sets (Ex-1) of Refs. (Levkovskij, 1991; Zhukova et al., 1970) above the 30 MeV are explained by the absence of ^{65}Cu in the target material. On the other hand, the present data agree with those recommended by the IAEA (Qaim et al., 2002) and also those reported by some other groups (Bryant et al., 1963; Shahid et al., 2015b; Szelecsényi et al., 2012; Tárkányi et al., 1992; Tárkányi et al., 2000; Zweit et al., 1987). The reported cross-sections by Szelecsényi et al. (Szelecsényi et al., 2001) are slightly higher and scattered, while those by some groups (Didik et al., 1994; Sonck et al., 1996) are much higher than the present ones around 17 MeV. The cross-sections reported by some groups (Levkovskij, 1991; Rizvi et al., 1987; Singh et al., 1994) are obviously affected by the energy shift while those by (Nassiff, 1983; Porile & Morrison, 1959) give, in addition to the energy shift, an unusual shape of the excitation function. Similarly, the evaluated cross-sections in the TENDL-2014 library (Koning et al., 2014) could not reproduce the data of the current study and give much lower values.

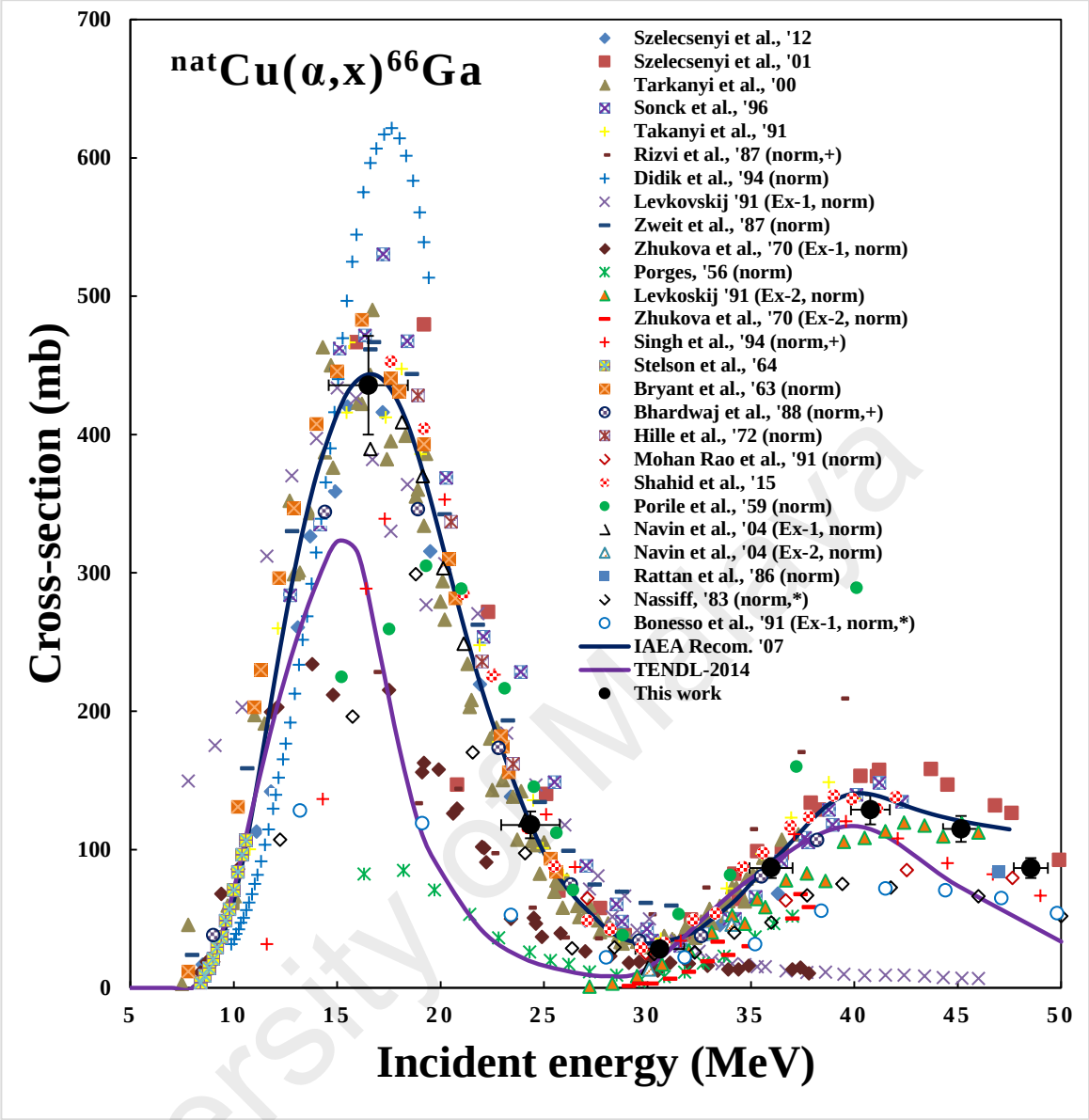

Figure 5.5: Excitation function of the ^{nat}Cu(α,x)^{66}Ga reactions. See the main text for the explanation of 'norm', 'norm,+' and 'norm,*'.

5.4.2 Independent Production Cross-sections of ^{67}Ga

The cross-sections for the beam monitor radionuclide ^{67}Ga ($T_{1/2}$ = 3.2617 d) was analysed using its interference-free γ line of E_γ = 300.217 keV (I_γ = 16.64%). The present cross-sections are shown in Fig. 5.6 together with the literature data and the extracted ones from the TENDL-2014 library. Several research groups (Basunia et al., 2005; Bhardwaj et al., 1988; Bonesso et al., 1991; Bryant et al., 1963; Cata-Danil et al., 2008; Didik et al., 1994; Graf & Münzel, 1974; Levkovskij, 1991; Mukherjee et al.,

1997; Navin et al., 2004; Porges, 1956; Porile & Morrison, 1959; Rao et al., 1991; Rattan et al., 1986; Rizvi et al., 1987; Shahid et al., 2015b; Singh et al., 1994; Szelecsényi et al., 2012; Szelecsényi et al., 2001; Tárkányi et al., 2000; Watson et al., 1973; Zhukova et al., 1970; Zweit et al., 1987) have reported the production of this radionuclide with, again, unacceptable discrepancy. Two experimental works (Basunia et al., 2005; Cata-Danil et al., 2008) show that the $^{63}Cu(\alpha,\gamma)^{67}Ga$ cross-section increases to 1 mb at about 8 MeV, while the $^{65}Cu(\alpha,2n)^{67}Ga$ reaction (E_{th} = 14.97 MeV) explains the major peak seen in the literature data. The reported cross-sections in some earlier studies (Navin et al., 2004; Porges, 1956; Porile & Morrison, 1959; Rizvi et al., 1987; Watson et al., 1973; Zhukova et al., 1970) are much lower than the present ones. The excitation function of the data reported by Zweit et al. (Zweit et al., 1987) is extremely too low though their ^{66}Ga production cross-sections shown in Fig.2 are reasonable. From the shape of the excitation function, energy shift seems to have affected the cross-section reported by some other authors (Graf & Münzel, 1974; Levkovskij, 1991) while other groups (Bonesso et al., 1991; Navin et al., 2004; Porges, 1956; Rizvi et al., 1987; Zhukova et al., 1970) reported much lower cross-sections than the present work. Some of the reported cross-sections (Mukherjee et al., 1997) gave an unusual shape of the excitation function of the studied radionuclide. The present data are in agreement with some previous studies (Bryant et al., 1963; Shahid et al., 2015b; Singh et al., 1994; Szelecsényi et al., 2012; Tárkányi et al., 2000) and the cross-sections recommended by the IAEA (Qaim et al., 2002), while those by Szelecsényi et al. (Szelecsényi et al., 2001) are slightly higher. On the other hand, the evaluated data in the TENDL-2014 library give lower values, especially at $\geq$ 22 MeV.

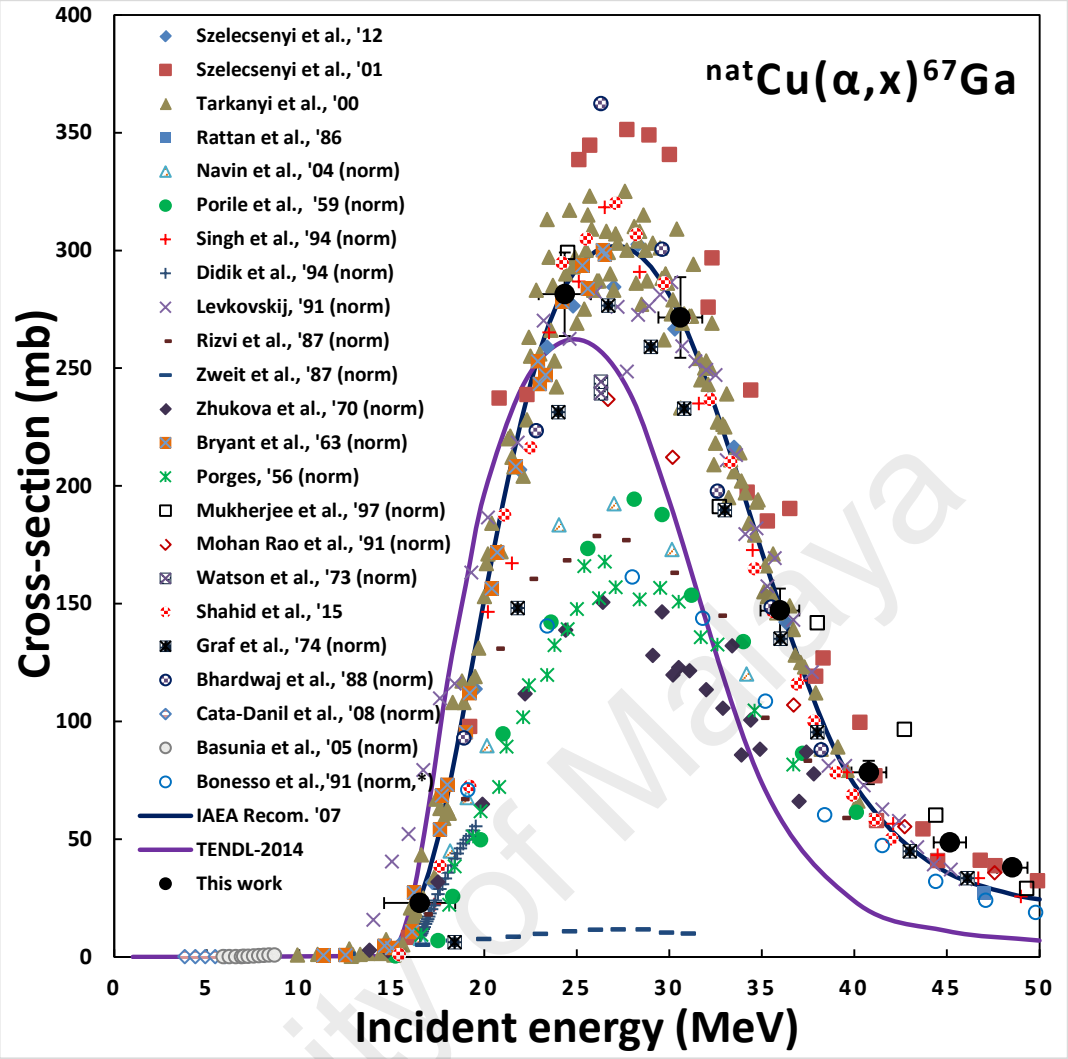

Figure 5.6: Excitation function of $^{nat}Cu(\alpha,x)^{67}Ga$ reactions. See the main text (Section 3) about 'norm' and 'norm,*'.

5.4.3 Cumulative Production Cross-sections of ^{65}Zn

The assessment of the long-lived beam monitor radionuclide ^{65}Zn ($T_{1/2}$ = 243.93 d) was done by its interference-free and highly intense γ line of E_γ = 1115.54 keV (I_γ = 50.04 %). The short-lived ^{65}Ga ($T_{1/2}$ = 15.2 min) formed by the $^{63}Cu(\alpha,2n)^{65}Ga$ (E_{th} = 17.7 MeV) and $^{65}Cu(\alpha,4n)^{65}Ga$ (E_{th} = 36.6 MeV) reactions completely decays to ^{65}Zn via EC and β^+ processes. Thus, the measured cross-section for ^{65}Zn is cumulative. Although many earlier studies (Bhardwaj et al., 1988; Bonesso et al., 1991; Houck & Miller, 1961; Lebowitz & Greene, 1970; Levkovskij, 1991; Lin & Alexander, 1977; Navin et al., 2004; Porges, 1956; Porile & Morrison, 1959; Rattan et al., 1986; Rizvi et

al., 1987; Ruddy & Pate, 1969; Shahid et al., 2015b; Singh et al., 1994; Tárkányi et al., 2000; Zhukova et al., 1970; Zweit et al., 1987) are available for the measurement of the $^{nat}Cu(\alpha,x)^{65}Zn$ reaction cross-sections, these studies could not yet address the discrepancies among the measured data. The present result is plotted together with the previous data in Fig. 5.7. The data reported by several groups (Bonesso et al., 1991; Lebowitz & Greene, 1970; Levkovskij, 1991; Navin et al., 2004; Porges, 1956; Porile & Morrison, 1959; Rattan et al., 1986; Rizvi et al., 1987; Zweit et al., 1987) are much lower than the present ones and also the the IAEA recommended values (Qaim et al., 2002). On the other hand, present cross-sections are closer to previous studies by some groups (Bhardwaj et al., 1988; Houck & Miller, 1961; Shahid et al., 2015b; Singh et al., 1994; Tárkányi et al., 2000) and the IAEA (Qaim et al., 2002) recommended values. The evaluated cross-sections in the TENDL-2014 library (Koning et al., 2014) are lower than the present experimental values even if the cross-sections of $^{nat}Cu(\alpha,x)^{65}Ga$ are added to the TENDL-2014 library data, as shown in the Figure below.

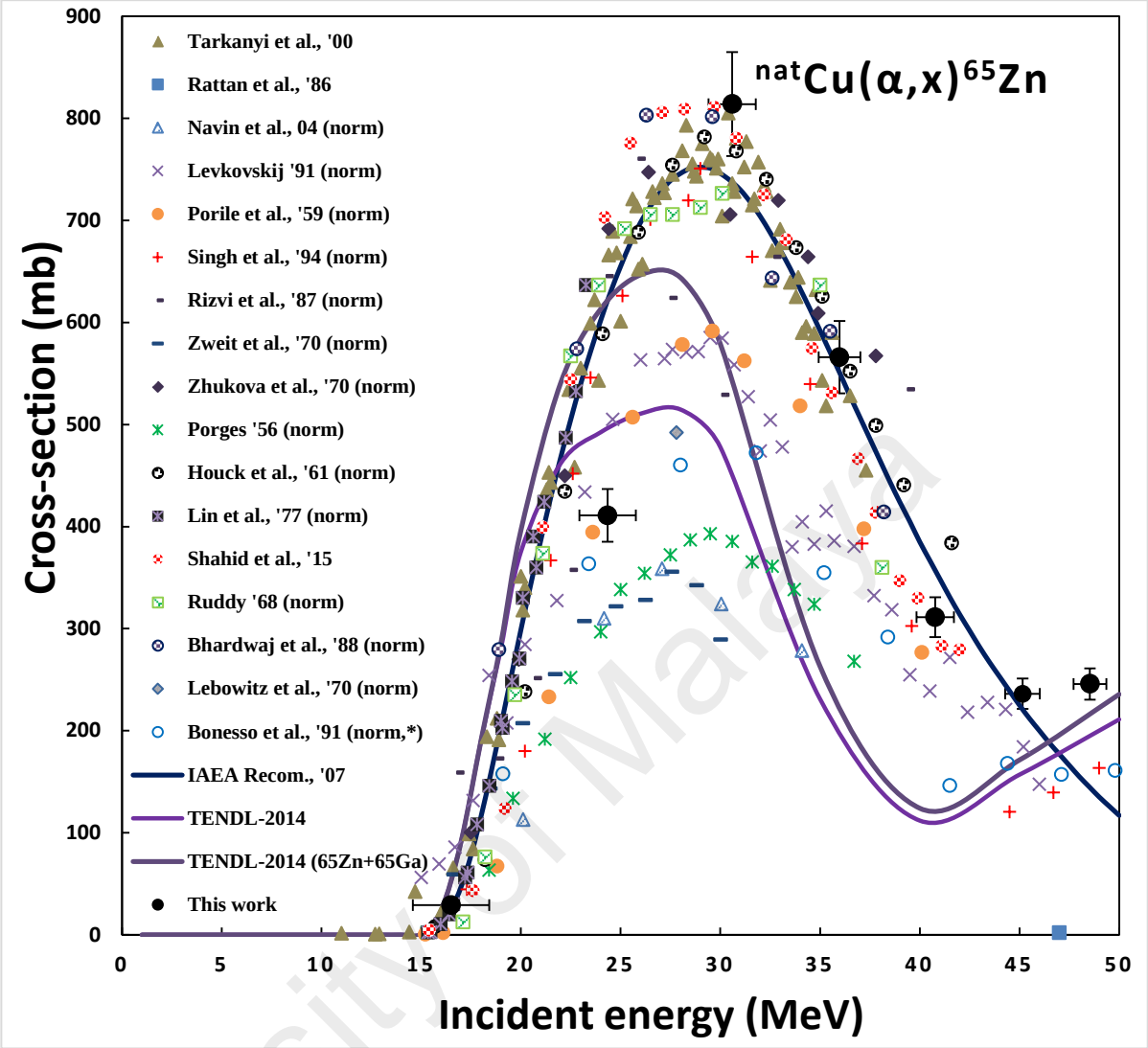

Figure 5.7: Excitation function of the ^{nat}Cu(α,x)^{65}Zn reactions. See the main text about 'norm' and 'norm,*'.

5.4.4 Independent Production Cross-sections of ^{57}Co

The independent cross-sections of ^{57}Co ($T_{1/2}$ = 271.74 d) were assessed via its interference-free γ line of E_γ = 122.0607 keV (I_γ = 85.60%). The main contributing reactions to the formation of ^{57}Co are listed in Table 5.2. The TENDL-2014 library evaluation shows that the ^{57}Co production is solely described by the ^{63}Cu(α,2nα)^{57}Co reaction below 50 MeV. Only two earlier studies (Ozafrán et al., 1989; Rattan et al., 1986) are available for the production of ^{57}Co via the ^{nat}Cu(α,x)^{57}Co reactions. In Fig. 5.8, the present data agree with the reported cross-sections of Rattan (Rattan et al., 1986) but larger than those reported by Ozafran's group (Ozafrán et al., 1989). The

TENDL-2014 library (Koning et al., 2014) reproduced the measured excitation function only in shape but not in magnitude.

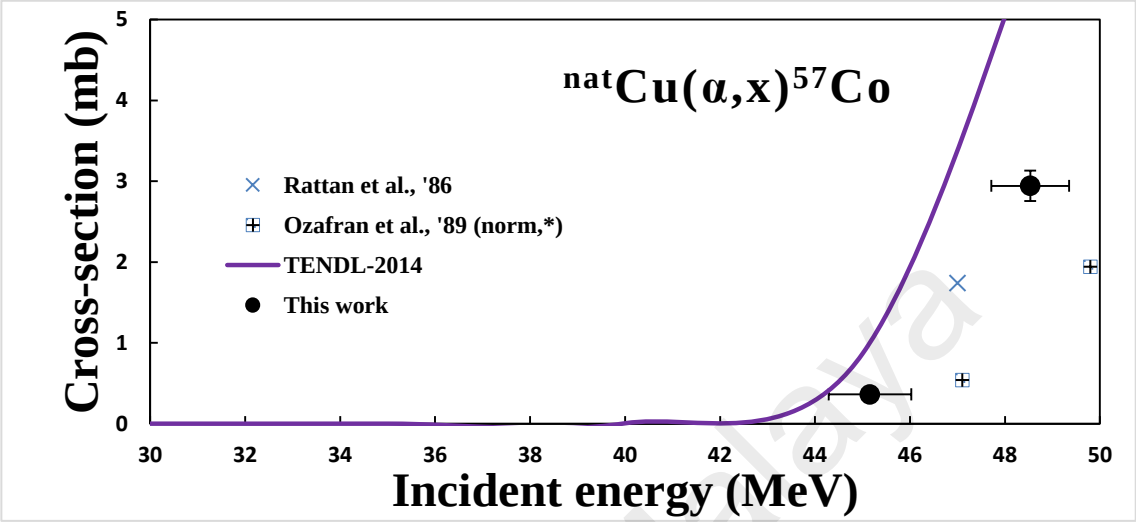

Figure 5.8: Excitation function of the ^{nat}Cu(α,x)^{57}Co reactions.

5.4.5 Independent Production Cross-sections of $^{58g+m}$Co

The cross-sections of ^{58g}Co ($T_{1/2}$ = 70.86 d) were assessed using the γ-ray spectra acquired after a sufficient cooling time for a complete IT decay from its metastable state ^{58m}Co ($T_{1/2}$ = 9.10 h). As indicated in Table 5.2, there are nine possible contributing reactions for the formation of this radionuclide, with the least threshold reaction as ^{63}Cu(α,n2α)^{58}Co (E_{th} = 17.3 MeV). The identification and analysis of this radionuclide were done via its abundant γ line of E_γ = 810.7593 keV (I_γ = 99.450%). As shown in Fig. 5.9, the excitation function of the present study agrees with the data of Rattan et al. (Rattan et al., 1986) and Shahid et al. (Shahid et al., 2015b). The TENDL-2014 library (Koning et al., 2014) reproduced well the present results including the literature data reported by Shahid (Shahid et al., 2015b) and Rattan (Rattan et al., 1986). The reported excitation functions by Levkoskij et al. (Levkovskij, 1991) and Ozafran et al. (Ozafrán et al., 1989) show a disagreement with the present study.

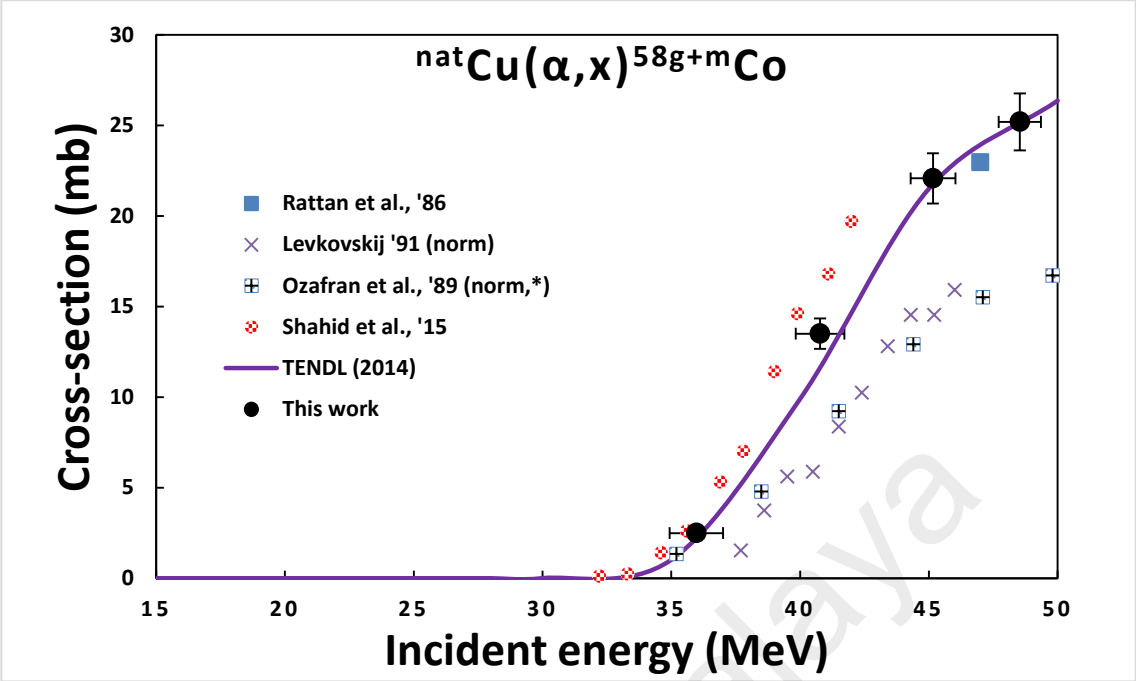

Figure 5.9: Excitation function of the ^{nat}Cu(α,x)$^{58g+m}$Co reactions. See the main text for the explanation of 'norm' and 'norm,*'.

5.4.6 Independent Production Cross-sections of $^{60g+m}$Co

The long-lived ^{60}Co ($T_{1/2}$ = 1925 d) is usually assessed by either or both of its two abundant γ lines of E_γ =1173.228 keV (I_γ = 99.85%) and 1332.492 keV (I_γ = 99.9826%). The reported cross-sections are for production of both the ground and metastable ($T_{1/2}$ = 10.467 min) states of ^{60}Co due to the complete IT decay (IT = 99.75%) of the metastable state. In addition to ^{65}Cu(α,n2α)^{60}Co, which has the least threshold energy (E_{th} = 17.1 MeV), other several nuclear reaction channels are leading to the formation of ^{60}Co as indicated in Table 5.2. Despite these possible reaction channels, the overall cross-sections are, however, very low. Only one previous work by Ozafran et al. (Ozafrán et al., 1989) and one recent study by Shahid et al. (Shahid et al., 2015b) are available for ^{60}Co production cross-sections. The present data are compared in Fig. 5.10 with the data of Shahid et al. (Shahid et al., 2015b) which gives slightly higher values above 40 MeV. The cross-sections reported in this work agree with those

reported by Ozafran et al. (Ozafrán et al., 1989). The data extracted from the TENDL-2014 library (Koning et al., 2014) are slightly lower than the present data.

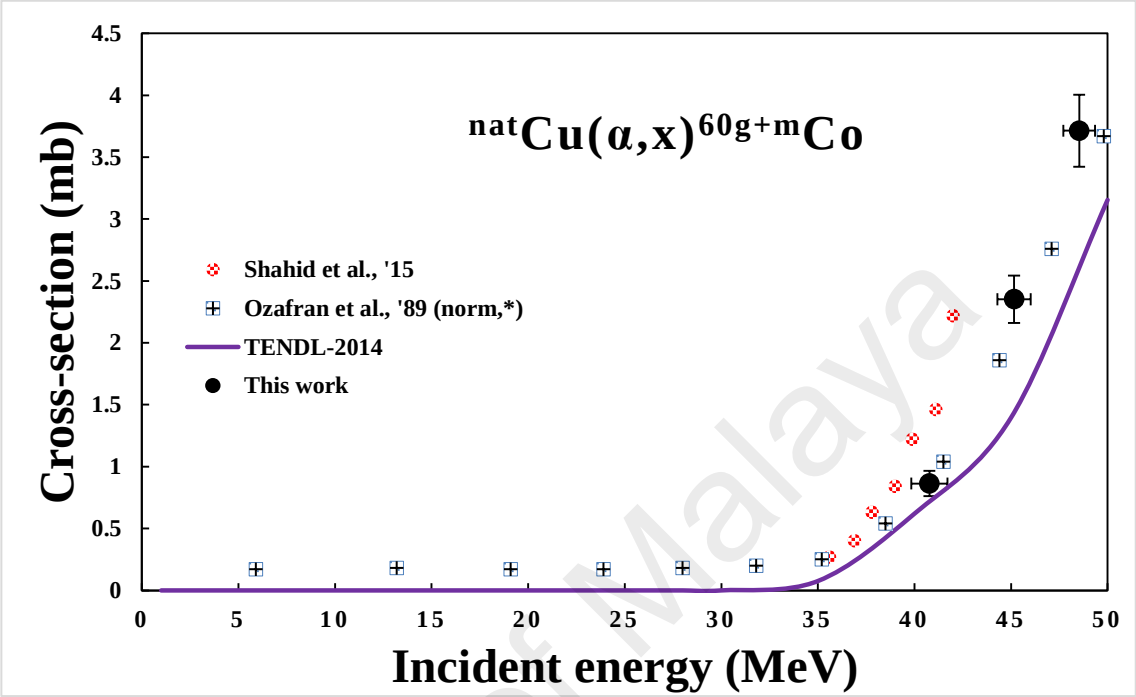

Figure 5.10: Excitation function of the $^{nat}Cu(\alpha,x)^{60g+m}Co$ reactions.

5.5 Conclusions

The production cross-sections of $^{66,67}Ga$, ^{65}Zn, and $^{57,58,60}Co$ radionuclides from the α-particle-induced reactions on natural copper were measured in the energy range of 50 MeV down to 16.5 MeV by using a stacked foil activation technique and HPGe γ-ray spectrometry. The measured data were compared with the available literature cross-sections as well as the theoretical data predicted by the TALYS-1.6 code and compiled in the TENDL-2014 library. From the reported excitation functions, the cross-sections of cobalt radionuclide productions are generally low and only obtainable at the upper part of the investigated energy region. Although there are several reported data on the production of ^{66}Ga, ^{67}Ga, and ^{65}Zn, they were found to be largely discrepant. The present results are useful to enrich the database of the investigated radionuclide productions thereby reducing the discrepancies among the previous measurements.

More so, the present data are also expected to further improve the prediction capability of the TALYS code and other nuclear reaction codes, especially for the Co radionuclide productions for which still very few experimental works have been performed so far.

CHAPTER 6: EXCITATION FUNCTIONS OF ALPHA-INDUCED REACTIONS ON NATURAL HOLMIUM

6.1 Introduction

This chapter presents the excitation functions of thulium (Tm) radionuclides obtained from irradiation of natural holmium targets. The holmium foils were parts of the stack bombarded with the 50.4 MeV alpha beam energy. The presented results are a part of the major components of this thesis. The Tm radionuclides have been reported to have several potential applications and the present chapter therefore exclusively presents only the results from the Ho targets.

Many of the radionuclides intended to investigate had very low gamma ray intensities, several interfering gamma lines among them, or, even having very low (less than 50 keV) gamma energies. Thus, such investigated radionuclides have not been reported in this study as the peaks of the gamma lines were sometimes either ambiguous or even not seen in the spectrum. Specifically, the following radionuclides are some of the attempts made without achieving the expected results; ^{161}Ho, ^{164g}Ho ^{166g}Ho, ^{167}Ho, as well as some radionuclides of Dy, Tb, Er, Eu, Sm, etc., although the q-tool system (Qtool, 2011) and Q-value calculator (QCalc, 2016) have predicted the production properties of these radionuclides. The following subsections will provide the details of the experimental component related to the holmium bombardment.

6.2 Literature Review

Holmium (Ho), a rare-earth metal, plays important roles in nuclear physics. It was used in nuclear reactors as a burnable poison due to its ability to absorb nuclear fission neutrons (Luo et al., 2015). Recently, there has been growing usage of therapeutic radionuclides in nuclear medicine. The rare-earth metals have attracted more attention as sources of these therapeutic radionuclides due to their ability to release low energy

electrons. They are usually pure emitters of the auger electrons which can transfer large local doses on tissues (Hermanne et al., 2009) as well as having outstanding chemical properties comparable to lanthanides such that they can be coupled to biomolecules with a single class of chelates as in DOTA for cancer treatment (Cutler et al., 2000). Several rare-earth metals are excellent sources of thulium radionuclides. Irradiation of these sources has recently been done using different charged particles.

The thulium-167, due to its low energy electrons, has been used as a tracer radionuclide during bone and tumour studies (Chandra et al., 1971; Nayak & Lahiri, 1999; Tárkányi et al., 2010). With a half-life of 9.25 days, ^{167}Tm has been considered as a suitable candidate in radiotherapy. In fact, its therapeutic properties are also due to its emission of Auger electrons, low energy γ- and X-rays (Tarkanyi et al., 2010; Uusijärvi et al., 2006). More precisely, some relatively small tumours, weighing below 1 mg, can effectively be treated (Sadeghi et al., 2012). On the other hand, the desirable decay characteristics of ^{165}Tm ($T_{1/2}$ = 1.25 d) radionuclide make it a potential replacement to the more popular ^{167}Tm (Nayak et al., 1999) counterpart.

Table 6.1 presents the major sources of ^{167}Tm via charged-particle-induced nuclear reactions (Sadeghi et al., 2012; Tarkanyi et al., 2010). As presented in the Table, the ^{167}Tm radionuclide can be produced through direct nuclear reactions as well as, in some cases, indirect formation by the decay of an intermediate radionuclide.

Table 6.1: Direct and Indirect Production Routes for ^{167}Tm.

Direct ^{167}Tm production	Indirect ^{167}Tm production
^{165}Ho(α,2n)^{167}Tm	^{169}Tm(p,3n) ^{167}Yb → ^{167}Tm
^{167}Er(p,n)^{167}Tm	^{nat}Yb(p,xn) ^{167}Lu → ^{167}Yb → ^{167}Tm
^{167}Er(d,2n)^{167}Tm	^{nat}Hf(p,x) ^{167}Lu → ^{167}Yb → ^{167}Tm
^{168}Yb(p,x)^{167}Tm (cumulative)	^{nat}Er(α,x) ^{167}Yb → ^{167}Tm
^{nat}Er(p,xn)^{167}Tm	
^{nat}Er(d,xn)^{167}Tm	

Aside the medical applications, measurements of low energy nuclear processes via (α, n) and (α, γ) reactions are very important in γ-process nucleosynthesis to improve determinations of certain astrophysical reaction rates (Kiss et al., 2014). The γ-process is the photodisintegration phenomenon of nuclei above Fe in explosive stellar processes (Kiss et al., 2014).

Currently, the production of these therapeutic radionuclides is mainly done via (n,γ) processes in nuclear reactors. Alternatively, however, charged-particles induced production routes are needed to achieve productions of these radionuclides with high specific activity or to produce an end-product at no-carrier-added level. Investigation of the various therapeutic radioactive candidates via various production routes has been intensified, with alpha production route as also a production pathway.

A comprehensive study of all previous studies on this production route with holmium (foils, compound, block, and so on) as target material from all previous works, as shown in a tabular summary in chapter two of this thesis, revealed that many of the previous measurements were made with one problem or the other. It would be seen from the table, as an example, that while several groups used scintillation detectors with poor resolutions, other groups used Ge(Li) detectors for the measurements of activities. The decay data used by several groups are also outdated relative to the present (decay) data available. Due to the importance and sensitivity of cross section data in nuclear physics

and medical applications, it is necessary that precise measurements and small details be well understood for optimisation in production since a little detail can make a huge difference in these relevant fields of knowledge.

Given these overwhelming reasons, new measurements are important to understand the uncertainties surrounding the previous measurements, and to improve the quality of the cross sections by using the most recent decay data of the measured residual radionuclides. In this thesis, new measurements are therefore made using a relatively large number of holmium foils so as to increase the energy points. Also, the present work presents results from relatively higher energy region (50 MeV) in comparison with several other studies in the literature.

6.3 Materials and Method

The overall procedure employed under this chapter is similar to the previous two chapters. The popularly known stack-foils method of activation was employed for irradiation. Measurements of activities from the activated target foils were achieved using a high resolution HPGe detector for the determination of the production cross sections. Further details on the materials and methods relevant to the studies of the excitation functions of several radionuclides from holmium bombardment have been presented under the following subheadings:

6.3.1 Selected Targets and Irradiation

High purity (>99 %,) holmium foils (thickness: 12.29 μm, supplier: Goodfellow, UK) served as the main target. The natural holmium has only one isotope (^{165}Ho: 100 %) (Berglund & Wieser, 2011). Other foils, which have been mentioned in the preceded chapters, served here as energy degraders of the initial beam energy down the stack. These are metallic foils of natural Cu (purity: 99.9%, nominal thickness: 9.71 μm,

supplier: Nilaco, Japan) and Ti (purity: >99.6%, nominal thickness: 10.40 μm, supplier: Goodfellow, UK) interleaved in between the Ti foils in the stack. All used foils were weighed using a high precision electronic balance for an accurate thickness determination.

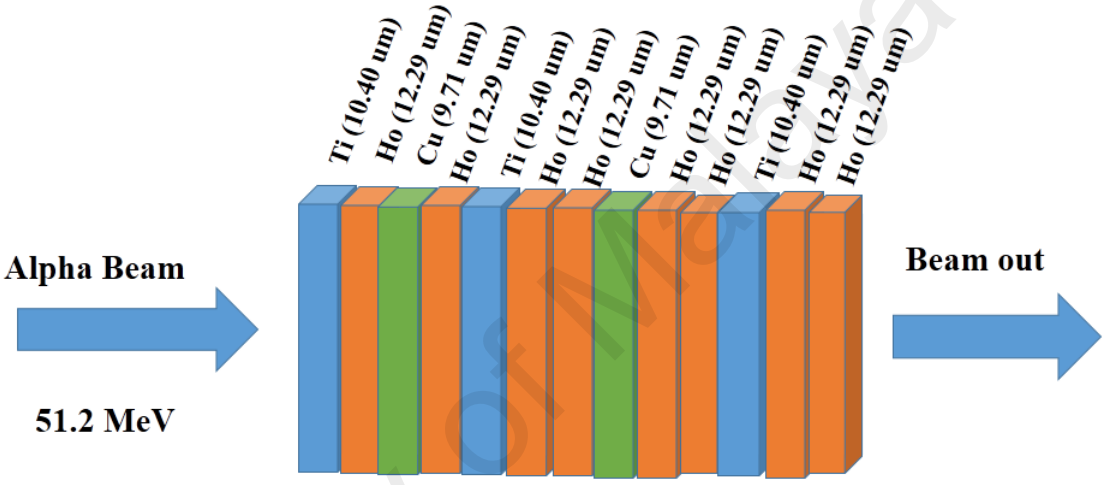

Figure 6.1: Stack arrangement for Ho and other metallic foils

For a successful focusing of the incident beam to the centre of the targets, all the holmium foils were prepared with the dimension of 15 × 15 mm^2 following the size of the target holder. Using the generated beam from the exit channel of the beam line of the AVF cyclotron of RKEN, the stack was then irradiated by focusing the alpha beam onto the target foils by collimating the beam to 9-mm diameter on the targets. Note that the target holder, a water-cooled container serving as a Faraday, held the foils during the whole 2.0 h irradiation time by the α beam, from which an average beam current of 194 nA was observed.

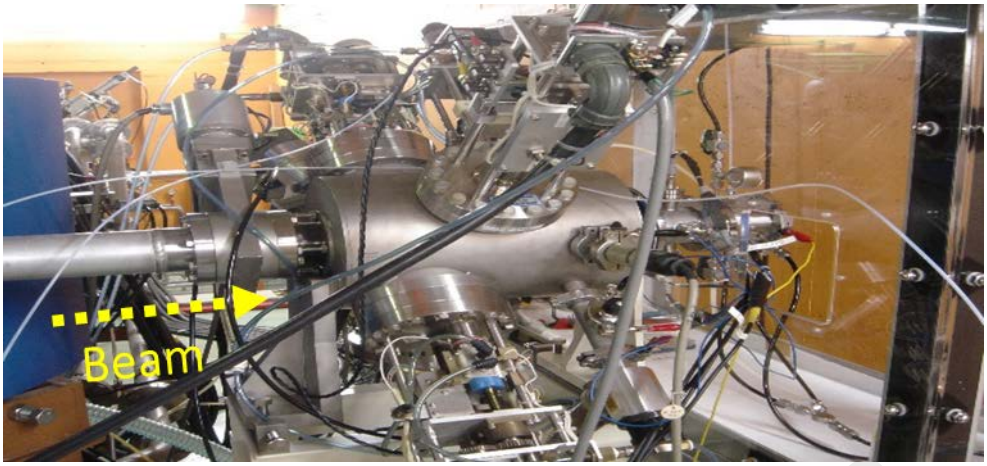

Figure 6.2: The beam line to irradiation chamber where target holder is placed.

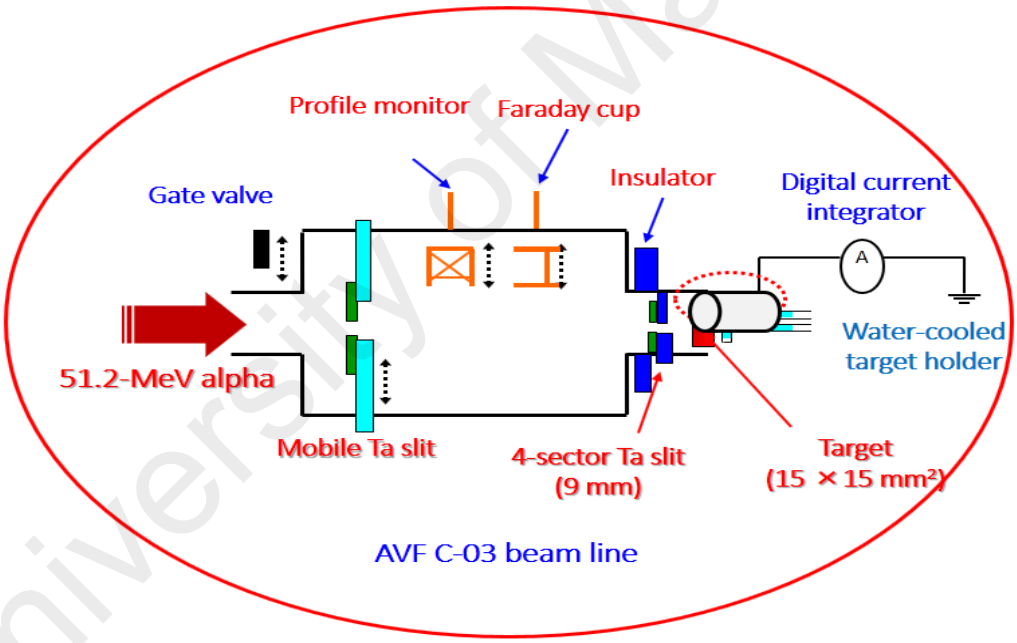

Figure 6.3: The schematic view of the irradiation chamber.

6.3.2 Activity Measurements and Data Analysis.

The irradiated holmium and other foils were removed from the container bombardment and transferred to a hot laboratory for measurements of the gamma rays of the residual radionuclides. Using a high-resolution gamma-ray HPGe detector, the Ho foils were repeatedly measured for the gamma activities to follow the decay of the residual radionuclides. Low dead time in detector was maintained during the measurements by proper utilisation of the various sample positioning locations from detector cap of the detector. Details on the detector specifications used for the measurements and other relevant information have been supplied in the previous chapters. Since there were 30 holmium foils, in addition to other foils from the other targets, with one dedicated detector, radionuclides with a half-life less than 30 mins could not effectively be measured. Details on the cooling periods used for each measured radionuclide have been presented in Table 6.2.

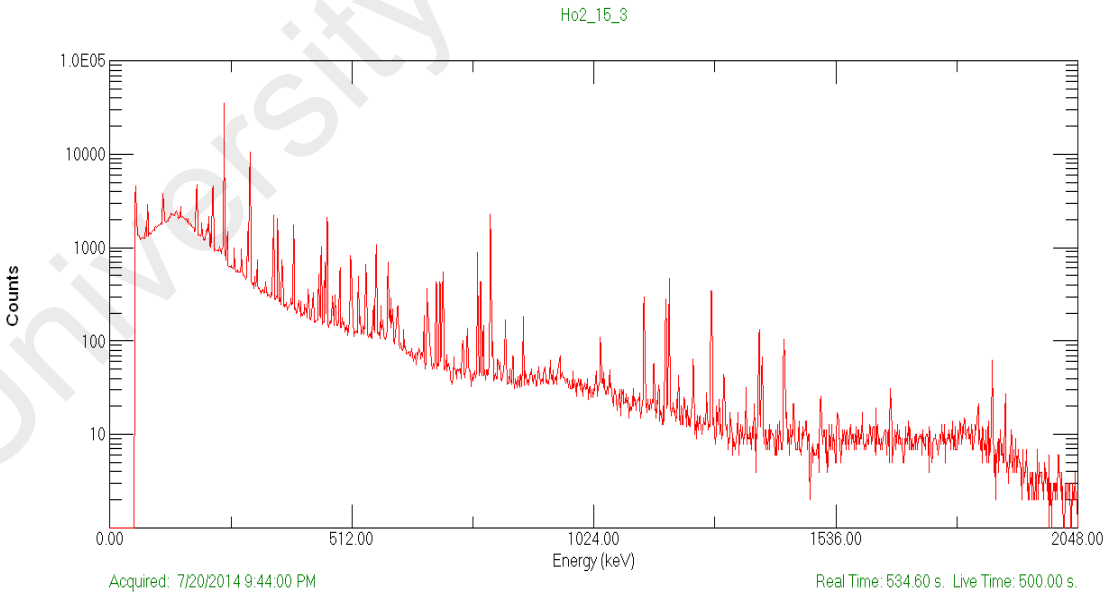

Figure 6.4: A holmium foil spectrum showing peaks for gamma lines.

In chapter 5 (excitation functions of copper-induced reactions) of this thesis, details on the procedure for the determination of efficiencies have been fully described. The efficiencies at various sample-to-detector distances were determined using a multi-nuclides gamma ray standard source for each used sample to detector distance.

Table 6.2: Cooling time used for all the assessed radionuclides

Measurement series	Cooling period	Radionuclide
III	7.7 - 20.7 h	^{166}Tm
IV	0.7 - 1.8 d	^{165}Tm
VII	9.5 - 18.0 d	^{167}Tm
VIII	19.3 – 42.6 d	^{168}Tm

The beam intensity was determined from the measured activities of the Ti foils in the stack for the cross-sections of the ^{51}Cr radionuclide. The IAEA recommended cross sections for the ^{nat}Ti(α,x)^{51}Cr monitor reaction (σ = 26.4 mb at E_α = 50 MeV) were used to determine the beam intensity and considered constant throughout the stack (Usman et al., 2016b).

As the beam traversed along the stack, its energy was degraded by the holmium foils as well as the other foils until it finally lost its energy toward the final foils in the stack. With the help of a computer program, SRIM-2003 software (Ziegler, 2004), the average alpha energy in each foil was calculated. The cross sections are therefore reported in this chapter as representative for each average foil energy.

The production cross sections of the studies radionuclides were calculated using the well-known activation equation (Khandaker et al., 2010; Khandaker et al., 2011; Usman

et al., 2016b). Further details on this aspect have fully been described in the previous chapters. The ENSDF library (Baglin, 2000, 2008, 2010; Jain et al., 2006) was the principal source of the decay data during the calculations of the cross sections and extracted through the Live Chart of Nuclides (IAEA, 2009b). The online Q-tool system (Qtool, 2011) was used for accessing of the Q-values and threshold energies for the reactions, which were calculated based on AME mass evaluation (Audi et al., 2003). Table 6.3 summarises the major relevant decay properties of the assessed radionuclides.

Table 6.3: Decay data used for the analysis of the thulium radionuclides.
(The data were obtained from the ENSDF library (Baglin, 2000, 2008, 2010; Jain et al., 2006) through the live chart of the nuclide, an IAEA online interface. The Q-values were obtained from the Q-tool online system.)

Nuclide	Half-life	Decay mode (%)	E_γ (keV)	I_γ (%)	Contributing reactions	Q-Value (MeV)	Threshold (MeV)
^{165}Tm	30.06 h	EC β^+:100	**242.917**	**35.5** *17*	^{165}Ho(α,4n)^{165}Tm	-31.83	32.60
			297.369	12.7			
^{166}Tm	7.70 h	EC β^+:100	705.333	11.1	^{165}Ho(α,3n)^{166}Tm	-24.80	25.40
			778.814	**19.1** *12*			
			785.904	904			
^{167}Tm	9.25 d	EC:100	**207.801**	**42.0** *8*	^{165}Ho(α,2n)^{167}Tm	-16.07	16.46
			531.54	1.61			
^{168}Tm	93.1 d	EC, β^+:99.99 β^-:0.01	198.251	54.49	^{165}Ho(α,n)^{168}Tm	-9.23	9.46
			815.989	**50.95** 16			

6.3.3 Uncertainties Evaluations on Cross-sections and Foil Energies

Using the procedure for the standard error propagation, all possible sources of uncertainties on cross sections were considered and evaluated in this work based on the experimental conditions during the experiment. Thus, the individual uncertainties were quadratically summed to obtain the cumulative uncertainties. The equations for the calculation of the uncertainties have been presented in chapters 4 and 5. The uncertainties considered were those enough to manifest and include; the uncertainties in gamma rays counts and intensity, the efficiency of the detector, flux and the

uncertainties due to the thicknesses of the used targets. Based on the experimental conditions, the uncertainties due to time scale were considered negligible and thus not included in the general uncertainties evaluations. The overall sources of the uncertainties on holmium excitation functions have been summarised in Table 6.4 and are also presented together with cross-sections in Table 6.5 and Figs. 6.5 to 6.8 of this chapter.

As the beam pass along the stack, its loses its energy by passing through each foil. There are thus uncertainties due to the beam straggling and foil thickness. The uncertainties on the energy on each foil depends on the position of the foil on the stack. The uncertainty on the first holmium foil was estimated as ±0.72 MeV but gradually increased along the stack and was found to be ±3.7 MeV on the last Ho foil. The estimated uncertainties in the α-beam energy for all energy points are indicated in the tables of cross sections and Figures of excitation functions of this chapter.

Table 6.4: Summary of uncertainties considered for analysis of holmium data.

Nuclide	**Uncertainties (%)**					
	γ-ray intensity (ΔIγ/ Iγ)	**beam intensity**	**detector efficiency**	**Target thickness**	**γ-ray counting statistics**	**Total uncertainty**
^{165}Tm	4.8	5	4	2	0.3 – 8.4	8.2 – 11.7
^{166}Tm	6.3				0.9 – 7.4	9.2 – 11.8
^{167}Tm	19.0				0.0 – 0.4	20.19– 20.20
^{168}Tm	0.3				0.4 – 3.17	6.7 – 7.4

6.4 Results and Discussions

The present section discusses the newly calculated cross-sections of the studied radionuclides from the irradiated holmium foils. The production cross-sections for the $^{165\text{-}168}$Tm radionuclides are provided in Table 6.5. Figs. 6.5 – 6.8 show the

corresponding excitation functions of the presented experimental data of Table.6.5. The figures also contain the excitation functions of the earlier experimental measurements (Gadkari et al., 1997; Glorius et al., 2014; Homma et al., 1980; Martin & Pilger, 1966; Mukhrjee et al., 1991; Rao et al., 1987; Rayudu & Yaffe, 1963; Sau et al., 1968; Singh & Prasad, 1995; Singh, 1992; Tarkanyi et al., 2010; Wilkinson & Hicks, 1949) accessed from the EXFOR library (Otuka et al., 2014). The evaluated data was extracted from the TENDL-2015 library (Koning et al., 2014) which provides the output of the TALYS code (Koning & Rochman, 2012).

Table 6.5: Cross sections of $^{165\text{-}168}$Tm radionuclides.

α - energy		^{165}Ho(α,4n)^{165}Tm		^{165}Ho(α,3n)^{166}Tm		^{165}Ho(α,2n)^{167}Tm		^{165}Ho(α,n)^{168}Tm	
E	**Δ*E***	***σ***	**Δ*σ***	***σ***	**Δ*σ***	***σ***	**Δ*σ***	***σ***	**Δ*σ***
(MeV)		**mb**		**mb**		**mb**		**mb**	
49.6	0.7	825.1	68.1	151.3	14.5	35.3	7.1	1.91	0.14
48.1	0.7	939.9	77.5	206.8	19.6	51.2	10.3	2.15	0.15
46.9	0.8	987.2	81.4	249.5	23.5	79.0	16.0	3.53	0.25
46.2	0.8	948.1	78.2	276.3	26.0	74.8	15.1	2.52	0.18
44.6	0.8	818.7	67.5	339.9	31.8	65.7	13.3	2.75	0.19
43.9	0.8	853.3	70.4	434.9	40.5	82.9	16.7	3.70	0.25
42.6	0.8	708.3	58.4	560.6	52.1	86.8	17.5	4.83	0.33
41.8	0.8	592.2	48.9	635.9	59.0	86.1	17.4	3.57	0.25
40.1	0.8	496.3	40.9	852.6	78.9	103.4	20.9	4.18	0.29
39.3	0.9	267.7	22.1	945.4	87.4	92.3	18.6	9.61	0.66
37.9	0.9	127.2	10.5	1072.8	99.1	109.3	22.1	6.25	0.43
37.0	0.9	63.3	5.3	1033.7	95.5	135.9	27.4	11.2	0.8
35.1	0.9	10.7	1.3	1069.6	98.8	161.7	32.6	8.85	0.60
34.2	0.9	0.76	1.02	1053.3	97.3	249.0	50.3	8.49	0.58
32.7	1.0			845.0	78.0	281.1	56.8	7.01	0.48
31.7	1.0			756.2	69.9	385.3	77.8	9.64	0.66
29.6	1.1			349.3	32.3	607.9	122.8	10.8	0.7
28.5	1.1			212.0	19.7	790.1	159.5	12.4	0.8
26.7	1.1			17.4	1.6	816.6	164.9	10.8	0.7
25.6	1.2			0.73	0.09	831.0	167.8	13.2	0.9
23.1	1.2					681.3	137.6	24.5	1.7
21.9	1.3					532.6	107.6	34.3	2.3
19.6	1.4					206.5	41.7	58.0	3.9
18.2	1.5					41.9	0.2	38.6	2.6
14.9	1.7							0.30	0.12
13.2	1.8							0.09	0.04

6.4.1 Production Cross-sections of ^{165}Tm

^{165}Tm ($T_{1/2}$ = 30.06 d) decays via EC β^+ (100%) process to ^{165}Er. The formation of ^{165}Tm was populated through ^{165}Ho(α,4n)^{165}Tm process. The cross sections of this radionuclide were measured via its relatively intense gamma line of E_γ = 242.917 keV (I_γ = 35.5%). Within the investigated energy region of 49.6 MeV as the upper region, the peak of the excitation function could be studied to some extent. The present study indicates a fine shape of the excitation function, showing a peak at around 48 MeV

alpha energy. At higher energy, the results of the present work are closer to the data of Mukherjee group (Mukhrjee et al., 1991). The theoretical excitation function from TENDL-2015 has not reproduced the present results or even the other literature data but looked rather energy shifted.

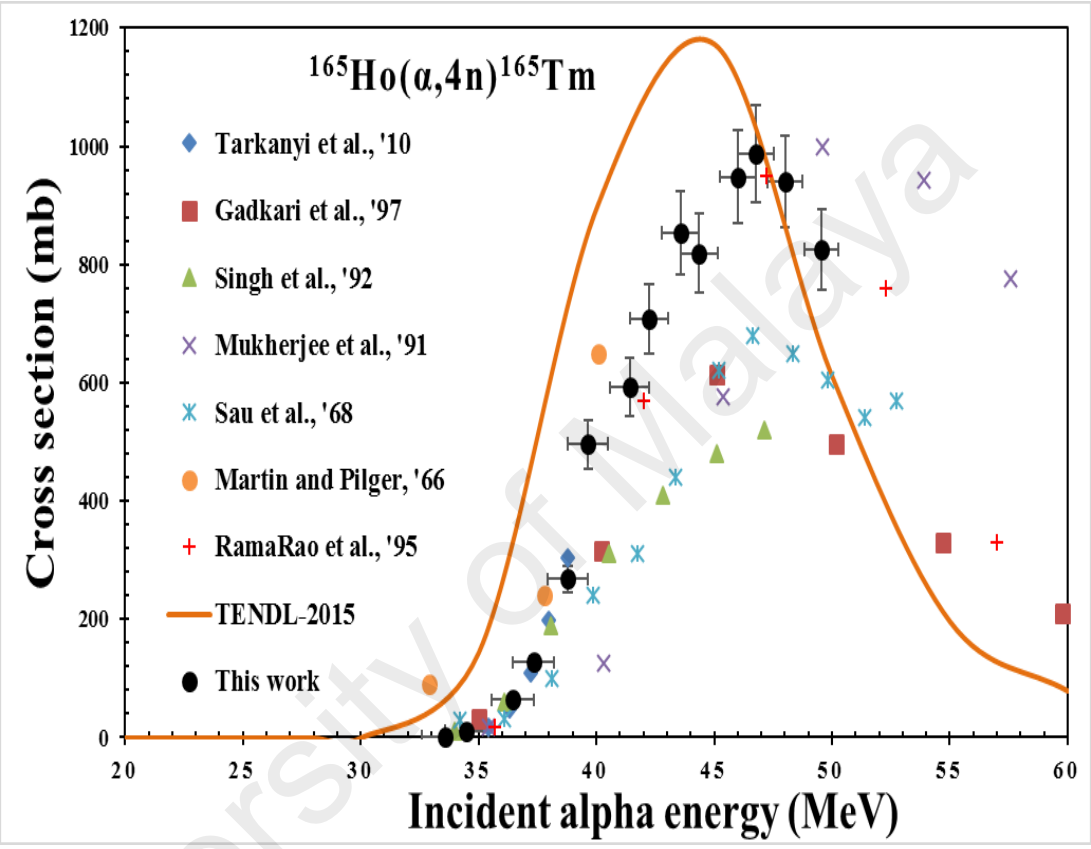

Figure 6.5: Excitation function of ^{165}Ho(α,4n)^{165}Tm reaction

6.4.2 Production Cross Sections of ^{166}Tm

The production cross sections of ^{166}Tm ($T_{1/2}$ = 7.7 h) was measured via its E_γ = 778.814 242.917 keV (I_γ = 19.1%) gamma line. Formation of the ^{166}Tm is via ^{165}Ho(α,3n)^{166}Tm reaction with a reaction Q-value of −24.8 MeV. The present results have been tabulated in Table 6.5 while the corresponding excitation function is presented in Fig. 6.6. From the Fig., present data is slightly higher than the recently measured cross sections by Tarkanyi group (Tarkanyi et al., 2010). There is an obvious discrepancy also among the previous measurements, with many of the previous works

presented much lower cross sections. The TENDL-2015 could not accurately predict the excitation function.

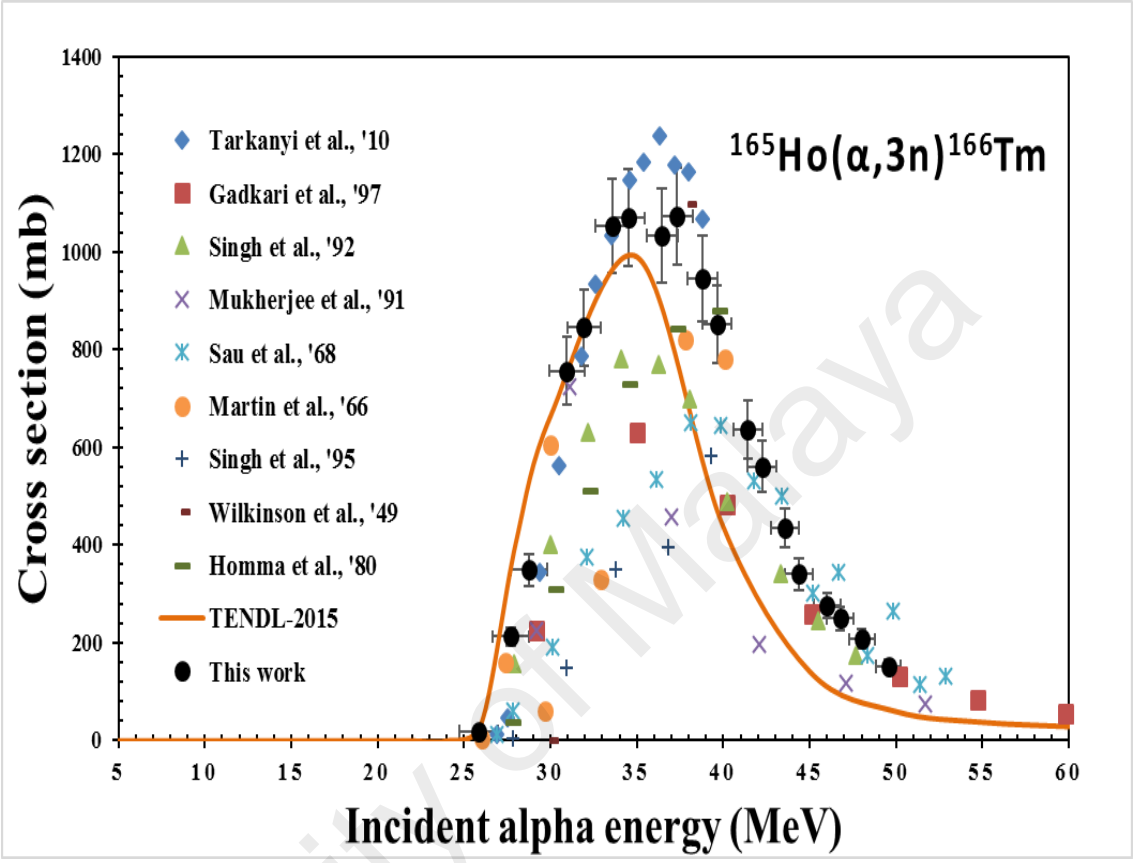

Figure 6.6: Excitation function of ^{165}Ho(α,3n)^{166}Tm reaction.

6.4.3 Production Cross Sections of ^{167}Tm

The popularly important ^{167}Tm ($T_{1/2}$ = 9.25 d) formation was via ^{165}Ho(α,2n)^{167}Tm. The cross section of this relatively long-life radionuclide was measured after sufficient cooling time as indicated in Table 6.2. The present cross sections have been plotted along other experimental studies in the Fig. 6.7. The results of this study present similar shape of some the previous studies. The present cross sections appear between the data of (Tarkanyi et al., 2010) and (Martin & Pilger, 1966; Mukhrjee et al., 1991; Singh, 1992). The prediction of the TENDL-2015 was only correct in shape but not magnitude.

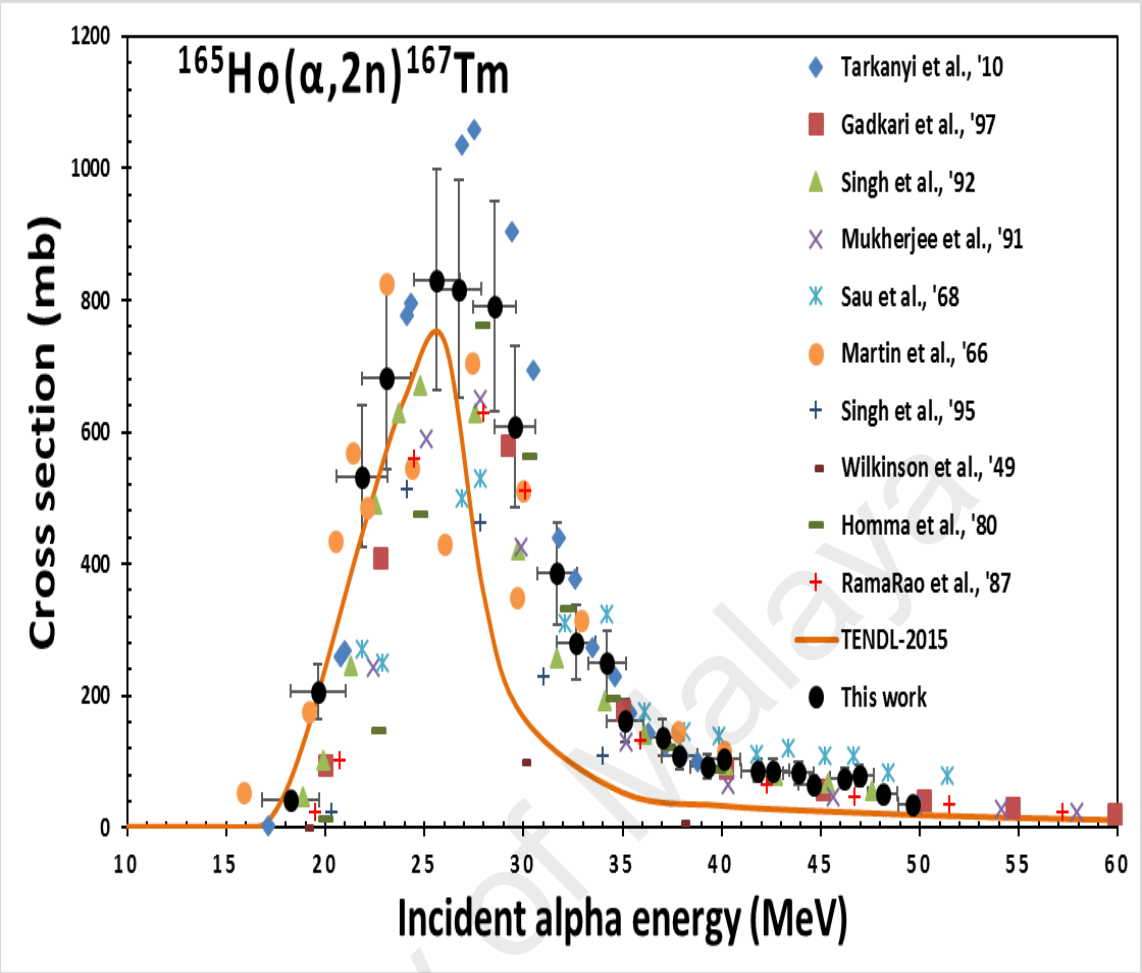

Figure 6.7: Excitation function of ^{165}Ho(α,2n)^{167}Tm reaction.

6.4.4 Production Cross Sections of ^{168}Tm

The radionuclide ^{168}Tm ($T_{1/2}$ = 93.1 d) is formed via ^{165}Ho(α,n)^{168}Tm nuclear reactions with the decay properties listed in Table 3. The measurement of this long-lived radionuclide was made after a cooling time of 19 to 43 days. The numeral data of the cross sections have been presented in Table 6.5 while the excitation function is plotted in Figure 6.8. The overall cross sections of this radionuclide are low compared to the other assessed radionuclides, with the maximum value seen at around 20 MeV energy. The present data agree with the recent earlier data by Tarkanyi group (Tarkanyi et al., 2010). The prediction of the Talys code via TENDL-2015 has underestimated the experimental values, although it maintained the experimental shape.

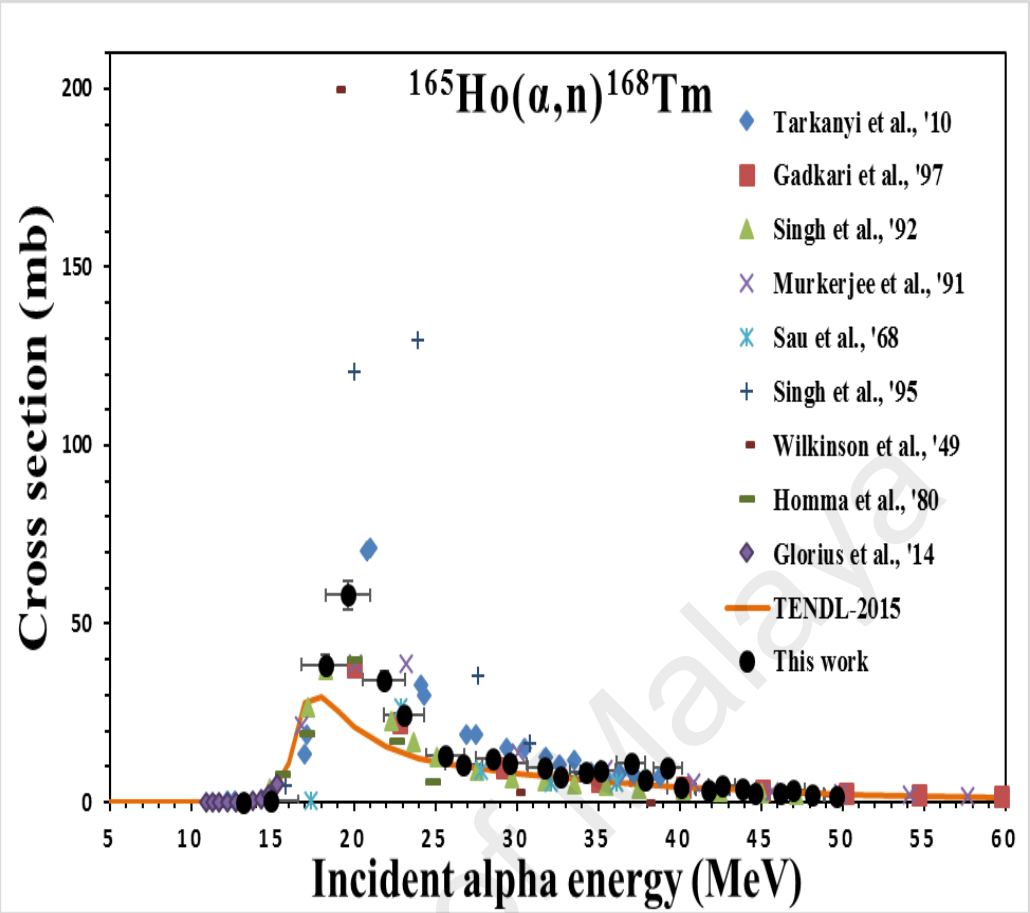

Figure 6.8: Excitation function of ^{165}Ho(α,n)^{168}Tm reaction.

6.5 Conclusions

Present chapter reports new experimental cross-sections of ^{165}Ho(α,4n)^{165}Tm, ^{165}Ho(α,3n)^{166}Tm, ^{165}Ho(α,2n)^{167}Tm and ^{165}Ho(α,n)^{168}Tm reactions in the region of 50.4 MeV down to respective reaction threshold. The new data have been compared with previous experimental measurements via same alpha particles bombardment on natural titanium. Present data compares well with some of the previous studies. The obtained new data has also been compared with Talys code, via its most recently calculated values which have been assessed through the TENDL-library (TENDL-2015). The prediction of the TENDL-2015 is not fully consistent with the measured experimental values. Therefore, the new cross-sections could help to enhance the prediction capacity of the Talys code further, average the discrepancies among the

previous measurements as well as enrich the database of the experimental studies for various applications.

CHAPTER 7: CONCLUSIONS AND RECOMMENDATIONS

This thesis presents the author's original research findings, discussions and conclusions of his PhD work. The research focused on the measurements of experimental production cross sections of several radionuclides from some selected metals using charged particles (deuteron and alpha beam) for the inducement of the reactions. The present chapter, therefore, summarises the previously presented results and conclusions of the various chapters of this thesis, following the objectives set at the beginning of the thesis. The chapter further highlights some limitations of the present work and gives some recommendations for future studies.

7.1 Conclusions

Just like how the presentation style of this thesis goes, where each chapter, from third to the sixth, represents a specific objective, thus, the conclusions would also take the same approach. The key experimental findings from those chapters are summarised under this section.

Taking the objectives one after the other, and recalling that the first was:

- To measure the excitation functions of $^{nat}Ni(d,x)^{x}Y$ nuclear reactions in the frame of 24 MeV.

From the natNi(d,x) nuclear processes, studies of production cross sections for the $^{55-58,60}Co$, ^{57}Ni, $^{52g,54}Mn$ and ^{61}Cu radionuclides have been made, and the numeral values have been presented in the Tables 3.4 and 3.5 of chapter 3 while the corresponding excitation functions have been graphically presented in the Figs. 3.3 to 3.11 of the same chapter. The TENDL-2014 and 2015 libraries, the output of the Talys nuclear reaction code, a very popular and efficient nuclear prediction code, were used to compare the

present experimental results with the theoretical cross sections. In some instances, such as in the production of $^{57,58(m+g),60}$Co, the code was found to overestimate the experiment cross sections while it underestimated the ^{55,56}Co, ^{52g,54}Mn and ^{61}Cu cross-sections. The integral thick target yields for ^{55}Co, ^{57}Co, and ^{58}Co radionuclides have also been calculated.

The following are additional details on the findings of the first objective;

- New cross-section results are presented for 24 MeV deuteron induced reactions on natural nickel.
- A critical review of the previous experimental data and their normalisations (in some cases) were made. The reviewed available experimental data were compared with the new measured results on the same graph for each studied radionuclide.
- The present study found that the IAEA recommended monitor reaction cross sections for ^{61}Cu are over estimated such that the IAEA values are higher not only to the data of the present study but also several recent studies. The recommended values, therefore, need to be revised.
- Before this work, there were only two studies which reported ^{60}Co via deuteron production route on Ni. The two previous works have rather scattered data, and it was hard to conclude on the best fit. The present results have improved the quality of the cross sections.
- The integral thick target yield calculations of some selected radionuclides have been presented.

❖ To study the cross sections and thick target yields of scandium radionuclides emitted from 50.4 MeV alpha-induced reactions on $^{nat.}$Ti.

From this second objective, above, the present thesis reports new experimental cross-sections for ^{43}K,^{43,44m,44g,46,47,48}Sc, ^{48}V and ^{48,49,51}Cr radionuclides via alpha particles bombardment on natural titanium in the region of 10.4 – 50.2 MeV. The comparison with the theoretical nuclear reaction codes was achieved via the TENDL-2014 and 2015 libraries.

The following are additional conclusions on the findings of this objective;

- Some data points for ^{46,48}Sc, ^{48}V and ^{48,49}Cr radionuclides in the high-energy region are reported here for the first time (except in the case where Michael et. al. 1983 data are available or Weinreich et. al. 1980).
- Integral thick target yields for the chromium and vanadium radionuclides have calculated. There was only one previous calculation in the literature
- Present thesis calculated the integral thick target yields for the first time for all the scandium radionuclides productions under the production route of this objective. The second measurement of ^{43}K has been made as well as its calculations of the integral yield.

❖ To measure the excitation functions of ^{nat}Cu(α,x)^{66,67}Ga,^{65}Zn,^{57,58,60}Co.

From the third objective above, using natural copper as the main target, the irradiation of the prepared copper foils with 50.4 MeV alpha beam was successfully carried out. From the analysed measured data of the bombarded copper target, new cross sections in tabular form for ^{nat}Cu(α,*x*)^{66,67}Ga,^{65}Zn,^{57,58,60}Co nuclear reactions have been reported, and the corresponding excitation functions are plotted separately in this thesis. A comprehensive evaluation of experimental literature from earlier experimental data on the studied radionuclides have been critically reviewed. The reviewed data have also been normalised and corrected for various reactions from some research groups

following the experimental conditions or definitions of terms of the literature data. For each nuclear reaction, the present results have been compared and presented together with the corresponding literature on the same Figure. The excitation functions for the assessed radionuclides from alpha-induced reactions on copper have also been compared with the output of the theoretical Talys nuclear reaction code, via its evaluated library, the TENDL-2014. The code underestimated the cross sections of ^{66}Ga between 10 to 30 MeV, the cross sections of ^{67}Ga between 20 to 50, the cross sections of ^{65}Zn between 22 to 47 MeV and the cross sections of $^{60m+g}$Co between 32 to 50 MeV while it overestimated ^{57}Co radionuclide via same production route.

The following could also be drawn from the findings under this objective;

- Most of the studies before the present on alpha-induced reactions on copper reported only the Ga and Zn radionuclides. The recent work has studied, in addition to the radionuclides mentioned above, the cobalt radionuclides. Specifically, there were only two previous studies each for ^{57}Co and ^{60}Co before this work.
- Despite the relatively sufficient experimental literature data on ^{66,67}Ga and ^{65}Zn, a significant portion of the previously reported cross sections was found to be largely discrepant, scattered or affected by energy shift. The present work has successfully improved the shape of the excitation functions through confirmation of some of the available data.
- The presented results of this thesis on the alpha-induced reactions on natural copper are some of the very few that have data points in the higher energy region around the 50 MeV.

The fourth objective of this thesis was as follows:

❖ To investigate the excitation functions of short-lived radionuclides via alpha production route on holmium foils.

For this objective, this thesis reports new experimental cross-sections of $^{165}Ho(\alpha,4n)^{165}Tm$, $^{165}Ho(\alpha,3n)^{166}Tm$, $^{165}Ho(\alpha,2n)^{167}Tm$ and $^{165}Ho(\alpha,n)^{168}Tm$ reactions in the interval of 50.4 MeV down to respective reaction threshold. The new data have been compared with previous experimental measurements via same alpha particles bombardment on natural titanium. Present data compare well with some of the previous studies. The obtained new data have also been compared with Talys code, via its most recently evaluated results, assessed through the TENDL-library (TENDL-2015).

7.2 Contributions

In a much shorter form, the following are some of the most obvious contributions of this thesis to this area of research:

- New results and data points for cross sections have been reported for all the assessed radionuclides via deuteron and alpha routes on the selected metals.
- In particular, the cross sections on $^{nat}Ni(d,x)^{60}Co$ have been improved. There were only two previous works on ^{60}Co via this route.
- Similarly, from alpha production route of ^{60}Co on Cu irradiation, there were only two previous studies for the $^{nat}Cu(\alpha,x)^{60g+m}Co$ nuclear reaction. The shape of the excitation function of this radionuclide has been improved following the new data from this thesis.
- From the Ti irradiation with 50.4 MeV alpha beam, new cross sections have been reported for ^{43}K, $^{43,44m,44g,46g+m,47,48}Sc$, ^{48}V and $^{48,49,51}Cr$ nuclear processes.

- There was only one prior report around 51 MeV high energy region on $^{43,44m,44g,46g+m,47,48}$Sc and another study on ^{48,49,51}Cr radionuclide. Only one earlier study has reported on ^{43}K via this production route.
- The present study does not found any previous work prior to the present work to calculate the experimental thick target yields for the scandium radionuclides via alpha bombardment on titanium. This work is thus the first calculation.
- New cross sections data have also been reported for $^{165\text{-}168}$Tm radionuclides through alpha production route on the holmium ^{165}Ho.
- The general evaluation of uncertainties in the cross sections in this thesis was done in a more broad, clear and coherent fashion, by its presentation in a separate Table in each experimental chapter of study, as well as the good definition of the individual uncertainties in each of these Tables.

7.3 Limitations of the study

- Efforts were made to report as many radionuclides as possible from Ho foils. A large number of Ho foils (and therefore data points) involved, which were shown under the section of results and discussions of chapter six, indicate how much reaction processes were intended to investigate from this broad energy interval (50 MeV to the threshold for each reaction process). The study of irradiation of Ho by alpha beam need more studies due to several factors which could not be solved by the present work. The present work, as stated earlier, had many Ho foils with the intention to measure many radionuclides at various energy points. However, this has some disadvantages, especially regarding the workforce and equipment for measurements, as the author could not measure the short-lived radionuclides.

More so, some gamma peaks from holmium bombardment have looked so thick and congested, due to many emission with closer gamma lines by several radionuclides. Measurements from these peaks may have some errors, even with an effort for separation of the possible interferences.

- This study could not have sufficient time for certain measurements, especially for the long-lived radionuclides and much shorter-lived ones (less than 30 mins) from all the studied production routes. For the short half-lives radionuclides, the gamma-ray detectors used in the studies are offline (in a hot laboratory), some few metres away from the irradiation room and the irradiated samples are also allowed to cool down so as to minimise radiation exposure during activity measurements.

7.4 Recommendation for Future Works

The contributions of the present thesis on this old but vibrant area have been highlighted in this chapter. However, it is impossible to address all the issues relevant to this study. For this reason, the following are some suggestions towards more contributions in the studied area.

- From the reported excitation function of $^{nat}Ni(d,x)^{60}Co$, it could be seen that further measurements are needed to support the shape of the excitation function. The presently measured cross sections of this radionuclide, as well as the few available experimental data, do not strongly agree with one another. Due to the long half-life of the ^{60}Co, some sufficient and dedicated experimental conditions could play vital roles to report a much more convincing shape of the excitation function.
- Despite the presence of several works on the production cross sections of the ^{48}Cr radionuclide, the excitation function reported by different studies

have not yet convincingly agree with one another. If additional dedicated studies are made, the new measurements could provide insights to help to determine the primary causes of the discrepancies in the ^{48}Cr production cross-sections via irradiation of copper.

- Future studies can be considered for holmium irradiation via alpha irradiation for the possible measurements of radionuclides with short half-lives, low gamma energy or low-intensity gamma energy. New work may have to employ some sufficient experimental conditions such as the workforce, much higher resolutions detectors, and if possible, more than one detector so that short half-lived radionuclides can be measured. These can provide better measurements of the thulium radionuclides cross sections, minimise the surrounding uncertainties on the cross-section as well as better chances of reporting new radionuclides that have not been previously reported via this production route. The introductory part of chapter six and the section 7.3 (limitation of the study) of the chapter have presented greater details of such (possibly) measurable radionuclides which could not be reported under the holmium-alpha production route of this study.

REFERENCES

Abe, K., Iizuka, A., Hasegawa, A., & Morozumi, S. (1984). Induced radioactivity of component materials by 16-MeV protons and 30-mev alpha particles. *Journal of Nuclear Materials, 123*(1), 972-976.

Adler, P., & Ghosh, S. (2003). Cobalt-induced ferromagnetic interactions and magnetoresistance in charge-ordered $Sr_{2/3}La_{1/3}Feo_3$. *Solid State Sciences, 5*(3), 445-450.

Al-Abyad, M., Spahn, I., & Qaim, S. M. (2010). Experimental studies and nuclear model calculations on proton induced reactions on manganese up to 45 MeV with reference to production of ^{55}Fe, ^{54}Mn and ^{51}Cr. *Applied Radiation and Isotopes, 68*(12), 2393-2397.

Al Saleh, F. S., Al Mugren, K. S., & Azzam, A. (2007). Excitation functions of (p,x) reactions on natural nickel between proton energies of 2.7 and 27.5 MeV. *Applied Radiation and Isotopes, 65*(1), 104-113.

Alliot, C., Kerdjoudj, R., Michel, N., Haddad, F., & Huclier-Markai, S. (2015). Cyclotron production of high purity ^{44m,44}Sc with deuterons from $^{44}CaCo_3$ targets. *Nuclear Medicine and Biology, 42*(6), 524-529.

Amjed, N., Hussain, M., Aslam, M. N., Tárkányi, F., & Qaim, S. M. (2016). Evaluation of nuclear reaction cross sections for optimization of production of the emerging diagnostic radionuclide ^{55}Co. *Applied Radiation and Isotopes, 108*, 38-48.

Amjed, N., Tarkanyi, F., Ditroi, F., Takacs, S., & Yuki, H. (2013). Activation cross-sections of deuteron induced reaction of natural ni up to 40 MeV. *Applied Radiation and Isotopes, 82*, 87-99.

Arbabi, A., Sadeghi, M., & Joharifard, M. (2009). Irradiation and dosimetry of nitinol stent for renal artery brachytherapy. *Applied Radiation and Isotopes, 67*(1), 129-132.

Aslam, M. N., & Qaim, S. M. (2014). Nuclear model analysis of excitation functions of proton, deuteron and alpha-particle induced reactions on nickel isotopes for production of the medically interesting copper-61. *Applied Radiation and Isotopes, 89*, 65-73.

Audi, G., Wapstra, A. H., & Thibault, C. (2003). The ame2003 atomic mass evaluation: (ii). Tables, graphs and references. *Nuclear Physics A, 729*(1), 337-676.

Baglin, C. M. (2000). Nuclear data sheets for A = 167. Nuclear Data Sheets, 90(3), 431-644.

Baglin, C. M. (2008). Nuclear data sheets for A = 166. *Nuclear Data Sheets, 109*(5), 1103-1382.

Baglin, C. M. (2010). Nuclear data sheets for A = 168. *Nuclear Data Sheets, 111*(7), 1807-2080.

Baglin, C. M., Norman, E. B., Larimer, R.-M., & Rech, G. A. (2004). Measurement of ^{107}Ag (alpha, gamma) ^{111}In cross sections. *Lawrence Berkeley National Laboratory*.

Baron, N., & Cohen, B. L. (1963). Activation cross-section survery of deuteron-induced reactions. , *Physical Review, 129*, 263-2642.

Basunia, M. S., Norman, E. B., Shugart, H. A., Smith, A. R., Dolinski, M. J., & Quiter, B. J. (2005). Measurement of cross sections for the ^{63}Cu (α, γ) ^{67}Ga reaction from 5.9 to 8.7 MeV. *Physical Review C, 71*(3), 035801.

Berglund, M., & Wieser, M. E. (2011). Isotopic compositions of the elements 2009 (iupac technical report). *Pure and Applied Chemistry, 83*(2), 397-410.

Bhardwaj, H. D., Gautam, A. K., & Prasad, R. (1988). Measurement and analysis of excitation functions for alpha-induced reactions in copper. *Pramana, 31*(2), 109-123.

Bhat, M. R. (1998). Nuclear data sheets for A = 57. *Nuclear Data Sheets, 85*(3), 415-536.

Blann, M., & Merkel, G. (1963). Reactions induced in ni 58 with 0-24 MeV deuterons: Statistical model analysis. *Physical Review, 131*(2), 764.

Bohr, N., & Wheeler, J. A. (1939). The mechanism of nuclear fission. *Physical Review, 56*(5), 426-450.

Bonardi, M., Birattari, C., Groppi, F., & Sabbioni, E. (2002). Thin-target excitation functions, cross-sections and optimised thick-target yields for ^{nat}Mo(p,xn)$^{94g,95m,95g,96(m+g)}$Tc nuclear reactions induced by protons from threshold up to 44 MeV. No carrier added radiochemical separation and quality control. *Applied Radiation and Isotopes, 57*(5), 617-635.

Bonesso, O., Ozafran, M. J., Mosca, H. O., Vazquez, M. E., Capurro, O. A., & Nassiff, S. J. (1991). Study of pre-equilibrium effects on α-induced reactions on copper. *Journal of Radioanalytical and Nuclear Chemistry, 152*(1), 189-197.

Brink, D. (1990). The compound nucleus at high excitation energy. *Nuclear Physics A, 519*(1-2), 3-16.

Brinkman, G. A., Helmer, J., & Lindner, L. (1977). Nickel and copper foils as monitors for cyclotron beam intensities. *Radiochemical and Radioanalytical Letters, 28*(1), 9 – 19.

Browne, E., & Tuli, J. K. (2010a). Nuclear data sheets for A = 65. *Nuclear Data Sheets, 111*(9), 2425-2553.

Browne, E., & Tuli, J. K. (2010b). Nuclear data sheets for A = 66. *Nuclear Data Sheets, 111*(4), 1093-1209.

Browne, E., & Tuli, J. K. (2013). Nuclear data sheets for A = 60. *Nuclear Data Sheets, 114*(12), 1849-2022.

Bryant, E. A., Cochran, D. R. F., & Knight, J. D. (1963). Excitation functions of reactions of 7- to 24- MeV He^3 ions with ^{63}Cu and ^{65}Cu. *Physical Review, 130*(4), 1512-1522.

Bryant, P. (1994). *A brief history and review of accelerators*. Paper presented at the CAS - CERN Accelerator school, 5th general accelerator physics course, held on 7-18, September 1992, University of Jyvaskyla, Finland. Retrived on 13/10/2017 from http://www.iaea.org/inis/collection/nclcollectionstore/_public/26/001/26001558.pdf

Budzanowski, A., Freindl, L., Grotowski, K., Rzeszutko, M. M., Slapa, M., Szmider, J., & Hodgson, P. E. (1963). Elastic scattering and total reaction cross-sections for the interaction of 12.8 MeV deuterons with ^{12}C, ^{58}Ni, ^{60}Ni and ^{209}Bi nuclei. *Nuclear Physics, 49*, 144-160.

Burrows, T. W. (2006). Nuclear data sheets for A = 48. *Nuclear Data Sheets, 107*(7), 1747-1922.

Burrows, T. W. (2007). Nuclear data sheets for A = 47. *Nuclear Data Sheets, 108*(5), 923-1056.

Burrows, T. W. (2008). Nuclear data sheets for A = 49. *Nuclear Data Sheets, 109*(8), 1879-2032.

C.D. Nesaraja, S.D. Geraedts, & B. Singh. (2010). Nuclear data sheets for A=58. *Nuclear Data Sheets, 111*, 897-1092.

Cata-Danil, I., Ivascu, M., Glodariu, T., Zamfir, N. V., Bucurescu, D., Filipescu, D., . . . Sava, T. (2008). Measurement of cross sections and thick target yields for (α, γ) process on ^{63}Cu. *Romanian Reports in Physics, 60*(3), 555-561.

Chakravarty, R., Dash, A., & R.A. Pillai, M. (2012). Electrochemical separation is an attractive strategy for development of radionuclide generators for medical applications. *Current Radiopharmaceuticals, 5*(3), 271-287.

Chandra, R., Hernberg, J., Braunstein, P., & Rosenfeld, W. (1971). ^{167}Tm: A new bone scanning agent 1. *Radiology, 100*(3), 687-689.

Chang, C.-N., Kent, J., Morgan, J., & Blatt, S. (1973). Total cross section measurements by x-ray detection of electron-capture residual activity. *Nuclear Instruments and Methods, 109*(2), 327-331.

Chen, J., Singh, B., & Cameron, J. A. (2011). Nuclear data sheets for A = 44. *Nuclear Data Sheets, 112*(9), 2357-2495.

Cline, C. K. (1971). Reaction mechanisms and shell structure effects in $^{54}Fe+^{6}Li$ and $^{58}Ni+d$ reactions at medium energies. *Nuclear Physics A, 174*(1), 73-96.

Cockcroft, J., & Walton, E. (1932). Experiments with high velocity ions. *Proceedings of the Royal Society A, 137*, 619-630.

Cockcroft, J. D., & Walton, E. T. S. (1932b). Disintegration of lithium by swift protons. *Nature, 129*(3261), 649-649.

Coetzee, P. P., & Peisach, M. (1972). Activation cross sections for deuteron-induced reactions on some elements of the first transition series, up to 5.5 mev. *Radiochimca Acta, 17*(1), 1-6.

Cogneau, M., Gilly, L. J., & Cara, J. (1967). Absolute cross sections and excitation functions for deuteron-induced reactions on the nickel isotopes between 2 and 12 MeV. *Nuclear Physics A, 99*(4), 686-694.

Craddock, M., & Symon, K. (2008). Cyclotrons and fixed-field alternating-gradient accelerators. *Reviews of Accelerator Science and Technology, 1*(01), 65-97.

Cutler, C. S., Smith, C. J., Ehrhardt, G. J., Tyler, T. T., Jurisson, S. S., & Deutsch, E. (2000). Current and potential therapeutic uses of lanthanide radioisotopes. *Cancer Biotherapy & Radiopharmaceuticals, 15*(6), 531-545.

De Cremer, K., Cornelis, R., Strijckmans, K., Dams, R., Lameire, N., & Vanholder, R. (2002). Behaviour of vanadate and vanadium–transferrin complex on different anion-exchange columns. Application to in vivo 48v-labelled rat serum. *Journal of Chromatography B, 775*(2), 143-152.

Deilami-nezhad, L., Moghaddam-Banaem, L., Sadeghi, M., & Asgari, M. (2016). Production and purification of scandium-47: A potential radioisotope for cancer theranostics. *Applied Radiation and Isotopes, 118*, 124-130.

Didik, V. A., Malkovich, R. S., Skoryatina, E. A., & Kozlovskii, V. V. (1994). Experimental determination of the cross sections of nuclear reactions by the method of analysis of the concentration profiles of transmutation nuclides. *Atomic Energy, 77*(1), 570-572.

Ditrói, F., Takács, S., Tárkányi, F., Baba, M., Corniani, E., & Shubin, Y. N. (2008). Study of proton induced reactions on niobium targets up to 70 MeV. *Nuclear Instruments and Methods in Physics Research Section B: Beam Interactions with Materials and Atoms, 266*(24), 5087-5100.

Dmitriev, P. P. (1986). *Radionuclide yield in reactions with protons, deuterons, alpha particles and helium-3: Handbook*: IAEA.

Duchemin, C., Guertin, A., Haddad, F., Michel, N., & Métivier, V. (2015). Production of scandium-44m and scandium-44g with deuterons on calcium-44: Cross section measurements and production yield calculations. *Physics in Medicine and Biology 60*(17), 6847-6864.

Dzoyem, J. P., Aro, A. O., McGaw, L. J., & Eloff, J. N. (2016). Antimycobacterial activity against different pathogens and selectivity index of fourteen medicinal plants used in southern africa to treat tuberculosis and respiratory ailments. *South African Journal of Botany, 102*, 70-74.

Fischer, U. (2009). Materials subjected to the irradiation by deuterons (and protons) in the ifmif accelerator and the lithium loop. Retrieved 13/01/2015, from IAEA Fusion Evaluated Nuclear Data Library FENDL3.0 https://www-nds.iaea.org/fendl3/vardocs.html

Fuying, Z., Zhenlan, T., & Zhenxia, W. (1983). Measurements of excitation functions for ^{56}Ni (d, α), ^{58}Ni (d, αn) and ^{58}Ni (d, t). *Chinese Jornal of Nuclear Physics, 5*, 166.

Gadkari, M. S., Patel, H. B., Shah, D. J., & Singh, N. L. (1997). Study of preequilibrium decay in (alpha, xn) reactions in holmium up to 70 MeV. *Physica Scripta, 55*(2), 147-151.

Glorius, J., Sonnabend, K., Goerres, J., Robertson, D., Knoerzer, M., Kontos, A., . . . Stech, E. (2014). Experimental cross sections of ^{165}Ho(α, n)^{168}Tm and ^{166}Er(α, n)^{169}Yb for optical potential studies relevant for the astrophysical γ process. *Physical Review C, 89*(6), 065808.

Goto, A. (1989). *Injector avf cyclotron at riken.* Paper presented at the Proc. 12th Int. Conf. on Cyclotrons and their Applications, Berlin, Germany.

Graf, H. P., & Münzel, H. (1974). Excitation functions for α-particle reactions with molybdenum isotopes. *Journal of Inorganic and Nuclear Chemistry, 36*(12), 3647-3657.

Heikkinen, P. (1994). *Cyclotrons*. Paper presented at the CAS - CERN Accelerator school, 5th general accelerator physics course, held on 7-18, September 1992, University of Jyvaskyla, Finland. Available at http://www.iaea.org/inis/collection/NCLCollectionStore/_Public/26/001/26001558.pdf, yellow report *2* (805-818), accessed on 13/10/2017

Heinle, R. W., Welch, A. D., Scharf, V., Meacham, G. C., & Prusoff, W. H. (1952). Studies of excretion (and absorption) of ^{60}Co labeled vitamin B12 in pernicious anemia. *Trans Assoc Am Physicians, 65*, 214-222.

Hermanne, A., Sonck, M., Takacs, S., Szelecsenyi, F., & Tárkányi, F. (1999a). *Monitoring of alpha-beam properties by the ^{nat}Ti (alpha , x)^{51}Cr reaction: New measurements and critical compilation.* Paper presented at the AIP Conference Proceedings.

Hermanne, A., Sonck, M., Takács, S., Szelecsényi, F., & Tárkányi, F. (1999b). Excitation functions of nuclear reactions induced by alpha particles up to 42 mev on ^{nat}Ti for monitoring purposes and tla. *Nuclear Instruments and Methods in Physics Research Section B: Beam Interactions with Materials and Atoms, 152*(2–3), 187-201.

Hermanne, A., Takács, S., Adam-Rebeles, R., Tárkányi, F., & Takács, M. P. (2013). New measurements and evaluation of database for deuteron induced reaction on ni up to 50 mev. *Nuclear Instruments and Methods in Physics Research Section B: Beam Interactions with Materials and Atoms, 299*(0), 8-23.

Hermanne, A., Tárkányi, F., Takács, S., Ditrói, F., & Amjed, N. (2014). Excitation functions for production of ^{46}Sc by deuteron and proton beams in ^{nat}Ti: A basis for additional monitor reactions. *Nuclear Instruments and Methods in Physics Research Section B: Beam Interactions with Materials and Atoms, 338*, 31-41.

Hermanne, A., Tárkányi, F., Takács, S., Ditrói, F., Baba, M., Ohtshuki, T., . . . Ignatyuk, A. V. (2009). Excitation functions for production of medically relevant radioisotopes in deuteron irradiations of pr and tm targets. *Nuclear Instruments and Methods in Physics Research Section B: Beam Interactions with Materials and Atoms, 267*(5), 727-736.

Hermanne, A., Tárkányi, F., Takács, S., Kovalev, S. F., & Ignatyuk, A. (2007). Activation cross sections of the ^{64}Ni(d,2n) reaction for the production of the medical radionuclide ^{64}Cu. *Nuclear Instruments and Methods in Physics Research Section B: Beam Interactions with Materials and Atoms, 258*(2), 308-312.

Hichwa, R. D., Kadrmas, D., Watkins, G. L., Wollenweber, S. D., Maniam, S., Boles Ponto, L. L., . . . Koeppel, J. A. (1995). Vanadium-48: A renewable source for transmission scanning with pet. *Nuclear Instruments and Methods in Physics Research Section B: Beam Interactions with Materials and Atoms, 99*(1–4), 804-806.

Hille, M., Hille, P., Uhl, M., & Weisz, W. (1972). Excitation functions of (p, n) and (α, n) reactions on Ni, Cu and Zn. *Nuclear Physics A, 198*(2), 625-640.

Hoehr, C., Oehlke, E., Benard, F., Lee, C. J., Hou, X., Badesso, B., . . . Schaffer, P. (2014). ^{44g}Sc production using a water target on a 13 MeV cyclotron. *Nuclear Medicine and Biology, 41*(5), 401-406.

Homma, Y., Sugitani, Y., Matsui, Y., Matsuura, K., & Kurata, K. (1980). Cyclotron production of ^{167}Tm from natural erbium and natural holmium. *The International Journal of Applied Radiation and Isotopes, 31*(8), 505-508.

Hong, H., Zhang, Y., Engle, J. W., Nayak, T. R., Theuer, C. P., Nickles, R. J., . . . Cai, W. (2012). In vivo targeting and positron emission tomography imaging of tumor vasculature with ^{66}ga-labeled nano-graphene. *Biomaterials, 33*(16), 4147-4156.

Houck, F. S., & Miller, J. M. (1961). Reactions of alpha particles with iron-54 and nickel-58. *Physical Review, 123*(1), 231-240.

Howard, A., Jensen, H., Rios, M., Fowler, W. A., & Zimmerman, B. A. (1974). Measurement and theoretical analysis of some reaction rates of interest in silicon burning. *The Astrophysical Journal, 188*, 131-140.

Huo Junde. (2008a). Nuclear data sheets for A=55. *Nuclear Data Sheets, 109* 787-942.

Huo Junde. (2008b). Nuclear data sheets for A=55. *Nuclear Data Sheets, 109*, 787-942.

Huo Junde, Huo Su, & Yang Dong. (2011). Nuclear data sheets for A=56. *Nuclear Data Sheets, 112*, 1513-1645.

IAEA. (2007). Charged particle reference cross sections, monitor reactions. Retrieved 15/03/2016, from International Atomic Energy Agency: https://www-nds.iaea.org/medical/monitor_reactions.html

IAEA. (2008). *Cyclotron produced radionuclides: Principles and practice* (Pillai, M. & Haji-Saeid, M. Eds.). Vienna, Austria: International Atomic Energy Agency.

IAEA. (2009a). *Cyclotron produced radionuclides: Physical characteristics and production methods* (Pillai, M. & Haji-Saeid, M. Eds.). Vienna, Austria.: International Atomic Energy Agency.

IAEA. (2009b). Livechart of nuclides. *International Atomic Anergy. Available at* https://www-nds.iaea.org/medical/monitor_reactions.html.

Iguchi, A., Amano, H., & Tanaka, S. (1960). (alpha, n) cross sections for ^{48}Ti and ^{51}V. *J. Atomic Energy Soc. Japan, 2*(11), 682-684.

Jain, A. K., Ghosh, A., & Singh, B. (2006). Nuclear data sheets for A = 165. *Nuclear Data Sheets, 107*(5), 1075-1346.

Junde, H., Xiaolong, H., & Tuli, J. K. (2005). Nuclear data sheets for A = 67. *Nuclear Data Sheets, 106*(2), 159-250.

Junde Huo, Su Huo, & Chunhui Ma. (2007). Nuclear data sheets for A=52. *Nucl. Data Sheets 108*, 773-882.

Jung, P. (1992). *Cross sections for the production of helium and long-living radioactive isotopes by protons and deuterons.* Paper presented at the Nuclear data for science and technology.

Khandaker, M. U., Haba, H., Kanaya, J., & Otuka, N. (2013). Excitation functions of (d,x) nuclear reactions on natural titanium up to 24 MeV. *Nuclear Instruments and Methods in Physics Research Section B: Beam Interactions with Materials and Atoms, 296*, 14-21.

Khandaker, M. U., Haba, H., Murakami, M., & Otuka, N. (2015). Production cross-sections of long-lived radionuclides in deuteron-induced reactions on natural zinc up to 23 MeV. *Nuclear Instruments and Methods in Physics Research Section B: Beam Interactions with Materials and Atoms, 346*(0), 8-16.

Khandaker, M. U., Haba, H., Otuka, N., & Usman, A. R. (2014). Investigation of (d,x) nuclear reactions on natural ytterbium up to 24 MeV. *Nuclear Instruments and Methods in Physics Research Section B: Beam Interactions with Materials and Atoms, 335*(0), 8-18.

Khandaker, M. U., Kim, K., Kim, G., & Otuka, N. (2010). Cyclotron production of the ^{105,106m}Ag, ^{100,101}Pd, ^{100,101m,105}Rh radionuclides by ^{nat}Pd(p,x) nuclear processes. *Nuclear Instruments and Methods in Physics Research Section B: Beam Interactions with Materials and Atoms, 268*(14), 2303-2311.

Khandaker, M. U., Kim, K., Lee, M., Kim, K. S., & Kim, G. (2011). Excitation functions of (p,x) reactions on natural nickel up to 40 mev. *Nuclear Instruments and Methods in Physics Research Section B: Beam Interactions with Materials and Atoms, 269*(10), 1140-1149.

Khandaker, M. U., Uddin, M. S., Kim, K. S., Lee, Y. S., & Kim, G. N. (2007). Measurement of cross-sections for the (p, xn) reactions in natural molybdenum. *Nuclear Instruments and Methods in Physics Research Section B: Beam Interactions with Materials and Atoms, 262*(2), 171-181.

Kiss, G. G., Szücs, T., Rauscher, T., Török, Z., Fülöp, Z., Gyürky, G., . . . Somorjai, E. (2014). Alpha induced reaction cross section measurements on ^{162}Er for the astrophysical γ process. *Physics Letters B, 735*, 40-44.

Kohara, S., Goto, A., Sakamoto, N., Kamigaito, O., Watanabe, S., Teranishi, T., . . . Yano, Y. (2004). Flattop acceleration system in the riken avf cyclotron. *Nuclear Instruments and Methods in Physics Research Section A: Accelerators, Spectrometers, Detectors and Associated Equipment, 526*(3), 230-238.

Koning, A. J., & Rochman, D. (2012). Modern nuclear data evaluation with the talys code system. *Nuclear Data Sheets, 113*, 2841–2934.

Koning, A. J., Rochman, D., Kopecky, J., Sublet, J. C., Bauge, E., Hilaire, S., . . . Mills, R. (2015). Tendl-2015: Talys-based evaluated nuclear data library. Retrieved 19/06/2016, Retrieved 19/01/2017 from NRG in Petten https://tendl.web.psi.ch/tendl_2015/tendl2015.html

Koning, A. J., Rochman, D., S.C van der Marck, Kopecky, J., Sublet, J. C., Pomp, S., . . . Hilaire, S. (2014). Tendl-2014: Talys-based evaluated nuclear data library. Retrieved 19/06/2016, from Nuclear Research and Consultancy Group (NRG) Petten, The Netherlands http://www.talys.eu/tendl-2014/

Koumarianou, E., Slastnikova, T. A., Pruszynski, M., Rosenkranz, A. A., Vaidyanathan, G., Sobolev, A. S., & Zalutsky, M. R. (2014). Radiolabeling and in vitro evaluation of ^{67}Ga-nota-modular nanotransporter – a potential auger electron emitting egfr-targeted radiotherapeutic. *Nuclear Medicine and Biology, 41*(6), 441-449.

Lagunas-Solar, M. C., & Jungerman, J. A. (1979). Cyclotron production of carrier-free cobalt-55, a new positron-emitting label for bleomycin. *The International Journal of Applied Radiation and Isotopes, 30*(1), 25-32.

Lagunas-Solar, M. C., Kiefer, P. M., Carvacho, O. F., Lagunas, C. A., & Ya Po, C. (1991). Cyclotron production of nca ^{99m}Tc and ^{99}Mo. An alternative non-reactor supply source of instant ^{99m}Tc and ^{99}Mo→^{99m}Tc generators. *International*

Journal of Radiation Applications and Instrumentation. Part A. Applied Radiation and Isotopes, 42(7), 643-657.

Lawrence, E. O., & Cooksey, D. (1936). On the apparatus for the multiple acceleration of light ions to high speeds. *Physical Review, 50*(12), 1131.

Lawrence, E. O., & Livingston, M. S. (1932). The production of high speed light ions without the use of high voltages. *Physical Review, 40*(1), 19.

Lebowitz, E., & Greene, M. W. (1970). An auxiliary cyclotron beam monitor. *International Jornal of Applied Radiation and Isotopes, 21*(10), 625-627.

Levkovskij, V. N. (1991). Cross sections of medium mass nuclide activation (a=40-100) by medium energy protons and alpha-particles (E=10-50 MeV). *Inter-Vesi, Moscow*.

Lin, S. Y., & Alexander, J. M. (1977). Reactions of ^{237}Np with ^{4}He near the interaction barrier. *Physical Review C, 16*(2), 688-693.

Lopez-Rodriguez, V., Gaspar-Carcamo, R. E., Pedraza-Lopez, M., Rojas-Calderon, E. L., Arteaga de Murphy, C., Ferro-Flores, G., & Avila-Rodriguez, M. A. (2015). Preparation and preclinical evaluation of ^{66}Ga-dota-E(c(RGDFK))$_2$ as a potential theranostic radiopharmaceutical. *Nuclear Medicine and Biology, 42*(2), 109-114.

Luo, J., An, L., Jiang, L., & He, L. (2015). Determination of the cross section for (n,p) and (n,α) reactions on ^{165}Ho at 13.5 and 14.8 MeV. *Applied Radiation and Isotopes, 98*, 40-43.

Mahaux, C., & Weidenmuller, H. (1979). Recent developments in compound-nucleus theory. *Annual Review of Nuclear and Particle Science, 29*(1), 1-31.

Mamtimin, M., Harmon, F., & Starovoitova, V. N. (2015). ^{47}Sc production from titanium targets using electron linacs. *Applied Radiation and Isotopes, 102*, 1-4.

Martin, G., & Pilger, R. (1966). Absolute cross sections and excitation functions for α-particle-induced reactions of ^{165}Ho, ^{164}Er, ^{166}Er and ^{167}Er. *Nuclear Physics, 89*(3), 481-496.

McCarthy, D. W., Shefer, R. E., Klinkowstein, R. E., Bass, L. A., Margeneau, W. H., Cutler, C. S., . . . Welch, M. J. (1997). Efficient production of high specific activity ^{64}Cu using a biomedical cyclotron. *Nuclear Medicine and Biology, 24*(1), 35-43.

Michel, R., Brinkmann, G., & Stück, R. (1983). Integral excitation functions of α-induced reactions on titanium, iron and nickel. *Radiochimica Acta, 32*(4), 173-190.

Milton, B. F., & Triumf. (1995). *Commercial compact cyclotrons in the '90s.* Paper presented at the International Conference on Cyclotrons and their Applications, Cape Town, South Africa.

Mohamed, M. B. (2006). *Study of the excitation functions for some cyclotron produced radionuclides.* (PhD), Mansoura University, Egypt.

Morton, A., Tims, S., Scott, A., Hansper, V., Tingwell, C., & Sargood, D. (1992). The ^{48}Ti (α, n)^{51}Cr and ^{48}Ti(α, p)^{51}V cross sections. *Nuclear Physics A, 537*(1), 167-182.

Moustapha, M. E., Ehrhardt, G. J., Smith, C. J., Szajek, L. P., Eckelman, W. C., & Jurisson, S. S. (2006). Preparation of cyclotron-produced ^{186}Re and comparison with reactor-produced ^{186}Re and generator-produced ^{188}Re for the labeling of bombesin. *Nuclear Medicine and Biology, 33*(1), 81-89.

Mukherjee, S., Kumar, B. B., & Singh, N. L. (1997). Excitation functions of alpha particle induced reactions on aluminium and copper. *Pramana, 49*(2), 253-261.

Mukhrjee, S., Rao, A. M., & Rao, J. R. (1991). Pre-equilibrium analysis of the excitation functions of (α, xn) reactions on silver and holmium. *Il Nuovo Cimento A (1965-1970), 104*(6), 863-874.

Murakami, M., Haba, H., Goto, S., Kanaya, J., & Kudo, H. (2014). Production cross sections of niobium and tantalum isotopes in proton-induced reactions on natzr and nathf up to 14 MeV. *Applied Radiation and Isotopes, 90*, 149-157.

Nassiff, S. J. (1983). *Cross-sections and thick target yields of alpha particles induced reactions*. IAEA contract: 2499/R1/RB. IAEA (unpublished).

Navin, A., Tripathi, V., Blumenfeld, Y., Nanal, V., Simenel, C., Casandjian, J. M., . . . Tryggestad, E. (2004). Direct and compound reactions induced by unstable helium beams near the coulomb barrier. *Physical Review C, 70*(4), 044601.

Nayak, D., Lahir, S., Ramaswami, A., & Manohor, S. B. (1999). Separation of carrier-free ^{163,165}Tm produced in 80 MeV ^{16}O irradiated eu_2o_3 target matrix *Radiochimica Acta* (Vol. 87, pp. 75).

Nayak, D., & Lahiri, S. (1999). Application of radioisotopes in the field of nuclear medicine. *Journal of Radioanalytical and Nuclear Chemistry, 242*(2), 423-432.

Nesaraja, C. D., Geraedts, S. D., & Singh, B. (2010). Nuclear data sheets for A = 58. *Nuclear Data Sheets, 111*(4), 897-1092.

Nichols, A. L., & Capote Noy, R. (2013). *Summary report of the first research coordination meeting on nuclear data for charged-particle monitor reactions and medical isotope production (INDC(NDS)-0630)*. Retrieved 07/05/2015 from IAEA: https://inis.iaea.org/search/search.aspx?orig_q=RN:44069163

Nikolic, J., Puzovic, J., Todorovic, D., & Rajacic, M. (2015). Application of photon simulation software on calibration of hpge detectors. *Nuclear Instruments and Methods in Physics Research Section A: Accelerators, Spectrometers, Detectors and Associated Equipment, 799*, 159-165.

NuDat 2.6. (2011). Radionuclide decay data sourse. Retrieved 15/07/2016, from National Nuclear Data Center, Brookhaven National Laboratory, USA http://www.nndc.bnl.gov/nudat2/

O'Donoghue, J. A., & Wheldon, T. E. (1996). Targeted radiotherapy using auger electron emitters. *Physics in Medicine and Biology, 41*(10), 1973-1992.

Oblozinsky, P. (1997). *Summary report of the 2nd research co-ordination meeting on development of reference charged-particle cross section database for medical radioisotope production*. Retrieved 30/03/2014 from IAEA: http://www.iaea.org/inis/collection/NCLCollectionStore/_Public/29/003/29003391.pdf

Ochiai, K., Nakao, M., Kubota, N., Sato, S., Yamauchi, M., Ishioka, N., . . . Konno, C. (2007). *Deuteron induced activation cross section measurement for IFMIF*. Paper presented at the International Conference on Nuclear Data for Science and Technology.

Ortec. (2012). Maestro gamma spectrum analyzer and mca emulator version 7.0: Software user's manual. Retrieved 13/10/2016, from http://www.ortec-online.com/products/application-software/maestro-mca

Osae, E. K., Nyarko, B. J. B., Serfor-Armah, Y., & Darko, E. O. (1999). An empirical expression for the full energy peak efficiency of an n-type high purity germanium detector. *Journal of Radioanalytical and Nuclear Chemistry, 242*(3), 617-622.

Otuka, N., Dupont, E., Semkova, V., Pritychenko, B., Blokhin, A. I., Aikawa, M., . . . Zhuang, Y. (2014). Towards a more complete and accurate experimental nuclear reaction data library (exfor): International collaboration between nuclear reaction data centres (nrdc). *Nuclear Data Sheets, 120*, 272-276.

Otuka, N., Lalremruata, B., Khandaker, M. U., Usman, A. R., & Punte, L. R. M. (2017). Uncertainty propagation in activation cross section measurements. *Radiation Physics and Chemistry,* 10.1016/j.radphyschem.2017.01.013.

Otuka, N., & Takacs, S. (2015). Definitions of radioisotope thick target yields. *Radiochimica Acta, 103*(1), 1-6.

Ozafrán, M. J., Bonesso, O., De La Vega Vedoya, M., & Nassiff, S. J. (1989). Study of (α, 2αxn) and (α, 4pxn) reaction on natural copper. *Journal of Radioanalytical and Nuclear Chemistry, 131*(2), 467-478.

Papash, A., & Alenitsky, Y. G. (2008). Commercial cyclotrons. Part i: Commercial cyclotrons in the energy range 10–30 MeV for isotope production. *Physics of Particles and Nuclei, 39*(4), 597-631.

Peng, X., He, F., & Long, X. (1998). Excitation functions for the reactions induced by alpha-particle impact of natural titanium. *Nuclear Instruments and Methods in Physics Research Section B: Beam Interactions with Materials and Atoms, 140*(1), 9-12.

Porges, K. G. (1956). Alpha excitation functions of silver and copper. *Physical Review, 101*(1), 225-230.

Porile, N. T., & Morrison, D. L. (1959). Reactions of ^{63}Cu and ^{65}Cu with alpha particles. *Physical Review, 116*(5), 1193-1200.

Qaim, S. M. (2004). Use of cyclotrons in medicine. *Radiation Physics and Chemistry, 71*(3–4), 917-926.

Qaim, S. M., Spahn, I., Scholten, B., & Neumaier, B. (2016). Uses of alpha particles, especially in nuclear reaction studies and medical radionuclide production. *Radiochimica Acta, 104*(9), 601-624.

Qaim, S. M., Tárkányi, F. T., Obložinský, P., Gul, K., Hermanne, A., Mustafa, M., . . . Takács, S. (2002). Charged-particle cross section database for medical radioisotope production. *Journal of Nuclear Science and Technology, 39*(sup2), 1282-1285.

QCalc. (2016). Q-value calcultor. Retrieved 13/01/2017, from National Nuclear Data Centre, NNDC: http://www.nndc.bnl.gov/qcalc/

Qtool. (2011). Calculation of reaction q-values and thresholds. Retrieved 23/01/2017, from US Department of Energy, USA http://t2.lanl.gov/nis/data/qtool.html

Rao, A. V. M., Mukherjee, S., & Rao, J. R. (1991). Alpha particle induced reactions on copper and tantalum. *Pramana, 36*(1), 115-123.

Rao, J. R., Rao, A. M., Mukherjee, S., Upadhyay, R., Singh, N., Agarwal, S., . . . Singh, P. (1987). Non-equilibrium effects in alpha-particle-induced reactions in light, medium and heavy nuclei up to 120 MeV. *Journal of Physics G: Nuclear Physics, 13*(4), 535-542.

Rattan, S. S., Singh, R. J., Sahakundu, S. M., Prakash, S., & Ramaniah, M. V. (1986). Alpha particle induced reactions of ^{209}Bi and ^{63,65}Cu. *Radiochimica Acta, 39*(2), 61-63.

Rayudu, G., & Yaffe, L. (1963). Reactions produced on erbium by protons of energies between 6 and 87 MeV. *Canadian Journal of Chemistry, 41*(10), 2544-2556.

Riken. (2017). Celebrating the naming of the new element nihonium. Retrieved from http://www.riken.jp/en/, accessed on 16/04/2017

Rizvi, I. A., Ansari, M. A., Gautam, R. P., Singh, R. K. Y., & Chaubey, A. K. (1987). Excitation function studies of (α, xpyn) reactions for ^{63,65}Cu and pre-equilibrium effect. *Journal of the Physical Society of Japan, 56*(9), 3135-3144.

Rorat, E., Petelenz, B., Marczewska, B., & Ochab, E. (2005). Thermoluminescence dosimetry of model line sources containing vanadium-48. *Radiation Measurements, 39*(5), 495-501.

Ruddy, F. H., & Pate, B. D. (1969). Formation and decay of the compound nucleus 68 ge:(i). Experiment and the independence hypothesis. *Nuclear Physics A, 127*(2), 305-322.

Ruth, T. J. (2003). Accelerators available for isotope production. *Handbook of Radiopharmaceuticals: Radiochemistry and Applications*, 71-85.

Ruth, T. J. (2009). The production of radionuclides for radiotracers in nuclear medicine. *Reviews of Accelerator Science and Technology, 02*(01), 17-33.

Sadeghi, M., Zandi, N., & Afarideh, H. (2012). Targetry and specification of tm-167 production parameters by different reactions. *Journal of Radioanalytical and Nuclear Chemistry*, *291*(3), 731-738.

Sau, J., Demeyer, A., & Chéry, R. (1968). Étude expérimentale et analyse des fonctions d'excitation ^{165}Ho (α, χn) et ^{169}Tm (α, χn). *Nuclear Physics A, 121*(1), 131-144.

Schmor, P. (2011). Review of cyclotrons for the production of radioactive isotopes for medical and industrial applications. *Reviews of Accelerator Science and Technology, 04*(01), 103-116.

Schröder, C., Bailey, B., Klingelhöfer, G., & Staudigel, H. (2006). Fe mössbauer spectroscopy as a tool in astrobiology. *Planetary and Space Science, 54*(15), 1622-1634.

Shahid, M., Kim, K., Naik, H., Zaman, M., Kim, G., Yang, S.-C., & Song, T.-Y. (2015a). Measurement of excitation functions in alpha-induced reactions on yttrium. *Nuclear Instruments and Methods in Physics Research Section B: Beam Interactions with Materials and Atoms, 342*, 158-165.

Shahid, M., Kim, K., Naik, H., Zaman, M., Yang, S.-C., & Kim, G. (2015b). Measurement of excitation functions in proton induced reactions on natural copper from their threshold to 43 MeV. *Nuclear Instruments and Methods in Physics Research Section B: Beam Interactions with Materials and Atoms, 342*, 305-313.

Singh, B., & Chen, J. (2015). Nuclear data sheets for A = 43. *Nuclear Data Sheets, 126*, 1-150.

Singh, B., & Prasad, R. (1995). Measurement and analysis of excitation functions for the reactions ^{165}Ho (α, xn)(x= 1-3) in the energy range ≈ 10–40 MeV. *Physica Scripta*, *51*(4), 440.

Singh, N. (1992). Pre-equilibrium neutron emission in alpha particle induced reactions. *Journal of Physics G: Nuclear and Particle Physics*, *18*(5), 927.

Singh, N. L., Patel, B. J., Somayajulu, D. R. S., & Chintalapudi, S. N. (1994). Analysis of the excitation functions of (α, xnyp) reactions on natural copper. *Pramana, 42*(4), 349-363.

Sloan, D. H., & Lawrence, E. O. (1931). The production of heavy high speed ions without the use of high voltages. *Physical Review, 38*(11), 2021-2032.

Sonck, M., Van Hoyweghen, J., & Hermanne, A. (1996). Determination of the external beam energy of a variable energy. Multiparticle cyclotron. *Applied Radiation and Isotopes, 47*(4), 445-449.

Srivastava, S. C. (1996). Is there life after technetium: What is the potential for developing new broad-based radionuclides? *Seminars in Nuclear Medicine, 26*(2), 119-131.

Steere, A. R. (2005). *A timeline of major particle accelerators.* Michigan State University, USA.

Stelson, P. H., & McGowan, F. K. (1964). Cross sections for (α, n) reactions for medium-weight nuclei. *Physical Review, 133*(4B), B911-B919.

Szelecsényi, F., Kovács, Z., Nagatsu, K., Fukumura, K., Suzuki, K., & Mukai, K. (2012). Investigation of direct production of ^{68}Ga with low energy multiparticle accelerator. *Radiochimica Acta International Journal for Chemical Aspects of Nuclear Science and Technology, 100*(1), 5-11.

Szelecsényi, F., Suzuki, K., Kovács, Z., Takei, M., & Okada, K. (2001). Alpha beam monitoring via ^{nat}Cu + alpha processes in the energy range from 40 to 60 MeV. *Nuclear Instruments and Methods in Physics Research Section B: Beam Interactions with Materials and Atoms, 184*(4), 589-596.

Szkliniarz, K., Sitarz, M., Walczak, R., Jastrzębski, J., Bilewicz, A., Choiński, J., . . . Zipper, W. (2016). Production of medical Sc radioisotopes with an alpha particle beam. *Applied Radiation and Isotopes, 118*, 182-189.

T.W. Burrows. (2006). Nuclear data sheets for A=48. *Nuclear Data Sheets 107* 1747-1922.

Takacs, S., Hermanne, A., Ditroi, F., Tarkanyi, F., & Aikawa, M. (2015). Reexamination of cross sections of the ^{100}Mo(p,2n)^{99m}Tc reaction. *Nuclear Instruments & Methods in Physics Research Section B-Beam Interactions with Materials and Atoms, 347*, 26-38.

Takacs, S., Sonck, M., Azzam, A., Hermanne, A., & Tarkanyi, F. (1997). Activation cross section measurements of deuteron induced reactions on ^{nat}Ni with special reference to beam monitoring and production of ^{61}Cu for medical purpose. *Radiochimica Acta, 76*(1-2), 15-24.

Takács, S., Sonck, M., Azzam, A., Hermanne, A., & Tárkányi, F. (1997). Activation gross section measurements of deuteron induced reactions on ^{nat}Ni with special

reference to beam monitoring and production of for ^{61}Cu medical purpose. *Radiochimica Acta, 76*, 15 - 24.

Takács, S., Szelecsényi, F., Tárkányi, F., Sonck, M., Hermanne, A., Shubin, Y., . . . Youxiang, Z. (2001). New cross-sections and intercomparison of deuteron monitor reactions on Al, Ti, Fe, Ni and Cu. *Nuclear Instruments and Methods in Physics Research Section B: Beam Interactions with Materials and Atoms, 174*(3), 235-258.

Takács, S., Tárkányi, F., Király, B., Hermanne, A., & Sonck, M. (2007). Evaluated activation cross sections of longer-lived radionuclides produced by deuteron induced reactions on natural nickel. *Nuclear Instruments and Methods in Physics Research Section B: Beam Interactions with Materials and Atoms, 260*(2), 495-507.

Tarkanyi, F., Hermanne, A., Kiraly, B., Takacs, S., & Ignatyuk, A. V. (2010). Study of excitation functions of alpha-particle induced nuclear reactions on holmium for ^{167}Tm production. *Applied Radiation and Isotopes, 68*(3), 404-411.

Tárkányi, F., Hermanne, A., Takács, S., Király, B., Spahn, I., & Ignatyuk, A. V. (2010). Experimental study of the excitation functions of proton induced nuclear reactions on ^{167}Er for production of medically relevant ^{167}Tm. *Applied Radiation and Isotopes, 68*(2), 250-255.

Tárkányi, F., Szelecsényi, F., & Kopecký, P. (1992). Cross section data for proton, ^{3}He and α-particle induced reactions on ^{nat}Ni, ^{nat}Cu and ^{nat}Ti for monitoring beam performance. In Qaim, S. (Ed.), *Nuclear data for science and technology* (10.1007/978-3-642-58113-7_151pp. 529-532): Springer Berlin Heidelberg.

Tárkányi, F., Szelecsényi, F., Takács, S., Hermanne, A., Sonck, M., Thielemans, A., . . . Youxiang, Z. (2000). New experimental data, compilation and evaluation for the ^{nat}Cu(α, x)^{66}Ga, ^{nat}Cu(α, x)^{67}Ga and ^{nat}Cu(α, x)^{65}Zn monitor reactions. *Nuclear Instruments and Methods in Physics Research Section B: Beam Interactions with Materials and Atoms, 168*(2), 144-168.

Toprek, D., Goto, A., & Yano, Y. (1999). Beam orbit simulation in the central region of the riken avf cyclotron. *Nuclear Instruments and Methods in Physics Research Section A: Accelerators, Spectrometers, Detectors and Associated Equipment, 425*(3), 409-414.

Tsoncheva, T., Genova, I., Paneva, D., Dimitrov, M., Tsyntsarski, B., Velinov, N., . . . Petrov, N. (2015). Cobalt- and iron-based nanoparticles hosted in SBA-15 mesoporous silica and activated carbon from biomass: Effect of modification procedure. *Solid State Sciences, 48*, 286-293.

Uddin, M. S., & Scholten, B. (2016). Excitation functions of alpha particle induced reactions on natti up to 40 MeV. *Nuclear Instruments and Methods in Physics Research Section B: Beam Interactions with Materials and Atoms, 380*, 15-19.

Ugur, Ö., Kothari, P. J., Finn, R. D., Zanzonico, P., Ruan, S., Guenther, I., . . . Larson, S. M. (2002). Ga-66 labeled somatostatin analogue DOTA-DPhe 1-Tyr 3-

octreotide as a potential agent for positron emission tomography imaging and receptor mediated internal radiotherapy of somatostatin receptor positive tumors. *Nuclear Medicine and Biology, 29*(2), 147-157.

Usman, A. R., Khandaker, M. U., Haba, H., Murakami, M., & Otuka, N. (2016a). Measurements of deuteron-induced reaction cross-sections on natural nickel up to 24 MeV. *Nuclear Instruments and Methods in Physics Research Section B: Beam Interactions with Materials and Atoms, 368*, 112-119.

Usman, A. R., Khandaker, M. U., Haba, H., Otuka, N., & Murakami, M. (2017). Excitation functions of alpha particles induced nuclear reactions on natural titanium in the energy range of 10.4 – 50.2 MeV. *Nuclear Instruments and Methods in Physics Research Section B: Beam Interactions with Materials and Atoms, 399*, 34-47.

Usman, A. R., Khandaker, M. U., Haba, H., Otuka, N., Murakami, M., & Komori, Y. (2016b). Production cross-sections of radionuclides from α-induced reactions on natural copper up to 50 MeV. *Applied Radiation and Isotopes, 114*, 104-113.

Uusijärvi, H., Bernhardt, P., Rösch, F., Maecke, H. R., & Forssell-Aronsson, E. (2006). Electron-and positron-emitting radiolanthanides for therapy: Aspects of dosimetry and production. *Journal of Nuclear Medicine, 47*(5), 807-814.

Valdovinos, H. F., Hernandez, R., Barnhart, T. E., Graves, S., Cai, W., & Nickles, R. J. (2015). Separation of cyclotron-produced ^{44}Sc from a natural calcium target using a dipentyl pentylphosphonate functionalized extraction resin. *Applied Radiation and Isotopes, 95*, 23-29.

van der Meulen, N. P., Bunka, M., Domnanich, K. A., Müller, C., Haller, S., Vermeulen, C., . . . Schibli, R. (2015). Cyclotron production of ^{44}Sc: From bench to bedside. *Nuclear Medicine and Biology, 42*(9), 745-751.

Vimalnath, K. V., Rajeswari, A., Chakraborty, S., & Dash, A. (2014). Large scale production of ^{51}cr for medical application in a medium flux research reactor: A comparative investigation of szilard–chalmers process and direct (n,γ) route. *Applied Radiation and Isotopes, 91*, 104-108.

Vlieks, A., Morgan, J., & Blatt, S. (1974). Total cross sections for some (α, n) and (α, p) reactions in medium-weight nuclei. *Nuclear Physics A, 224*(3), 492-502.

Vonach, H., Haight, R., & Winkler, G. (1983). (α, n) and total α-reaction cross sections for ^{48}ti and ^{51}v. *Physical Review C, 28*(6), 2278.

Vorozhtsov, S., Vorozhtsov, A., Perepelkin, E., Watanabe, S., Kubono, S., Mitsumoto, T., & Goto, A. (2008). *Calculations of the beam transmission and quality in the riken avf cyclotron.* Paper presented at the Report presented at this Conference.

Watanabe, T., Fujimaki, M., Fukunishi, N., Imao, H., Kamigaito, O., Kase, M., . . . Wakasugi, M. (2014). *Beam energy and longitudinal beam profile measurement system at the ribf.* Paper presented at the 5th International Particle Accelerator Conference (IPAC2014), Jacow, Dresden, Germany.

Watson, I. A., Waters, S. L., Bewley, D. K., & Silvester, D. J. (1973). A method for the measurement of the cross-sections for the production of radioisotopes by charged particles from a cyclotron. *Nuclear Instruments and Methods, 106*(2), 231-235.

Weinreich, R., Probst, H. J., & Qaim, S. M. (1980). Production of chromium-48 for applications in life sciences. *International Journal of Applied Radiation and Isototopes, 31*(4), 223-232.

Wilkinson, G., & Hicks, H. G. (1949). Radioactive isotopes of the rare earths. I. Experimental techniques and thulium isotopes. *Physical Review, 75*(9), 1370.

Wu, S. C. (2000). Nuclear data sheets for A = 46. *Nuclear Data Sheets, 91*(1), 1-116.

Xiaolong, H. (2006). Nuclear data sheets for A = 51. *Nuclear Data Sheets, 107*(8), 2131-2322.

Xuan Tham, L., Nagasawa, N., Matsuhashi, S., Ishioka, N. S., Ito, T., & Kume, T. (2001). Effect of radiation-degraded chitosan on plants stressed with vanadium. *Radiation Physics and Chemistry, 61*(2), 171-175.

Yang Dong, & Huo Junde. (2014). Nuclear data sheets for A=54. *Nuclear Data Sheets 121*, 1-142.

Yano, Y. (2007). The riken ri beam factory project: A status report. *Nuclear Instruments & Methods in Physics Research Section B-Beam Interactions with Materials and Atoms, 261*(1-2), 1009-1013.

Zhukova, O. A., Kanashevich, V. I., Laptev, S. V., & Chursin, G. P. (1970). Excitation functions of reactions induced by alpha particles with maximum energy of 38 MeV on copper isotopes. *Izv. Akad. Nauk Kaz. SSR, Ser. Fiz.-Mat., No. 4*, 1-8.

Ziegler, J. F. (2003). Stopping and range of ions in matter srim-2003. *SRIM Code.* Retrieved 15/09/2016, from www.srim.org

Ziegler, J. F. (2004). Srim-2003. *Nuclear Instruments and Methods in Physics Research Section B: Beam Interactions with Materials and Atoms, 219–220*(0), 1027-1036.

Zweit, J., Sharma, H., & Downey, S. (1987). Production of gallium-66, a short-lived, positron emitting radionuclide. *International Journal of Radiation Applications and Instrumentation. Part A. Applied Radiation and Isotopes, 38*(7), 499-501.

Zweit, J., Smith, A. M., Downey, S., & Sharma, H. L. (1991). Excitation functions for deuteron induced reactions in natural nickel: Production of no-carrier-added ^{64}Cu from enriched ^{64}Ni targets for positron emission tomography. *International Journal of Radiation Applications and Instrumentation. Part A. Applied Radiation and Isotopes, 42*(2), 193-197.

LIST OF PUBLICATIONS AND PAPER PRESENTATIONS

A. ISI PUBLICATIONS:

1. **Usman, A. R.**, Khandaker, M. U., Haba, H., Murakami, M., & Otuka, N. (2016). **Measurements of deuteron-induced reaction cross-sections on natural nickel up to 24 mev**. *Nuclear Instruments and Methods in Physics Research Section B: Beam Interactions with Materials and Atoms, 368*, 112-119.

2. **Usman, A. R.**, Khandaker, M. U., Haba, H., Otuka, N., Murakami, M., & Komori, Y. (2016). **Production cross-sections of radionuclides from α-induced reactions on natural copper up to 50mev.** *Applied Radiation and Isotopes, 114*, 104-113.

3. **Usman, A. R.**, Khandaker, M. U., Haba, H., Otuka, N., & Murakami, M. (2017). **Excitation functions of alpha particles induced nuclear reactions on natural titanium in the energy range of 10.4 – 50.2 MeV**. *Nuclear Instruments and Methods in Physics Research Section B: Beam Interactions with Materials and Atoms, 399*, 34-47.

4. Otuka, N., Lalremruata, B., Khandaker, M. U., **Usman, A. R**., & Punte, L. R. M. (2017). **Uncertainty propagation in activation cross section measurements.** ***Radiation*** *Physics and Chemistry*, DOI: 10.1016/j.radphyschem.2017.01.013. (Accepted Manuscript).

B. PAPER PRESENTED AT INTERNATIONAL CONFERENCES:

1. **New measurements of alpha-induced reactions on natural copper up to 50 MeV.** International Conference on Computational Environmental Sciences and Engineering (ICCESEN -2015) – Antalya, Turkey.
2. **Cyclotron production of ^{48}V via ^{nat}Ti(d,x)^{48}V nuclear reaction; a Promising Radionuclide.** International Nuclear Science and Technology Conference (INST-2016), Bangkok, Thailand.